BRL

REPORT NO. 1292

A FAILURE CRITERION FOR BLAST LOADED CYLINDRICAL SHELLS

by

William J. Schuman, Jr.

MAY 1965

U. S. ARMY MATERIEL COMMAND
BALLISTIC RESEARCH LABORATORIES
ABERDEEN PROVING GROUND, MARYLAND

Destroy this report when it is no longer needed.
Do not return it to the originator.

DDC AVAILABILITY NOTICE

Qualified requesters may obtain copies of this report from DDC.

The findings in this report are not to be construed as an official Department of the Army position, unless so designated by other authorized documents.

BALLISTIC RESEARCH LABORATORIES

REPORT NO. 1292

MAY 1965

A FAILURE CRITERION FOR BLAST LOADED CYLINDRICAL SHELLS

W. J. Schuman, Jr.

Terminal Ballistics Laboratory

RDT&E Project No. 1P014501A33E

ABERDEEN PROVING GROUND, MARYLAND

B A L L I S T I C R E S E A R C H L A B O R A T O R I E S

REPORT NO. 1292

WJSchuman/blw
Aberdeen Proving Ground, Md.
May 1965

A FAILURE CIRTERION FOR BLAST LOADED CYLINDRICAL SHELLS

ABSTRACT

The results of an extensive experimental program to study the plastic response of thin-walled, unstiffened cylindrical shells to external blast loading are presented. Empirical relations between the shell and blast parameters that satisfy a failure criterion based on a given level of plastic deformation are given.

A comparison of calculated and actual overpressure values for 159 shells that had responses satisfying the failure criterion (permanent deformation in the radial direction - 5 percent to 10 percent of the original diameter) is made. The average deviation between these values is 14 percent.

Intentionally Left Blank.

TABLE OF CONTENTS

TABLE OF CONTENTS (Contd)

LIST OF TABLES

Intentionally Left Blank.

LIST OF FIGURES

LIST OF FIGURES (Contd)

TABLE OF SYMBOLS

p = peak overpressure

p_i = peak incident overpressure

p_r = peak reflected overpressure

p_{cr} = failure pressure for dynamic lateral loading

$\bar{p}_{cr}$ = failure pressure for dynamic longitudinal loading

p_o = ambient pressure

$\bar{p}$ = failure pressure for static lateral loading

p_w = pressure required at weight W

p_{w_o} = pressure required at weight W = 1 pound

p_D = pressure required at diameter D

p_{D_o} = pressure required at diameter D = 1 inch

ΔT = shock duration

T = shock arrival time

τ = natural period of vibration

u = peak particle velocity

U = shock velocity

I = impulse

I_i = incident impulse per unit area

I_r = reflected impulse per unit area

I_a = theoretical impulse per unit area

I_o = impulse per unit mass

I_t = total impulse

E = modulus of elasticity

ν = Poisson's ratio (= 1/2 for plastic materials)

$$S_i = \frac{\sqrt{2}}{2}\left[(S_x - S_y)^2 + (S_y - S_z)^2 + (S_z - S_x)^2 + 6(\tau_{xy}^2 + \tau_{yz}^2 + \tau_{zx}^2)\right]^{1/2}$$

S_x, S_y, S_z, τ_{xy}, τ_{yz}, τ_{zx} = stress components (S's are direct stresses and τ's are shear stresses)

S_o = yield stress

S_u = ultimate stress

e = strain

$$e_i = \frac{\sqrt{2}}{3}\left[(e_x - e_y)^2 + (e_y - e_z)^2 + (e_z - e_x)^2 + 3/2(\gamma_{xy}^2 + \gamma_{yz}^2 + \gamma_{zx}^2)\right]^{1/2}$$

e_x, e_y, e_z, γ_{xy}, γ_{yz}, γ_{zx} = strain components (e's are direct strains and γ's are shear strains)

e_m = maximum strain

e_o = yield strain in tension

D = shell diameter

D_o = width of plastic hinge

a = shell mean radius

L = shell length

t = shell thickness

d = charge diameter

Z = scaled distance = $R/W^{1/3}$

W = charge weight

R = charge distance

K = scale factor

x = cylindrical coordinate

x_m = maximum displacement

x' = x/L

TABLE OF SYMBOLS (Contd)

φ = cylindrical coordinate

$y = a\varphi$

$u, v, w,$ = displacements of shell element

$\dot{u}, \dot{v}, \dot{w},$ = velocities of shell element

$w(x', \varphi)$ = deflection pattern

w_o = maximum radial displacement

$w(e_i)$ = function of e_i

r = radial distance from the midsurface to any element within the shell thickness

$\overline{K}$ = bulk modulus of material

ψ = multiplying factor

ρ = mass density of shell material

$\theta = e_x + e_y + e_z$

λ = parameter involved in plastic-linear hardening stress-strain law

ξ, a, β, γ = functions describing the integrand of the energy integrals

$F_{L/D}$ = length-to-diameter ratio factor

F_w = charge weight factor

F_D = diameter factor

F_t = thickness factor

V_o = work done in deforming shell per unit volume

V = work done in deforming shell

$\overline{V} = \dfrac{\sqrt{3}V}{S_o taL}$

dm = element of mass

T_E = initial kinetic energy put into shell by pressure pulse

Intentionally Left Blank.

1. INTRODUCTION

1.1 General Remarks

One of the major problems in the design of structures is that of determining their useful life. One would like to clearly define the limiting environment that the structure can tolerate and if it fails, the reasons for failure. There are many theories of failure for static loadings. In some instances the onset of yielding would constitue an end to the useful life of the structure. In other design conditions complete rupture of a particular element would be the limiting case. There are also theories for the failure of unstable structures and of structures that must withstand fluctuating loads.

An important need at this time is a theory and criterion of failure for structures such as aerospace vehicles that include as part of their life expectancy an encounter with a nuclear environment that numbers blast loading among its many effects. A toleration level to this type of loading is required so that design judgments may be made as to whether a given vehicle will survive or fail to survive a particular encounter of this type.

The majority of these vehicles are primarily composed of elements that may be approximated by cylindrical shells. Therefore an experimental study of the response of cylindrical shells to external blast loading is worthwhile in leading to the determination of relationships between shell and blast parameters that will predict the deformation required to satisfy a given failure criterion.

Before proceeding to a specific statement of the problem to be investigated, a discussion of blast parameters will be presented.

1.2 Definition of Blast Parameters

As a result of a detonation of a chemical or nuclear explosive, a pressure wave of finite amplitude is propagated into the surrounding medium. The velocity of propagation of the disturbances is greater than the velocity of sound in the undisturbed medium. The pressure wave changes its form

and, in particular in air, the pressure front becomes steeper and steeper until it is limited by viscosity and heat conductivity. When this relatively stable form is reached the pressure rise occurs within a very narrow region which may be considered to be a perfect discontinuity. Such a disturbance is termed a shock wave. For gases, the thickness of the shock front is of the order of the mean free path of a molecule[44]*.

A simplified form of the pressure-time history of the shock at a point in space is as shown in the top part of Figure 1.1. The peak over-pressure-p declines exponentially to the ambient pressure p_o (represented by the dashed horizontal line), in the time $-\Delta T$ (called duration). In fact, the decline is to a value less than ambient (atmospheric) as shown by the curve continuing below the dashed line. The integral of the over-pressure with respect to time over the duration $-\Delta T$ is termed the impulse -I and is indicated by the shaded area. Thus, the main blast parameters important for the problem studied here are over-pressure, impulse and duration.

Major complications in studies of the dynamical response of targets or structures to the transient loads of air blast are the interactions, e.g., diffraction effects, between the structure and the air blast, which change considerably the subsequent flow characteristics of the blast and hence the actual load imposed on the target. This report is restricted to reporting free air blast (absence of target) and termed incident, and blast imposed on a semi-infinite rigid target by normal (90^o) incidence of a blast wave-termed reflected. The true values of peak pressure and impulse to which a target is subjected will fall between these two limiting values.

A general law of similitude was proposed by Sachs[37] to account for the effect of changes in the ambient air pressure and temperature on the peak overpressure and positive impulse of the blast. A special case of this law is Hopkinson's law[48] for size scaling. It pertains only to the propagation of air blast under sea-level atmospheric conditions.

---

* *Reference numbers refer to items listed in the Biblography on page 79.*

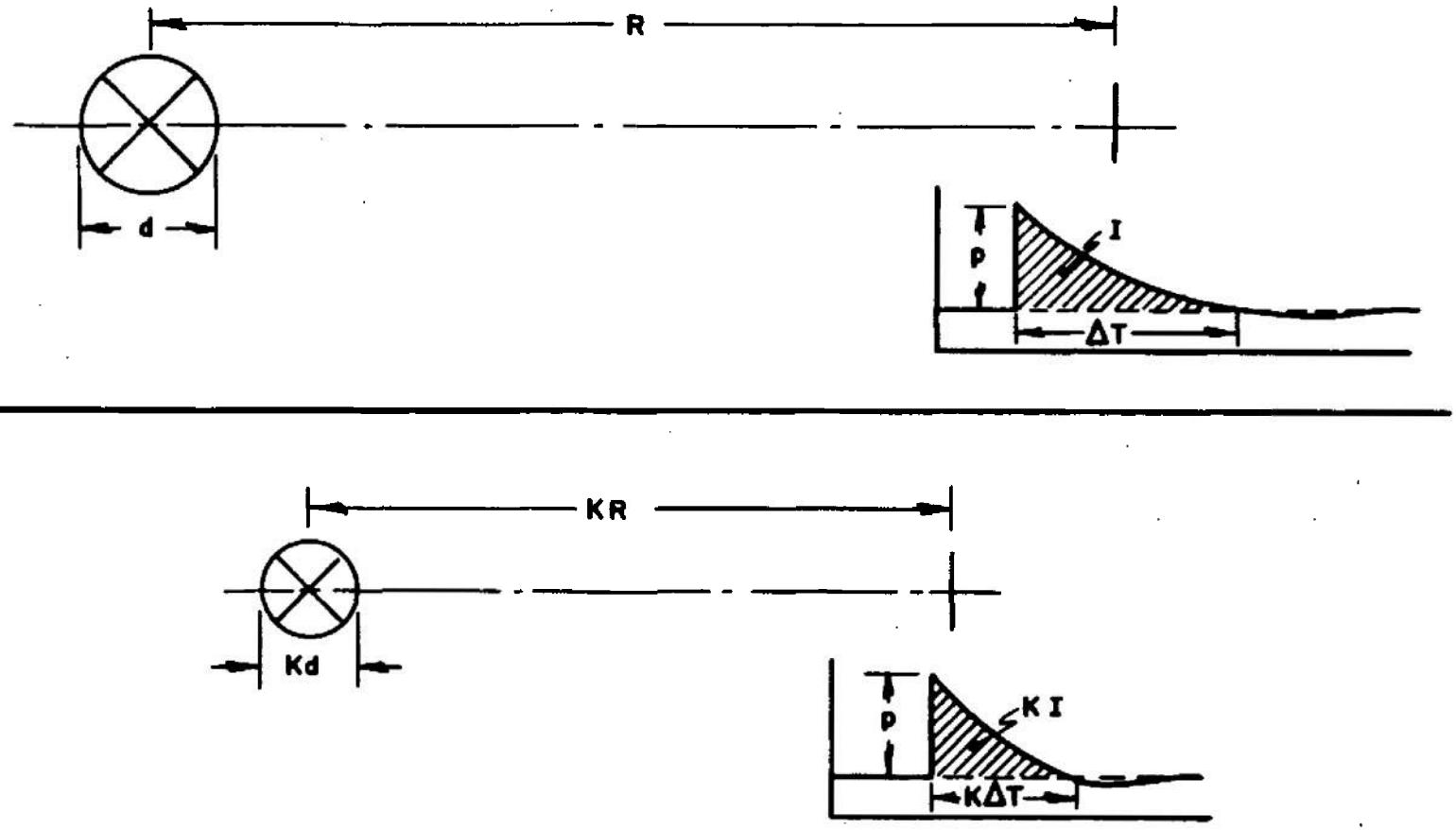

FIG. I-1 BLAST WAVE SCALING

According to size scaling the peak overpressure and scaled impulse, $I/W^{1/3}$, are functions of the scaled distance, $R/W^{1/3}$, where R is the distance to the center of the explosive and W is the weight of the explosive.

This type of blast wave scaling is shown in Figure 1.1. If one has an explosive of weight W (which is proportional to the cube of the diameter d^3) located at a distance, R, from a point in space, then there will be an overpressure, p, an impulse, I, and duration, ΔT at that point. If one then takes a scaled explosive of weight, K^3W, (which is proportional to the cube of the scaled diameter, $(Kd)^3$, located at a scaled distance, KR, from a point in space) then there will be an overpressure, p, as before but the duration will be $K \cdot \Delta T$ and impulse will be KI.

A plot of scaled air blast data[7] is given in Figure 1.2. This is a plot of peak incident overpressure, p_i, scaled duration, $\Delta T/W^{1/3}$, scaled shock arrival time, $T/W^{1/3}$, shock velocity, U, and peak particle velocity, u, versus scaled distance, $Z = R/W^{1/3}$. Similar curves are given for peak reflected pressure in Reference (16).

The curves discussed above pertain to explosive charges that are suspended above the ground. If the charges are located close to or on the ground, the portion of the shock wave striking the ground will be reflected (the amount depending upon the composition of the ground) and will then propagate through the previously heated air and therefore at some point overtake the initial shock wave. These two shocks will then combine and the target will be subjected to a blast wave that would be the result of an explosive weight approximately twice the initial magnitude. This factor termed the reflection factor, may very from one to eight, but is generally closer to two. Therefore, free-field blast overpressure measurements are usually taken at a few points to establish the exact value of the reflection factor when the explosive is detonated on or close to the ground. The explosive charge weights given in subsequent tables of data include the reflection factor; i.e., they are effective weights.

FIG. 1.2 – COMPILED FREE-AIR BLAST DATA ON BARE SPHERICAL PENTOLITE

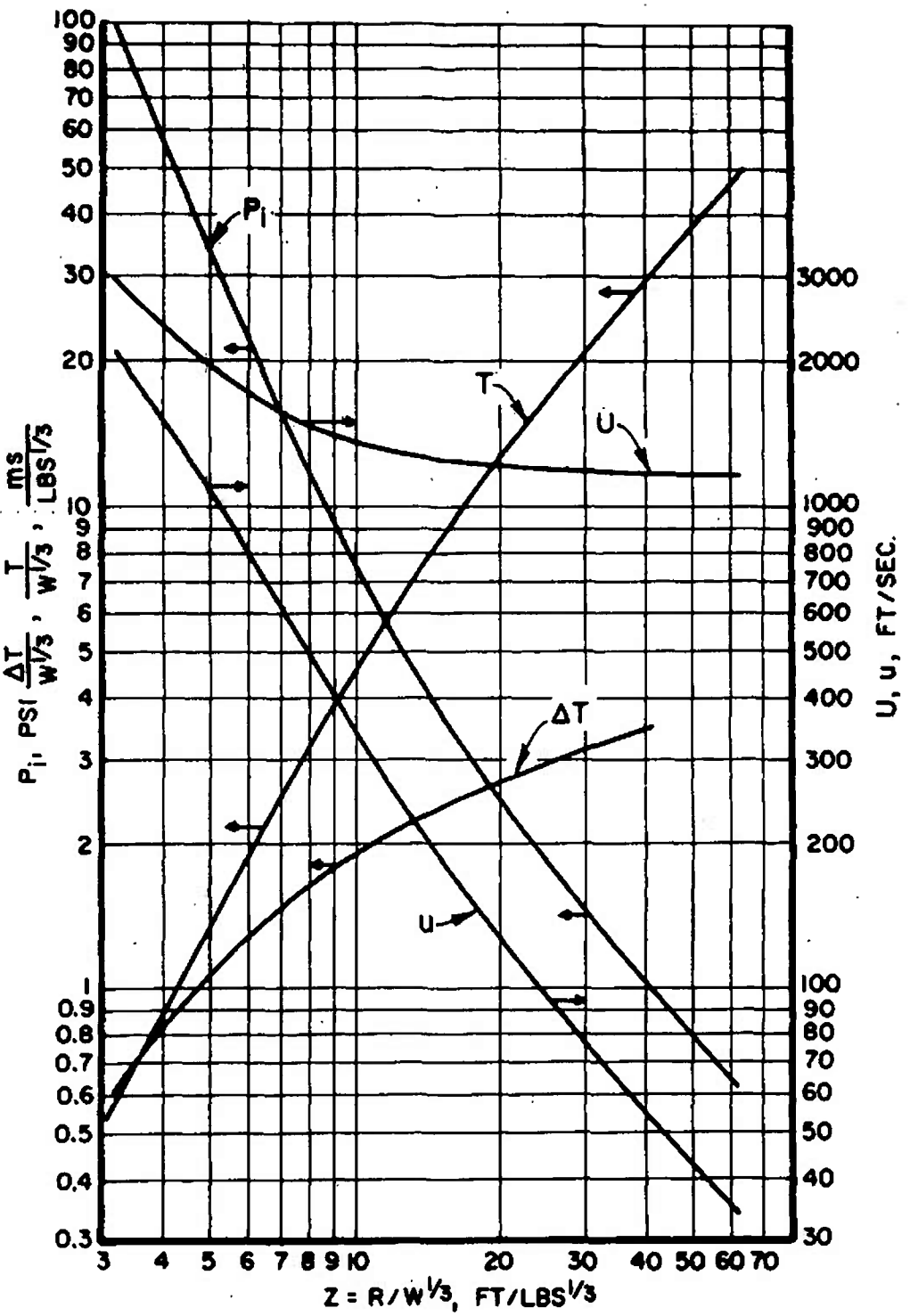

1.3 Statement of the Problem

The general problem to be studied in this report is an experimental study of the response of cylindrical shells to external blast loading. Comparisons with theory will also be made.

An aerospace vehicle may suffer failure or be "killed" by blast loading in one of three different ways: deformation of the outer skin and subsequent crushing of internal components, failure of internal components due to high accelerations or the vehicle may be overturned on the firing pad with subsequent damage upon impact, i.e., crushing, g-loading, or overturning.

This study will be limited to the case of deformation of the outer skin. Therefore a right-circular, thin-walled, unstiffened shell of finite length will be used for the simulation. It will be assumed that the heavy bulkheads and attachment rings between sections can be simulated by considering the shell sections to have clamped ends and that there are no pre-loads such as bending, compression or torsion.

As described in the Section 1.5, Previous Related Studies, the simulation techniques used by other researchers in the past have not been able to reproduce the true blast effects, namely, very-high rise time (measured in microseconds), an exponential decay of overpressure with time and diffraction effects on the shell. Hence, the blast loading can be best produced by using actual charges of high explosive.

It will be assumed that a given level of damage or deformation of the shell will be representative of that required to "kill" a real vehicle. Based on previous experience in determining the vulnerability of actual missiles, the level of damage that will constitute a failure criterion may be stated as follows: a radial permanent deformation approximately 5 percent to 10 percent of the original diameter. This range of deformation values is rather broad, but in keeping with the accuracy of blast field work. The problem of accuracy will be discussed in more detail in later portions of this report.

The specific problem may now be stated as follows:

Determine the relationships between the shell and blast parameters that enable one to determine if failure has occurred, according to the failure criterion chosen. These relationships should be sufficiently general to be adaptable to variation in the magnitudes of the deformation defined by the failure criterion, and to changes in the failure level.

1.4 Scope of the Study

The study consisted of an extended experimental program involving a wide spectrum of shell geometries and explosive charge weights. The shells were fabricated from steel and a number of different aluminum alloys. The shells were mounted so the ends are clamped to end caps restrained from moving in order that bending and axial compressive stresses may be neglected. The explosive charges were oriented so there were two different loadings: asymmetric, which is of the most interest, and axisymmetric. Relationships between certain shell parameters (length, diameter, thickness and material) and the blast parameters of overpressure and charge weight were determined that will predict the deformation required to satisfy the failure criterion. The results were compared with other published work.

The text of this report consists of five sections and three appendices.

Section 1 deals with introductory considerations, defines blast parameters, states the problem, outlines the scope of the investigation, presents a review of previous research on response of cylinders to blast loading and defines structural scaling.

Section 2 describes the test specimens and related equipment and discusses the experimental procedures involved.

The data obtained are presented in Section 3 with some discussion of the shell-blast parameter relationships.

In Section 4 these parameter relationships are determined so that they satisfy the failure criterion. A comparison of the calculated and actual values as well as comparisons with theoretical analyses are given.

Section 5 contains a summary of the results of the investigation, and the conclusions that can be drawn from these results. In addition, suggestions for further research are given.

Photographs of firing areas and of the instrumentation are presented in Appendix A. Miscellaneous tables of data are given in Appendix B. A selected portfolio of deformation pattern pictures is produced in Appendix C.

1.5 Previous Related Studies

The problem of shell response has been studied since at least 1828 when the first papers were published. A very excellent bibliography by Nash[30] lists 1,455 publications through the end of 1953. Although a small portion of these were concerned with the vibration of shells, most were concerned with static shell problems.

The earliest studies on the response of cylindrical shells to impulsive loading were reported by Mindlin and Bleich[29] in 1952. The author started the present study in 1959. Since 1960 the number of researchers concerned with this problem has increased so that the majority of the studies made were concurrent with this study.

The theoretical analyses will be reviewed first, followed by a discussion of the experimental studies. The theoretical analyses will be divided into elastic and plastic studies. The plastic analyses are of major concern as the failure criterion is based on a plastic deformation level.

It will be shown that the scope of this report is unique and presents for the first time relationships between shell and blast parameters that are based on the effects of a real blast against real, three-dimensional cylindrical shells with clamped ends. Furthermore the results are in reasonable agreement with a failure criterion.

Theoretical Analyses - Elastic Studies. Bleich and DiMaggio[10] studied the axisymmetric case of infinite cylindrical shells under a suddenly applied uniform radial pressure above the buckling load. It was assumed that the deformation was inextensional and the shell generators remained straight.

Radknowski, Humphreys, Bodner, Payton and Budiansky[32] considered the axisymmetric cases of a distributed impulse and a moving pressure load and also the asymmetric case of a point impulse. Solutions were based on linear membrane shell theory with a failure criterion based on yield stress.

Wood, O'Neill and Koval[49] considered axisymmetric and asymmetric loading with the addition of a static axial compressive load. The analyses used were based on a linear theory and a buckling type of failure.

DeHart and Basdekas[13] have studied the response of aircraft and missile structures to axisymmetric and asymmetric blast loading. A linear-elastic approach was used since it was assumed that the typical materials will tear before large plastic strains can occur. In some instances a static analysis was considered as a first approximation. The cylindrical shells were stiffened by both rings and stringers. Wah, Rastrelli, Basdekas and DeHart[45] studied the axisymmetric and asymmetric response of cylindrical shells with various end conditions. Linear-elastic theories were again used. DeHart, Rastrelli, Basdekas, Minor and Pape[14] have studied the response of missiles in various configurations (on the transporter, in the launch position, etc.) and considered rolling of the transporter and overturning of the missile also. The failure of the missile itself was still based on elastic considerations as above[13,45].

Mindlin and Bleich[29] studied the response of an infinitely long, elastic cylindrical shell to a step shock wave with a front parallel to the shell axis. The motions were restricted to dilatational, translational and inextension-flexural modes. The shell was submerged in an acoustic

fluid. A modal analysis was used with incipient elastic buckling as the failure criterion. Baron and Bleich[9] refined the solution to include extensional effects in all modes.

An elastic failure criterion is extremely conservative in determining the vulnerability of missiles. Therefore, plastic studies are needed to correlate with the experimental data.

Theoretical Analyses - Plastic Studies. Hodge[20] presented an analysis for a rigid-plastic shell loaded for a short time with a pressure greater then the static collapse load. The pressure was a uniform radial step function. The shell was assumed to follow a simplified yield condition and the plastic flow law. Hodge[21] then extended this analysis to cover an arbitrary dynamic loading shape. The deformations were limited to a maximum of five times the thickness of the shell. Hodge[22] also studied the effect of variations of loading shape on shells. The shells considered were a central portion, between ring stiffeners, of a long shell. Sankarnaranayanan[38] studied shells, clamped at one end and free at the other, that were subjected to uniform lateral and hydrostatic pressures.

Abrahamson and Goodier[5], Abrahamson and Florence[4] and Abrahamson[2] studied the response of beams and circular rings, cylindrical shells and plates to impulsive loadings. The cylindrical shells had free ends and were subjected to uniform radial impulse. It was assumed that there was a slight imperfection in the uniformity of the initial velocity of the shell elements and strain hardening takes place in the material. These two assumptions are necessary for buckling to ensue. The asymmetrically loaded case was not studied. Some of the author's data[40] were used as the basis for estimating bounds on the strength of reentry vehicles in another report by Abrahamson[3]. Lindberg studied shells that had a higher radius-to-thickness ratio. The shell ends were still considered free. A modal analysis was used in determining the deformation patterns.

Rosendorf[34] has studied the response of various shells (cylindrical, conical, hemispherical) to blast loading from high explosives. A method of predicting buckling based on a triangular pressure pulse and a "dynamic load factor" was developed. The results in the form of predicted pressures, do not agree very well with the pressures predicted by the author in an earlier report[39].

Witmer, Herrmann, Leech and Pian[46] studied the response of plates and shells to impulsive loads. They were concerned with scabbing and fracture as well as deformation. It was proposed to use an approximate energy method for predicting the final degree of deformation. The energy method consisted of equating the total kinetic energy imparted to the shell by the applied loading to the energy absorbed by the structure in reaching its final deformed state. One must know what shape the deformation will take in order to determine the energy required or else one can assume plausible patterns. It was suggested that static properties be used to compute the absorbed energy. No details were presented for computing this energy for cylindrical shells.

Leech, Pian, Witmer and Herrmann[27] presented analyses to cover two and three-dimensional structures. Specifically, beams rings and shells (restricted to axisymmetric deformation) were treated. Numerical methods were presented based on non-linear differential equations. The material was treated as an elastic, perfectly plastic solid. A specific yield condition and flow rule was assumed. Witmer, Balmer, Leech and Pian[47] further extended the analyses to include (a) elastic, (b) perfectly-plastic, (c) elastic, strain-hardening, or (d) elastic, strain-hardening, strain-rate sensitive material behavior and large structural deflections in a general numerical method. The method can still only handle axisymmetrical response of shells with rotational symmetry. Pian[31] presented general equations for the dynamic response of three-dimensional shells of elastic-plastic material in tensor form. It is shown that the solution of the general shell problem involves exactly the same basic steps as that for two-dimensional structures. Pian remarked that the finite difference formulation may have to be modified when actual

boundary conditions are taken into consideration. Balmer and Witmer[8] carried out an extensive detailed evaluation of the adequacy of the elastic-plastic two-dimensional analysis previously discussed[46]. The evaluation was based on experimental work with circular rings and beams performed by Picatinny Arsenal. The application of the analysis to finite cylindrical shells have not been attempted except in very general terms.

Greenspon[17-19] has studied theoretically the response of cylindrical shells to blast loading. His results are very closely related to this report study and will therefore be left to a more detailed discussion given in Section 4. The plastic analysis by Greenspon is the only complete analysis that includes both axisymmetric and asymmetric impulsive loadings on shells of finite length.

Experimental Studies. Abrahamson and Goodier[5] and Abrahamson[1,2] studied experimentally the response of cylindrical shells. The loading was simulated by the use of sheet explosive placed over all or portions of the shell surface. A layer of attenuator material was placed between the shell and explosive to prevent spalling. The shells had free ends. The plastic analysis described earlier was used and it compared well with the experimental data. Lindberg[28] studied the case of a finite, very thin shell with clamped ends exposed to a uniform radial impulse over one-half of the shell surface. Loads were applied by detonating explosive gaseous mixtures of oxygen, hydrogen and helium. The elastic analysis predicted the number of lobes in the buckled pattern but not the amplitudes. The impulses in these studies were very short, simulating the energy deposition from X-rays rather than blast. There were no diffraction effects and the boundary conditions were different from those in the present problem.

DeHart and Basdekas[13] studied the response of shells to bending loads. Wah, Rastrelli, Basdekas and DeHart[45] conducted tests on cylindrical shells with various end conditions. The loading was obtained from the detonation of small quantities (5 lbs. to 30 lbs.) of TNT. The shells

were freely suspended on nylon ropes. Only one shell had rigid end caps to simulate clamped ends. However, the permanent deformation was only 0.25 inches for an original diameter of 12 inches and certainly falls well below the failure level specified for this study. The comparisons of computed and experimental deformations are considered good by these authors where the computed values are given as a range ± 10 percent wide and the experimental values vary from the average of this band by 10 to 40 percent.

Wood, O'Neill and Koval[49] studied the buckling of cylindrical shells. The loading was a combination of a dead-weight axial compression with either axisymmetric transient and oscillatory pressures or asymmetric lateral transient pressures. A modified loudspeaker was used to drive a column of air and thus load mylar shells. The rise times of the loading were an order of magnitude greater than those obtained from blast loadings. The boundary conditions were different from the present problem.

Laing[26] studied the response of cylindrical shells to the blast loading from a large charge weight (20 tons) of high explosive. Unfortunately the shells suffered either no amount or excessive amounts of deformation and the results were too sparse to determine the conditions required to just cause failure. The experimental technique used was similar to that of the author but the program was limited.

Rosendorf[33,35,36] has studied the response of various shells (cylindrical, conical, hemi-spherical) to blast loading from high explosives. He presents data obtained from instrumented models. The models, composed of a cylindrical portion with a hemisphere attached to one end and a truncated cone with hemisphere attached to the other end, were instrumented with pressure transducers and strain gages. In addition some data on plastic response of uninstrumented shells is presented[36]. A comparison of the deformations of the cylindrical portions with those predicted by the author[41] shows that the actual deformations were higher. This was to be expected as there were no bulkheads at the ends of the cylindrical portion and therefore the ends could not be considered clamped.

Sevin[43] studied the details of blast loadings on a series of five horizontal cylindrical shells that were instrumented with pressure transducers and strain gages. These shells were exposed to the blast from a nuclear explosion. All deformations were elastic. The pressure-time histories were erratic giving random results. No quantative strain results were presented because of their interpretation difficulties.

Dewey[50] has studied the loading on various geometric shapes (sphere, cube, cylinder) by the use of pressure transducers mounted in rigid models. Some data are given for the cylinder, but Dewey is not satisfied with the available transducers and has suspended further testing.

This survey shows clearly the lack of extensive and systematic data for the plastic response of finite shells to blast loading.

In addition to the sparsity of experimental data relevent to the problem of the report, there are only the analyses of Greenspon that have considered the response of a three-dimensional cylinder to impulsive loading. These are the only analyses that are directly applicable to this study.

1.6 Definition of Structural Scaling

As in many other branches of science, tests of suitably scaled models can be substituted for full-scale experiments, and the response of the full-scale structures inferred from a knowledge of the model laws. Such scaling has been applied by several investigators to the problem of small deflection elastic response of structures to dynamic loads. We wish to predict the plastic response of large structures to transient forces. A report by Baker, Ewing and Hanna[6] reviewed the model laws for blast loading from explosive charges and for the small-deflection elastic response of structures to such loading, discussed such laws for large-deflection elastic response and for plastic response, and presented the results of experiments conducted to confirm the modeling. They concluded that the entire elastic-plastic response of a structure to blast loading should scale geometrically, as described below.

The same geometrical scaling which governs the shock transmission process (See 1.2 Definition of Blast Parameters) also provides the proper modeling for structural response to the transient pressures generated during the blast process. The effect of gravity and strain-rate are assumed negligible. Perhaps the "geometrical" modeling can be best described by imagining the following experiment. An energy source of characteristic dimension, d, is initiated a distance, R, from an elastic structure of characteristic dimension, L, which produces a transient pressure loading on the structure of amplitude, p, and duration, ΔT, and causes the structure to respond in its natural modes of vibration with periods τ_1, τ_2, --- τ_n, --- and corresponding displacement amplitudes X_1, X_2, --- X_n, ---. Strain-time histories of the structure's response are characterized by the periods τ_n and corresponding strain amplitudes e_n. Let the entire experiment be scaled geometrically by a scale factor, K, making the energy source of characteristic dimension, Kd, and locating the structure of characteristic dimension, KL, at a distance, KR, from the source. Then, geometrical modeling predicts that the pressure loading on the structure will be similar in form to that obtained in the first experiment, with amplitude, p, and duration, $K\Delta T$; and that the structural response will also be similar in character, with the natural periods being $K\tau_1$, $K\tau_2$, ---$K\tau_n$, ---, displacement amplitudes KX_1, KX_2, --- KX_n, ---, and strain amplitudes e_1, e_2, -- e_n, ---. The blast scaling is shown graphically in Figure 1.1 and the corresponding response in Figure 1.3.

2. PROCEDURE USED IN THE INVESTIGATION

2.1 Test Specimens and Equipment

Test Specimens. The thin-walled cylindrical shells were fabricated from steel sheet and aluminum foil, sheet, and tubing. The steel shells were cold formed from 1040 hot-rolled steel and were butt-welded along a longitudinal seam. The properties of this material were determined by tensile tests and are listed in Table 2.1. The aluminum shells

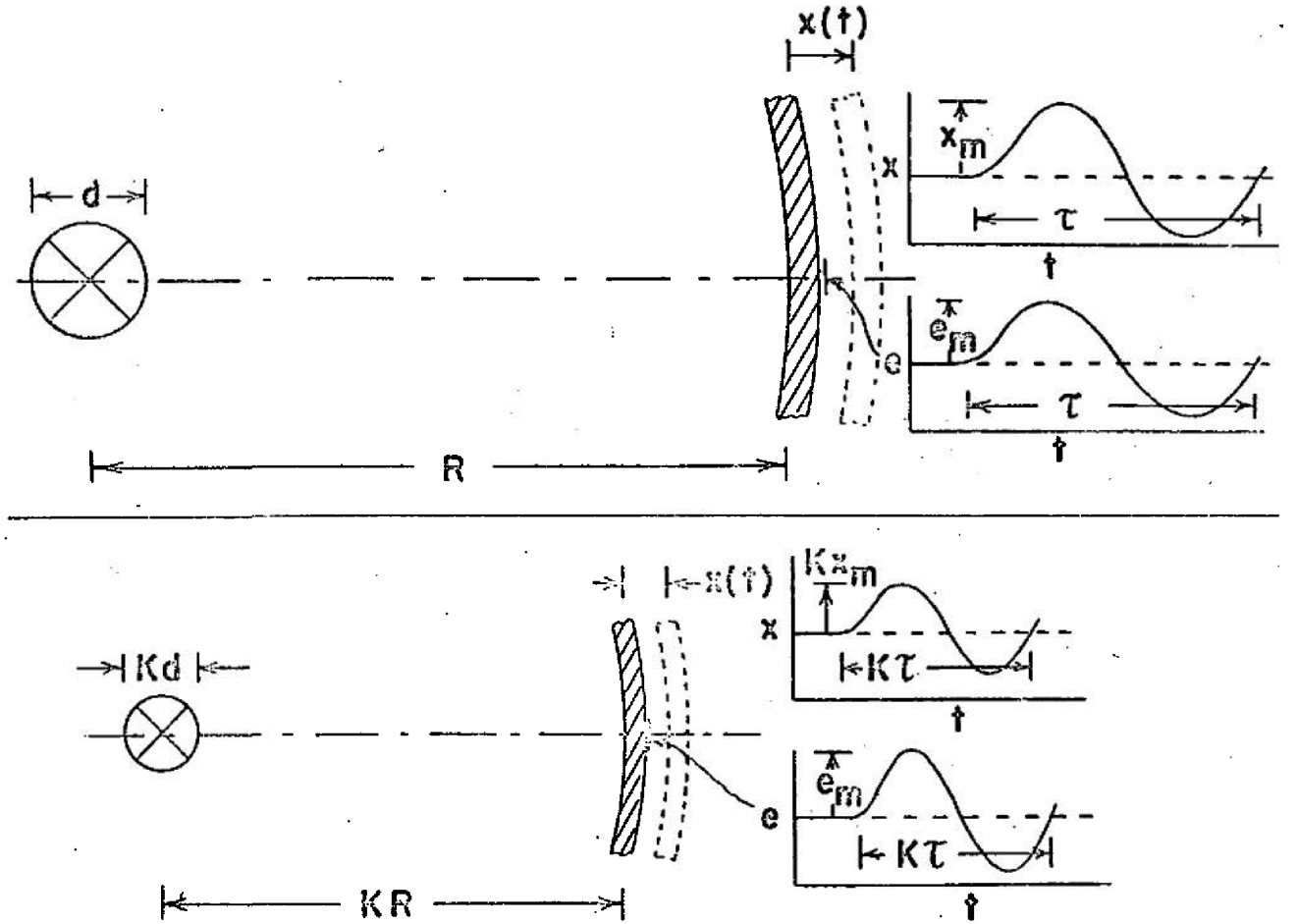

Fig. 1.3 Structural Response Scaling

TABLE 2.1

Shell Material Properties

Material	Modulus of Elasticity E(psi)	Yield Stress S_o (psi)	Ultimate Stress S_u (psi)
Steel Sheet[1] - 1040	29.0×10^6	34,500	45,400
Aluminum Foil[2]- 5052-H38	10.2×10^6	37,000	42,000
1100-0	10.0×10^6	5,000	13,000
Aluminum Tubing[2]- 6061-T6	10.0×10^6	40,000	45,000

---

[1] Obtained from Tensile Tests

[2] Taken from Alcoa Aluminum Handbook, Aluminum Company of America, 1957

were either sections of 6061-T6 seamless drawn tubing or formed from 1100-O or 5052-H38 foil. The foil shells were fastened along a longitudinal seam by solder, a crimped seam, or by cloth-backed adhesive tape. The material properties for the various aluminum alloys were taken from the Alcoa Aluminum Handbook and are also listed in Table 2.1.

The shell dimensions were chosen so that they were scaled models of a variety of actual missiles structure. A scale factor was chosen so that the shell sizes would be convient for handling in the field. A number of the shells were scale models of other shells in the series to validate the structural response scaling. The dimensions of the shells tested are presented in Table 2.2. The shell diameters varied from 3 to 24 inches, the lengths from 1 to 75 inches, and the thicknesses from 0.003 to 0.136 inches. These dimensions provided shells that had length-to-diameter ratios of 0.3 to 25 and diameter-to-thickness ratios of 60 to 2,000.

A few representative shells were instrumented to measure details of response. Baldwin-Lima-Hamilton FAB-25-35, 350-ohm foil strain gages were applied to the inside walls of the shells in a number of locations to indicate both longitudinal and circumferential strains. The strain gage pattern is shown in Figure 2.1.

The shells were fastened to heavy end caps and this assembly was then fastened over a rigid tube. This tube prevented rotation of the end caps about an axis perpendicular to the longitudinal axis of the shell and therefore minimized bending in the shell. The tube also prevented any axial load by restricting motion of the end caps in the axial direction. A schematic of the shell and support tube assembly is shown in Figure 2.2.

Explosives. The blast loading was provided by detonation charges of high explosive ranging in weight from 1 pound to 500 tons. The smaller charges (up to 64 pounds) were cast spheres of Pentolite. The

TABLE 2.2

Shell Dimensions

Shell No.	Diameter D (in.)	Length L (in.)	Thickness t (in.)	L/D	D/t	Material
1-2	3.0	6.0	0.019	2.0	158	1040
3-7	3.0	8.62	0.019	2.87	158	Steel Sheet
8-16	3.0	9.0	0.019	3.0	158	"
17-18	3.0	11.62	0.019	3.87	158	"
19-20	3.0	14.62	0.019	4.87	158	"
21-23	3.0	18.0	0.019	6.0	158	"
24-25	3.0	24.0	0.019	8.0	158	"
26-27	3.0	8.62	0.035	2.87	86	"
28-31	3.0	9.0	0.035	3.0	86	"
32	3.0	18.0	0.035	6.0	86	"
33-38	6.0	18.0	0.019	3.0	316	"
39-40	6.0	17.5	0.035	2.91	172	"
41-44	6.0	18.0	0.035	3.0	172	"
45-46	6.0	17.5	0.076	2.91	79	"
47	6.0	18.0	0.076	3.0	79	"
48	12.0	36.0	0.035	3.0	343	"
49-51	12.0	35.38	0.076	2.94	158	"
52	12.0	35.38	0.136	2.94	88	"
53	24.0	48.0	0.035	2.0	686	"
54	24.0	48.0	0.076	2.0	316	"
55-58	24.0	47.25	0.136	1.98	176	"
59	3.0	6.0	0.003	2.0	1,000	5052-H38
60-67	3.0	9.0	0.003	3.0	1,000	Aluminum Foil
68	3.0	15.0	0.003	5.0	1,000	"
69-71	3.0	6.0	0.004	2.0	750	"
72-73	3.0	9.0	0.004	3.0	750	"
74	3.0	3.0	0.006	1.0	500	"
75	3.0	6.0	0.006	2.0	500	"
76-84	3.0	9.0	0.006	3.0	500	"
85	3.0	15.0	0.006	5.0	500	"
86	3.0	23.0	0.006	7.67	500	"
87	3.0	24.0	0.006	8.0	500	"
88	3.0	30.0	0.006	10.0	500	"
89-91	3.0	6.0	0.008	2.0	375	"
92-94	3.0	9.0	0.008	3.0	375	"
95-96	3.0	9.0	0.010	3.0	300	"
97-104	3.0	9.0	0.012	3.0	250	"
105-111	3.0	9.0	0.024	3.0	125	"
112-120	6.0	18.0	0.003	3.0	2,000	"
121-122	6.0	18.0	0.004	3.0	1,500	"
123-128	6.0	18.0	0.006	3.0	1,000	"

TABLE 2.2 (Cont'd.)

Shell No.	Diameter D (in.)	Length L (in.)	Thickness t (in.)	L/D	D/t	Material
129-130	6.0	18.0	0.012	3.0	500	5052-H38
131	6.0	18.0	0.024	3.0	250	Aluminum Foil
132-134	12.0	36.0	0.008	3.0	1,500	"
135	3.0	1.0	0.022	0.33	136	6061-T6
136	3.0	2.0	0.022	0.67	136	Aluminum Tubing
137	3.0	3.0	0.022	1.0	136	"
138	3.0	6.0	0.022	2.0	136	"
139-145	3.0	9.0	0.022	3.0	136	"
146	3.0	30.0	0.022	10.0	136	"
147	3.0	36.0	0.022	12.0	136	"
148	3.0	40.0	0.022	13.3	136	"
149	3.0	48.0	0.022	16.0	136	"
150	3.0	54.0	0.022	18.0	136	"
151	3.0	60.0	0.022	20.0	136	"
152	3.0	75.0	0.022	25.0	136	"
153-157	3.0	9.0	0.042	3.0	71	"
158-165	6.0	18.0	0.042	3.0	143	"
166	6.0	18.0	0.083	3.0	72	"
167	7.5	7.5	0.063	1.0	119	"
168	7.5	7.5	0.125	1.0	60	"
169	9.0	27.0	0.065	3.0	138	"
170	3.0	2.0	0.006	0.67	500	1100-0
171	3.0	3.0	0.006	1.0	500	Aluminum Foil
172	3.0	5.0	0.006	1.67	500	"
173	3.0	6.0	0.006	2.0	500	"
174-181	3.0	9.0	0.006	3.0	500	"
182	3.0	12.0	0.006	4.0	500	"
183-184	3.0	15.0	0.006	5.0	500	"
185	3.0	23.0	0.006	7.67	500	"
186-188	3.0	9.0	0.010	3.0	300	"
189-190	3.0	2.0	0.012	0.67	250	"
191-193	3.0	3.0	0.012	1.0	250	"
194-197	3.0	9.0	0.012	3.0	250	"
198	6.0	9.0	0.006	1.5	1,000	"
199	6.0	11.0	0.006	1.83	1,000	"
200	6.0	4.0	0.012	0.67	500	"
201	6.0	6.0	0.012	1.0	500	"
202	6.0	9.0	0.012	1.5	500	"
203-204	6.0	11.0	0.012	1.83	500	"

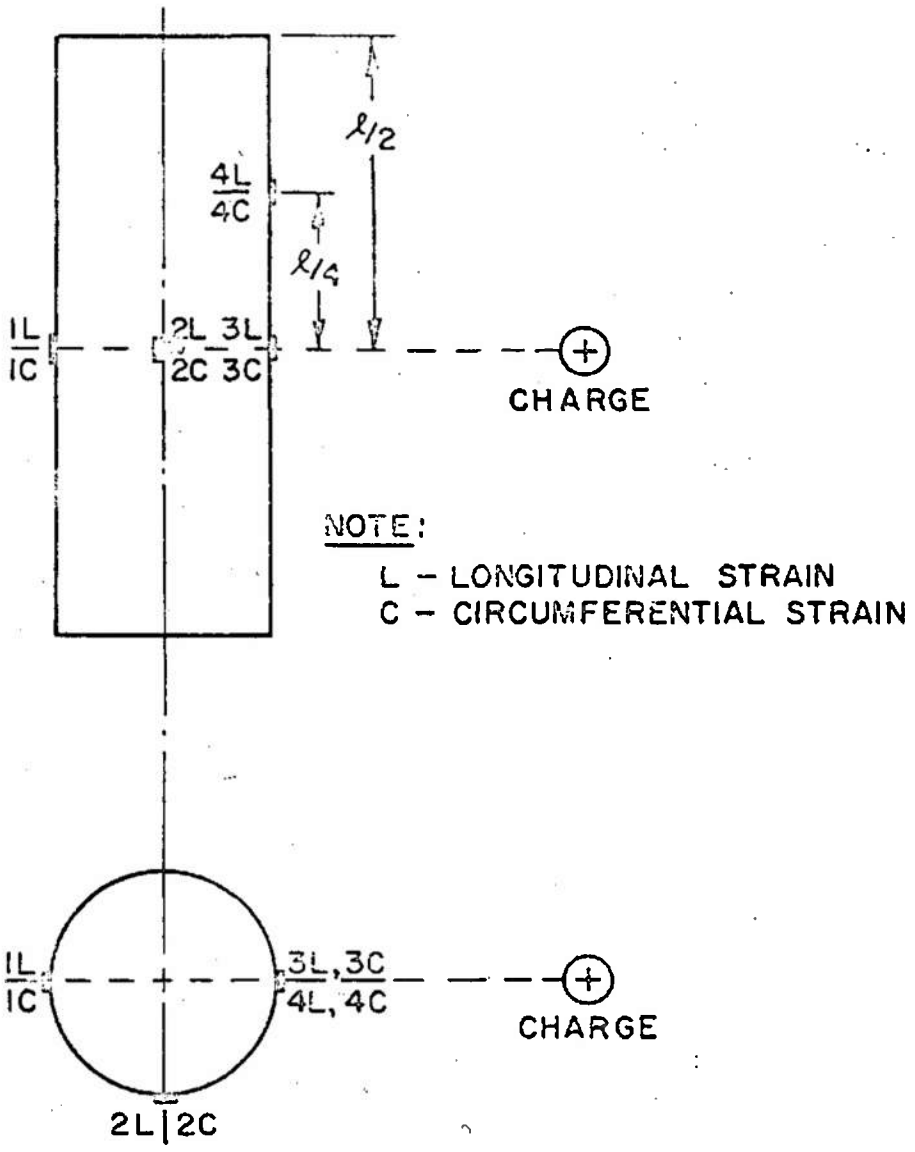

Fig. 2.1 Strain Gage Pattern

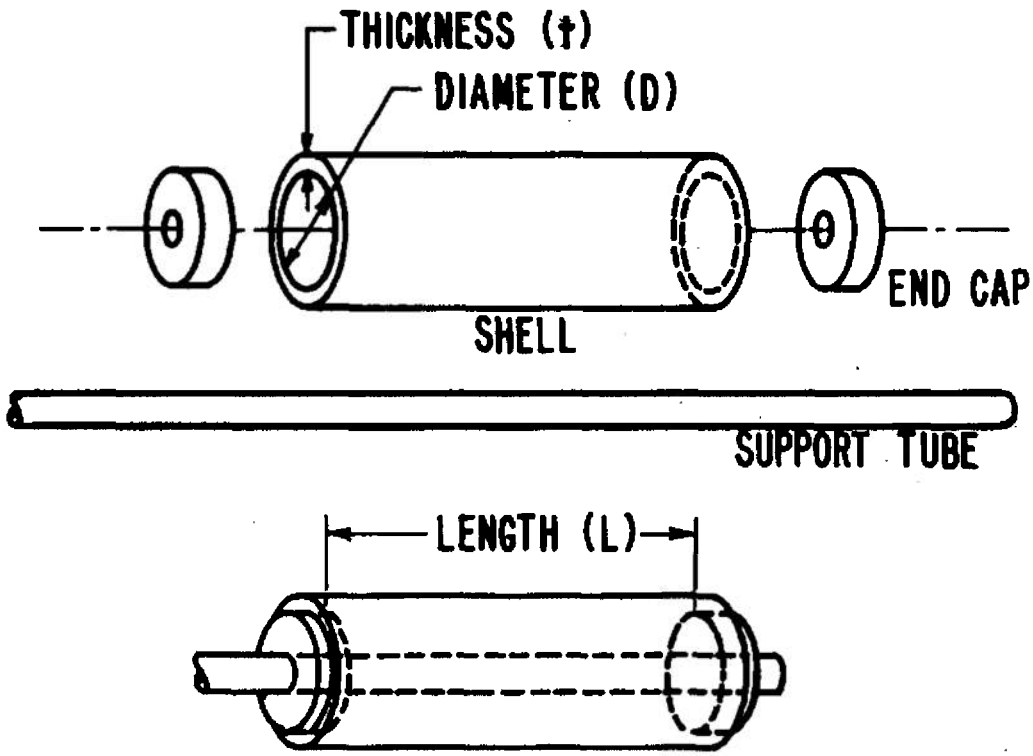

FIGURE 2.2 TYPICAL SHELL SPECIMEN

larger charges were composed of cast blocks of Trinitrotoluene (TNT). The blast parameters for equal weights of these two different explosives are approximately equal and the explosives can be considered interchangable.

For field work 1-pound and 8-pound charges are the most practical to use. They are normally cast as spheres and therefore produce uniform, reproducable spherical shock waves. These charge weights are easy to handle in the field.

Larger charge weights are required to simulate the very long durations obtained from nuclear detonations. The overpressure of the shock wave is independent of the charge weight but the duration varies directly as the cube root of the charge weight. (See Figure 1.2) However, the larger charges can be placed near the ground so that the shock wave will be reflected and effect on the shells will be the same as if approximately twice the charge weight had been detonated.

Instrumentation. Instrumentation was chosen to record three types of information; magnitudes of the blast parameters, response-time history of the shell and final shell deformation patterns. Piezoelectric and self-recording gages provide pressure-time histories from which the other blast parameters can be determined. Strain gages with appropiate recording equipment provide response-time history of the shells. High-speed motion picture cameras supplement these data by providing a visual response-time history. Still cameras provide a visual record of the final shell deformation patterns. This instrumentation is shown in Figures A.3 to A.9, Appendix A.

The piezoelectric gage is used for recording the incident pressure-time history associated with blast waves. A blast gage array is shown in Figures A.4 and A.5. The two gages are staggered so that the shock arrives at each at a different time. This gives a measure of the shock velocity and thus another check on the effective charge weight. The sensitive element of the gage is a stack of four wafer-shaped crystals

(made of tourmaline or a synthetic piezoelectric material), approximately .050 inches thick, with silver foil electrodes between crystals to collect the charge. The crystals are usually one inch or one-half inch in diameter.

A group of self-recording gages, used to record pressure-time histories of the shock wave, were buried flush with the ground and at predetermined distances from the explosive charge. These gages were designed by Ballistic Research Laboratories[23] to record relatively long duration shock waves from large scale detonations. Figures A.6 and A.7 show a gage with and without its cylindrical housing. The gage utilizes a corrugated metal capsule as its pressure sensing element. Attached to a center post on the capsule is a leaf-spring arm with an osmium tipped stylus. The stylus rests on an aluminum glass disc which is attached to a turntable. During operation the shock wave fills the corrugated capsule and, in turn, deflects the stylus. The glass disc, rotating at a fixed rate, records the pressure deflection as a function of time. The record is then photographically reproduced and the data obtained. Because of the mechanical design, the gage has a frequency response of only 0 to approximately 100 cps.

The pressure recording equipment is shown in Figure A.8. This is a 16-channel unit with 8 dual-beam cathode-ray oscilloscopes. The oscilloscopes are photographed by a streak camera. The equipment, built by the Consolidated Electrodynamics Corporation has a maximum writing speed of 400 in. per second and a frequency response of 0 to 100 kilocycles (kc.).

The strain recording equipment is shown in Figure A.9. The unit on the right is a Consolidated Electrodynamics Corporation 50-channel oscillograph recorder with galvonometers. The recorder has a writing speed of 0.10 in. per second to 100 in. per second with a frequency response of 0 to 200 cps. for the galvonometers.

The cameras used were 16-mm high speed (400-2,500 frames/second) 100-feet capacity cameras from Red Lake Laboratories. A typical field arrangement is shown in Figures A.3.

2.2 Experimental Procedure

Portions of this test were conducted at three different areas: the Spesutie Island Ranges of the Ballistic Research Laboratories; the Yuma Test Station, Yuma, Arizona; and the Suffield Experimental Station, Ralston, Alberta, Canada.

The general procedure for each of the areas was similar. The shell and support tube assemblies were mounted on stands at a height of six feet to minimize ground effects. They were oriented with respect to the charge so that the blast impinged on the shells either along a line perpendicular to the longitudinal axis (lateral loading) or along an extension of the longitudinal axis (longitudinal loading). A nose cone was added to the shell for the longitudinal loading orientation to minimize the disturbance of the flow. This is shown schematically in Figure 2.3. The specific procedures at each of the three areas will be given in the next three sections.

Ballistic Research Laboratories. Tests were conducted with both uninstrumented and instrumented shells at the Ballistic Research Laboratories. The charge weights varied from 1 pound to 500 lbs. The smaller charges were supported above the ground (as shown in Appendix A, Figure A.1) to avoid ground reflection, while the larger charges were stacked on small frangible tables over a thick plate of armour steel to provide maximum reflection and minimum cratering.

A small group of shells were then positioned about the explosive charge at various distances such that the blast parameter values would be below those required to cause failure. The shells were then repositioned in increments until failure (defined as permanent radial deformation of approximately 5 percent to 10 percent of the original diameter) was obtained.

In the case of the shells instrumented to record response-time histories, a single shell was positioned and firings repeated until acceptable records were obtained.

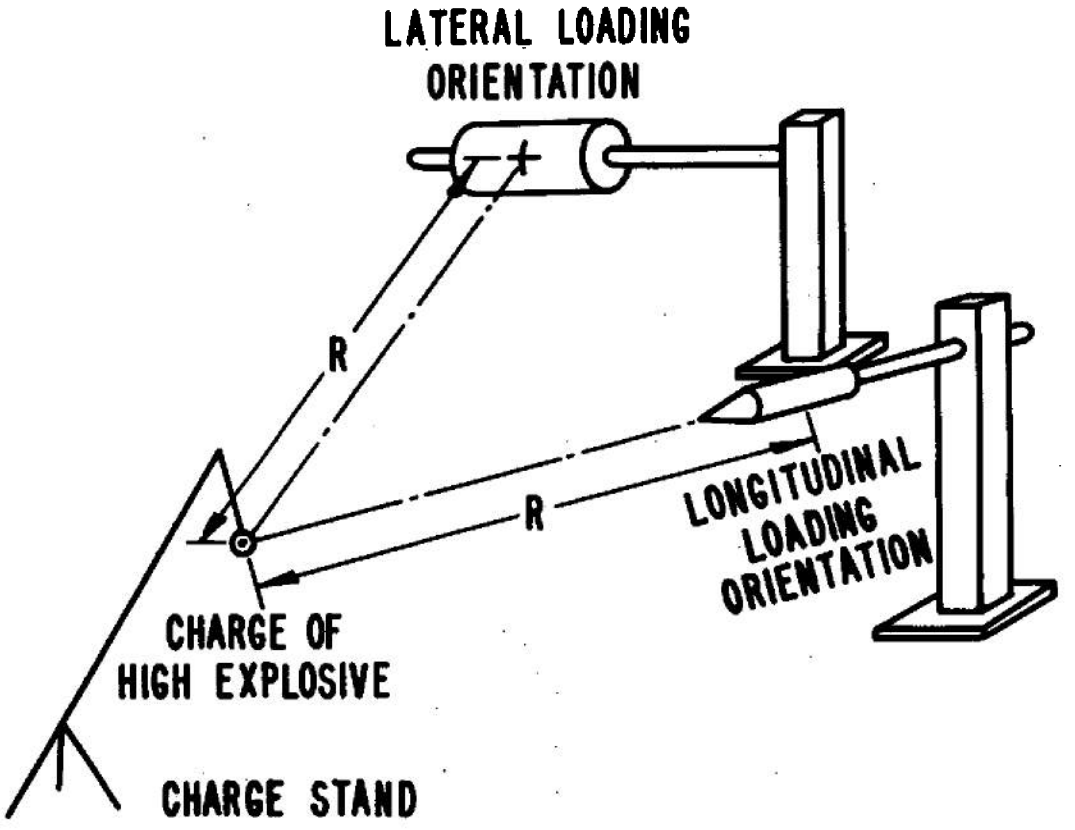

FIGURE 2.3 TYPICAL FIELD ARRANGEMENT

Yuma Proving Ground. Tests were conducted with uninstrumented shells only at the Yuma Proving Ground. The weights of the charges were 1,000; 10,000 and 30,000 pounds. The charges consisted of hemispherical stacks of cast blocks of TNT on tables that ranged in height from six feet to thirteen feet. No armour steel was available, but the desert floor had proven a very effective reflector in the past.

A group of 24 shells were exposed on nine of the ten firings of Project Big Bird. For the early firings 3 each of 8 different shells were positioned at 3 different radii to bracket the failure region. For the later firings, as the data were processed and better estimates could be made, only 2 each of each shell were positioned and more different shells could be exposed. A typical field arrangement is shown in Appendix A, Figure A.2.

Suffield Experimental Station. Tests were conducted with both uninstrumented and instrumented shells at the Suffield Experimental Station during two different firing programs. The first test firing was conducted in 1960 with a charge weight of 20 tons. The second test firing was conducted in 1964 with a charge weight of 500 tons. The charges in each case were hemispherical stacks of cast TNT blocks placed on a stablizing platform in direct contact with the ground.

One shell, instrumented with strain gages, was exposed on the first firing. Three each of 11 different shells (33 total) were positioned on the second firing. Four of the shells were instrumented with strain gages and photographed by high speed motion cameras. (Appendix A, Figure A.3.)

Safety Requirements. Special precautions had to be taken to insure the safety of the operating personnel, the base personnel, and the inhabitants of the local communities. Safety required special handling of the explosives, laying of the firing lines and capping of explosives with a detonator by trained personnel.

In addition meteorological data were assessed to determine if focussing conditions existed. Certain changes in temperature and wind velocity with altitude can cause shock wave paths to bend and converge. Where these paths converge the pressure can be said to focus and the magnitude may be multiplied by one hundred. In such cases property damage including breakage of windows with attendant flying glass may occur. Numerous delays in firing programs were caused by such adverse weather conditions.

3. EXPERIMENTAL RESULTS

3.1 Uninstrumented Shells

The data for the laterally-loaded shells, having approximately failure deformation, have been plotted in Figures 3.1 through 3.4. The data for the four different materials were plotted separately. The limited data for the longitudually loaded shells have not been plotted. Values of the blast parameters were obtained for each case and are listed in Table B.1, Appendix B. The table includes both the laterally-loaded and longitudinally-loaded shells. For the smaller charges, where reflection was not a problem, the values of the blast parameter were taken from published data as listed in References 7 and 16. For the larger charges, the blast instrumentation was used to determine the reflection factor and then the values of the blast parameters were taken as above. The explosive weights listed in Table B.1 are effective weights, i.e., the reflection factor has been taken into account.

A total of 204 data points were obtained from the series of 316 firings on 299 shells.

Iso-damage curves were drawn through those points that represent the various combinations of incident pressure and incident impulse for an equivalent deformation of a specific shell geometry (See points 3 - 4 - 5 - 8 - 9 - 10 - 11 - 12 - 13, 33 - 34 - 35 - 36 - 37, etc., Figure 3.1). These curves form the boundaries between safe and failure regimes.

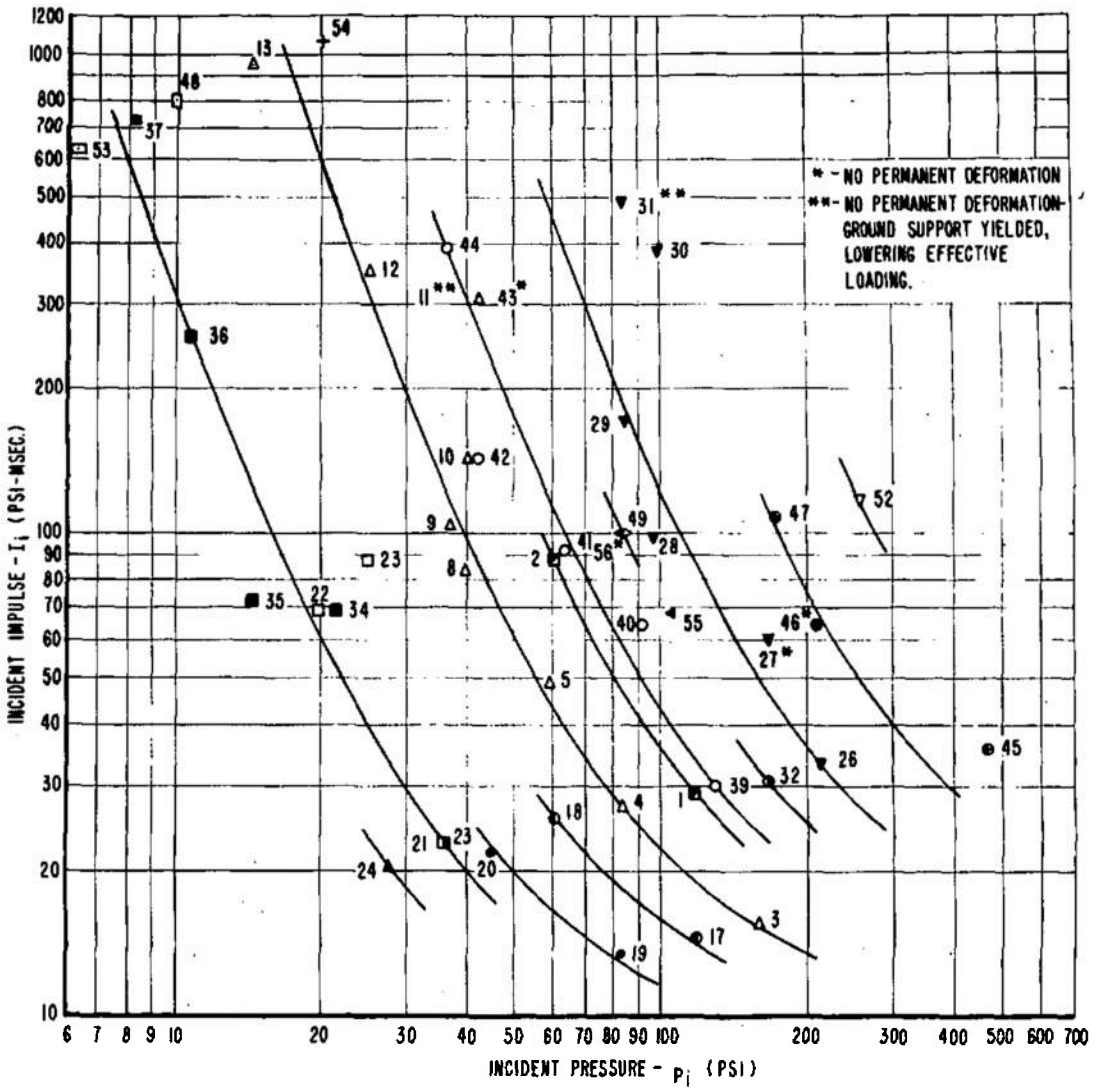

FIG. 3.1 - ISO DAMAGE CURVES FOR LATERALLY LOADED STEEL SHELLS

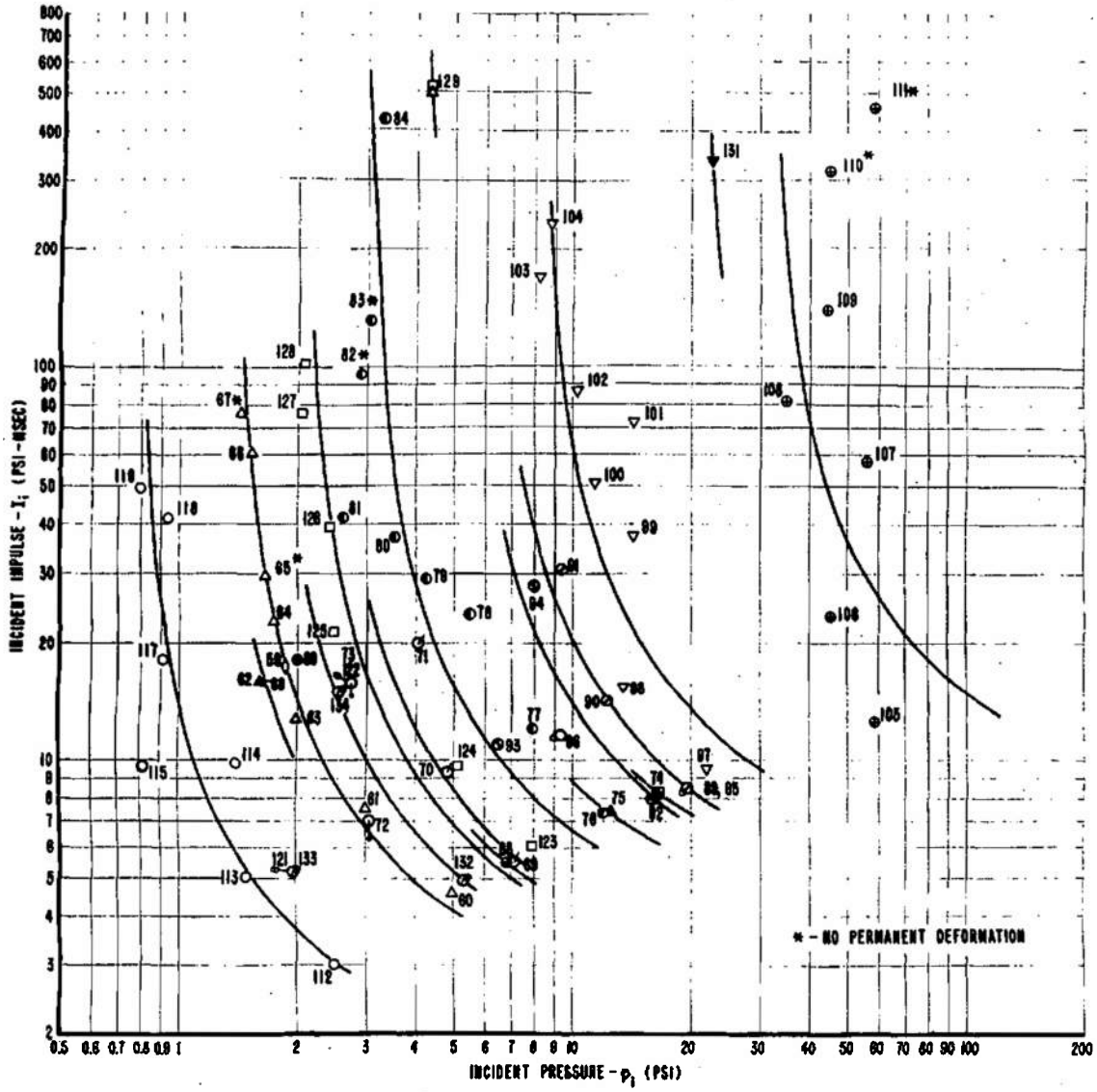

FIG. 3.2-ISO-DAMAGE CURVES FOR LATERALLY LOADED ALUMINUM (5052-H38) SHELLS

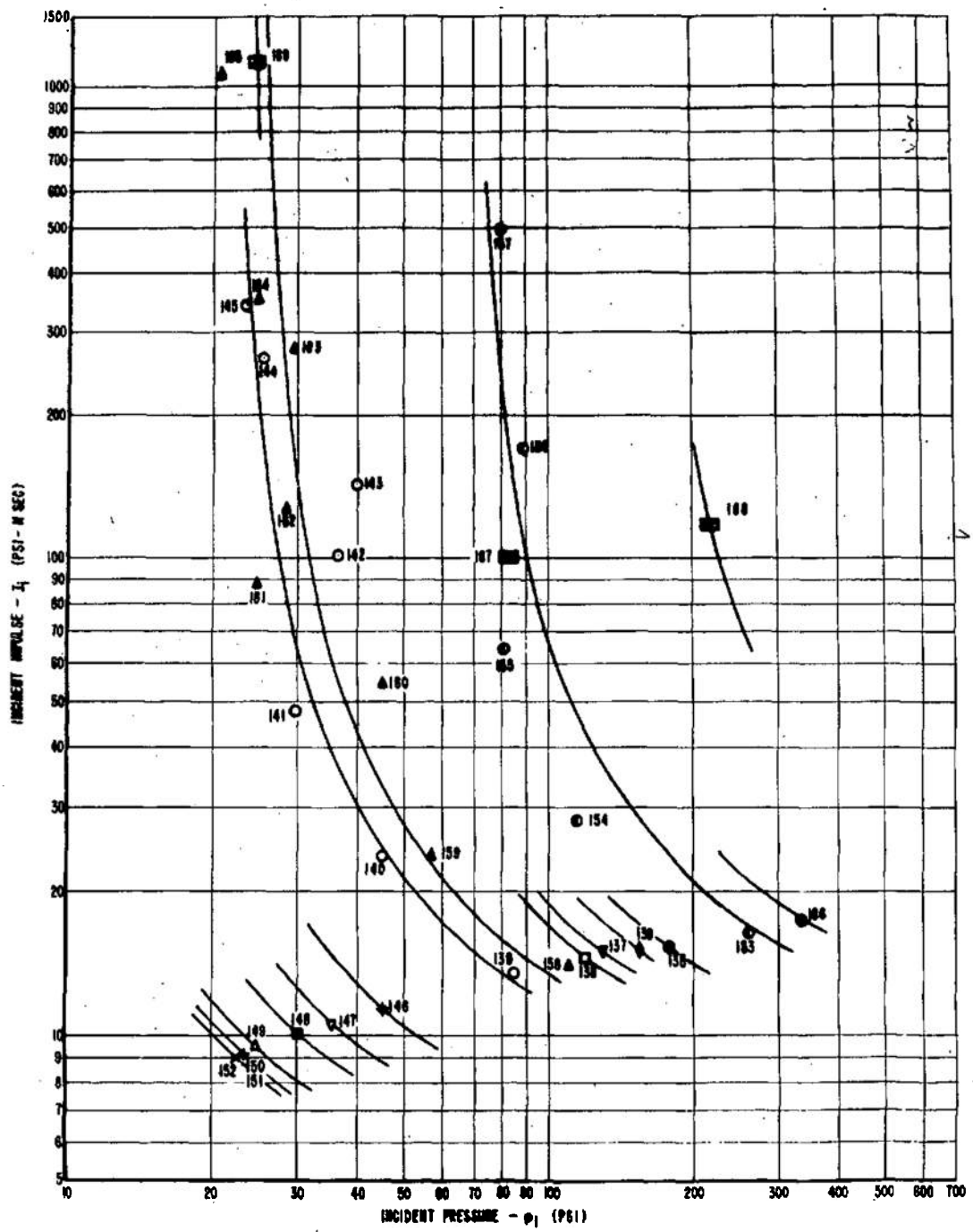

FIG. 3.3-I60 - DAMAGE CURVES FOR LATERALLY LOADED ALUMINUM (6061-T6) SHELLS

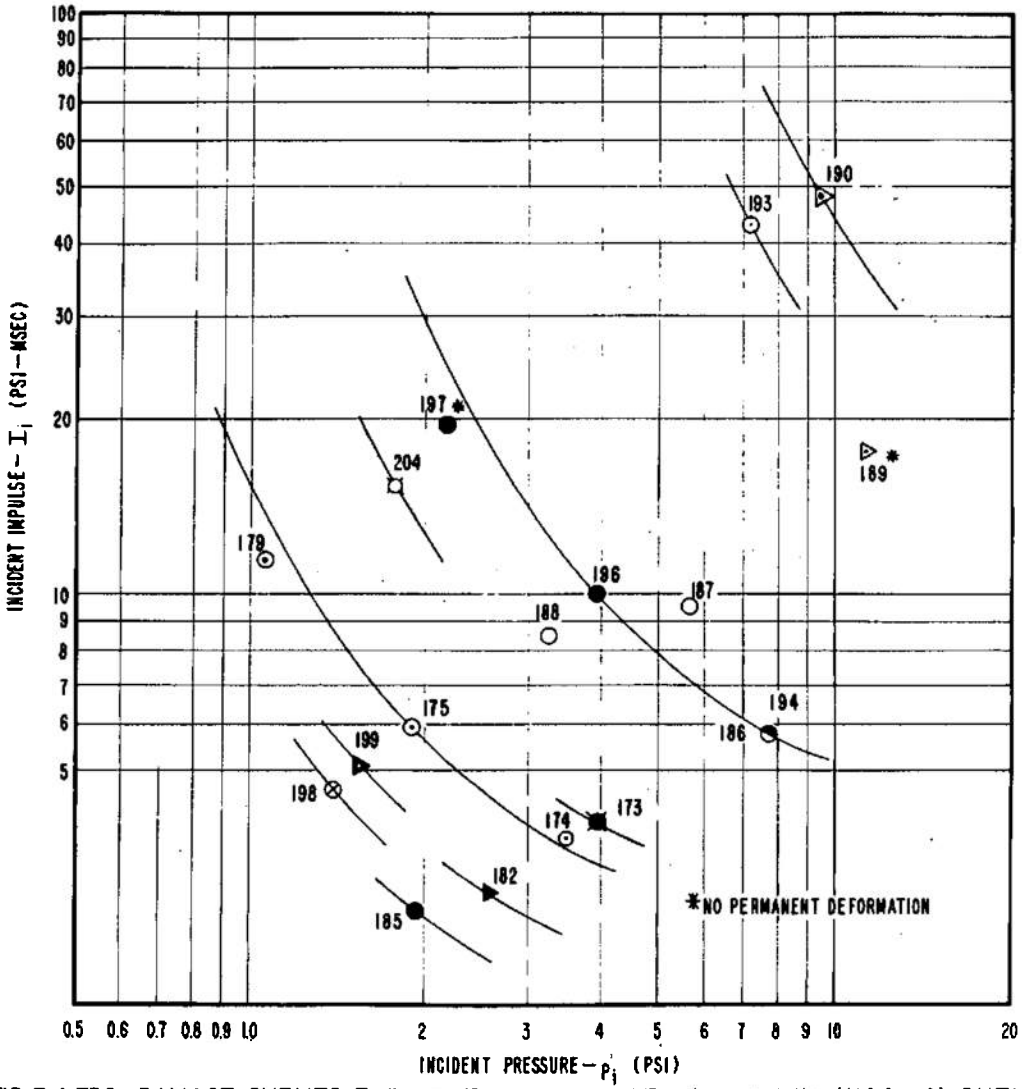

FIG. 3.4 ISO-DAMAGE CURVES FOR LATERALLY LOADED ALUMINUM (1100-O) SHELLS

The iso-damage curves represent a separate family of curves for each material. One curve shape was fitted to all the data for a particular material. From these curves the variation of required over-pressure values with respect to charge weight can be determined for a given shell material. As the explosive charge weight increases, moving from lower right to upper left along an iso-damage curve, the values of impulse increase; while the values of pressure decrease. For very large charges, the curves for the two tempered aluminums (5052-H38, Figure 3.2 and 6061-T6, Figure 3.3) approach asymptotically some minimum values of pressure. However, the mild steel and untempered aluminum (Figures 3.1 and 3.4) still show a considerable decrease in pressure for these same weights.

The variations of pressure and impulse with changes in shell length, diameter and thickness were also determined. A further discussion of these parameters will be deferred to Section 4, which deals with development of relations for the failure criterion.

As expected, the deformation patterns produced by the two different types of loading, (lateral or longitudinal) were quite different. There were two basic deformation patterns for the asymmetric lateral loading. The first pattern, which we call a collapse mode, is characterized by a single, transverse plastic hinge line. (See Figures C.1 to C.3, Appendix C.) If the loading conditions are made more severe, by decreasing the charge-shell distance, the hinge line lengthens. At slightly higher levels of loading, a small hinge will start on the back side, away from the charge.

A specialized case occurred where two parallel hinge lines formed, pushing the material between them in the outward radial direction. This is the only case where this happened and is shown in Figures C.4 and C.5, Appendix C.

The second lateral loading pattern, which we will call a buckling mode, is characterized by one or more longitudinal lobes. A single lobe is shown in Figure C.6, Appendix C, and multiple lobes are shown in Figures C.7 and C.8, Appendix C. The lobes vary in depth around the shell.

The two lateral loading patterns seem to be primarily a function of the shell geometry. The "thicker" shells with lower $D/_t$ values deform in a collapse mode while the "thinner" shells with higher $D/_t$ values are unstable and deform in a buckling mode. However a few shells fall on the borderline and can apparently go either way. One such shell is shown in Figure C.9, Appendix C. Here we see a combination of one hinge line and one lobe. These patterns will be discussed in more detail in Section 4.

In all the lateral loading cases the maximum deflection occurs approximately in the center of the shell at the point closest to the charge. However, there is deformation along the complete length of the finite shell as shown by the sharp creases where the shell meets the end caps. For the shells of sufficient length to be considered infinite this is not true and there is no deformation at the ends.

The deformation pattern for the longitudinal loading is axisymmetric. The maximum deflection does not occur at the mid-length of the shell but closer to the forward endcap as shown in Figures C.10 and C.11, Appendix C. A thin ring of high pressure propagates along the length of the shell. As it deforms the forward portion of the shell, the air inside is compressed toward the rear. This tends to further strengthen the aft portion, as shown in Figure C.11, Appendix C, where the high pressure of the compressed air has torn the aft portion of shell loose from the end cap and increased the diameter, while the forward portion has been torn loose and decreased in diameter. The longitudinal loading orientation is the stronger of the two. The values of blast parameters required to satisfy the failure criterion will be established in the next section.

One shell was tested statically to compare its deformation pattern with those tested dynamically. This shell and support tube assembly was mounted on V-blocks in a testing machine. A line load was applied perpendicular to the center-line of the shell at the center with a 1/4 x 4-inch striker plate. The deformation pattern shown in Figure C.12, Appendix C, is very similar to the dynamic collapse mode. The shell

commenced to deform at a 3-lb. load and the load had to be increased continuously to increase the deformation. The load was increased to a maximum value of 10-lb. and then removed. This requirement that the load must be increased in order to increase the deformation agrees with the dynamic loading results. A more complete collection of deformation pattern pictures is given in References 40 and 41.

3.2 Instrumented Shells

Some difficulty was experienced in obtaining sufficient output from the original 120-ohm strain gages. The records obtained from the first Suffield Experimental Station firing were not read because of the combination of low output and very low loading level. The low loading level was caused by improperly positioning the shell at too great a distance from the explosive charge.

The 350-ohm strain gages provided an adequate level of output and a series of tests were conducted at the Ballistic Research Laboratories to check the system. The results are shown in Table B.2, Appendix B. The reproducibility of the strain readings was quite good. Only peak values were read at this time.

The results from the second Suffield Experimental Station firing are given in Table B.3, Appendix B. (The shell numbers refer to Table 2.2.) The iso-damage curves were extrapolated incorrectly for this firing and the shells experienced slightly higher than anticipated deflections and the strain traces overlapped badly, with subsequent difficulty in following the traces. The recorder stopped momentarily (time length unknown) when struck by the blast so that the elapsed time was unknown; and because of this malfunctioning, time histories could not be ascertained.

4. DEVELOPMENT OF RELATIONS FOR THE FAILURE CIRTERION

4.1 Discussion of Experimental Data

An examination of the experimental data indicates that geometrical modeling laws apply for the large deformations discussed in Section 1. The scaling parameters are shown in Figure 4.1. The pressure will be the same on both shells if the charge with the scaled shell is increased in diameter by the scale factor K (weight increased by K^3), and the shell-charge distance is increased by the scale factor K. The scaled shell will have the same strain as the original shell if all dimensions are increased by the scale factor K.

For example, refer to Figure 3.1. Point 3 on Figure 3.1 and in Table B.1, Appendix B represents a shell of given geometry (3-in. diameter, 9.0-in. length, 0.019-in. thickness) laterally loaded by a charge weight of 1.1 lb at a distance of 2.5 ft. The deformation (in percent of original diameter and therefore equivalent to strain) should be the same for a shell-charge combination with a scale factor of 2. Consider shell 39 (6-in. diameter, 18.0-in. length, 0.35-in. thickness) exposed to a charge weight of 8.4 lb located at a distance of 5.8 ft. The dimensions of shell 39 are all approximately 2 times those of shell 3. The charge weight is approximately 8 times ($K^3 = 2^3 = 8$) the original charge weight. The incident pressures for the two shells (3 and 39) are 159 psi and 130 psi respectively, showing fairly good agreement. The results for these two shells and 11 other pairs are given in Table 4.1.

4.2 Development of Relations for the Failure Criterion

In Section 3 it was shown that the iso-damage curves formed a family for each material. The data for each material can then be represented by one curve with appropiate constants. In the preceeding section it was also shown that the scaling laws are applicable and, therefore, the results should lead to a method of extrapolation that would cover a wide spectrum of shell-charge weight configurations.

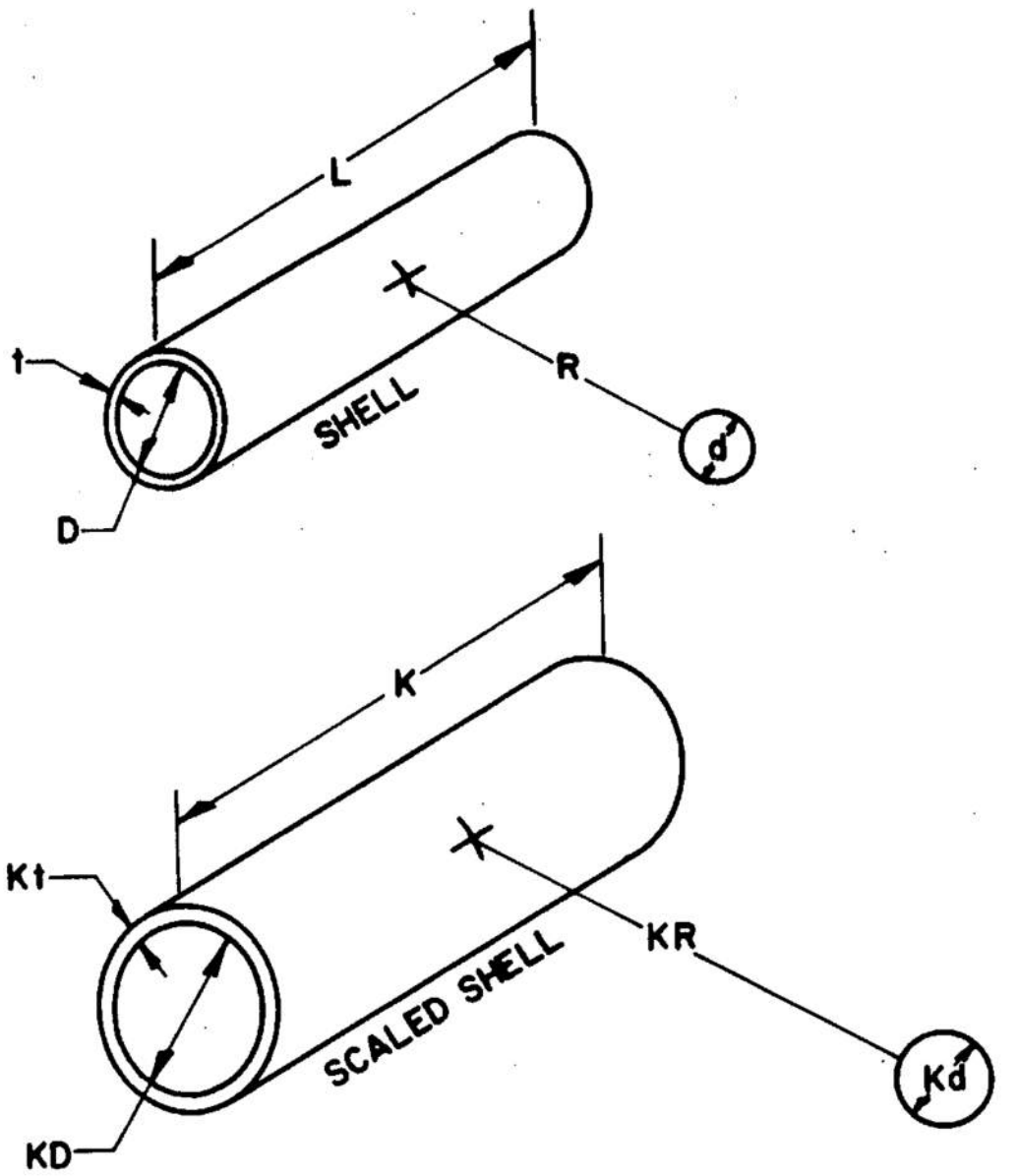

FIGURE 4.1 SHELL SCALING PARAMETERS

TABLE 4.1

Comparison of Scaled Shells

Shell No.	Material	Diameter D (in.)	Length L (in.)	Thickness t (in.)	Chg. Wt. $W^{1/3}$ $(lb)^{1/3}$	Pressure Incident p_i	Pressure Calculated p_{cr}
3	1040 Steel	3	9	0.019	1.02	159	160
39	"	6	18	0.035	2.03	130	113
4	"	3	9	0.019	2.03	82.4	83.3
40	"	6	18	0.035	4.0	91.3	74.6
5	"	3	9	0.019	4.0	58.0	55.3
41	"	6	18	0.035	7.3	63.6	55.6
10	"	3	9	0.019	13.0	40.2	33.7
43	"	6	18	0.035	28.4	41.5*	35.6
26	"	3	9	0.035	2.03	213	232
46	"	6	18	0.076	4.0	209*	276
27	"	3	9	0.035	4.0	166*	154
47	"	6	18	0.076	7.3	174	204
60	5052-H38 Aluminum	3	9	0.003	1.02	5.05	4.62
124	"	6	18	0.006	2.03	5.14	3.97
62	"	3	9	0.003	7.3	1.62	1.91
126	"	6	18	0.006	12.6	2.43	2.36
65	"	3	9	0.003	12.7	1.66*	1.73
127	"	6	18	0.006	27.5	2.05	2.17
139	6061-T6 Aluminum	3	9	0.022	1.02	85.2	88.0
159	"	6	18	0.042	2.03	57.5	58.8
141	"	3	9	0.022	4.9	29.6	34.3
161	"	6	18	0.042	9.5	25.0	31.2
143	"	3	9	0.022	13.0	40.2	27.6
163	"	6	18	0.042	28.4	29.5	28.7

* No permanent deformation

From a practical standpoint, it is more convenient to work with incident pressure and charge weight rather than incident pressure and incident impulse. Only two of these three quantites are independent. Therefore the relationships between pressure and charge weights, shell diameters, lengths, and thicknesses need to be determined. The effects of variations of incident pressure with charge weights was determined from the iso-damage curves as discussed in the last section.

The effects of variation of shell length-to-diameter (L/D) on the values of pressure has been found. The data for 6061-T6 aluminum shells with wide variations in length-to-diameter values have been plotted in Figure 4.2. Since the diameter was held constant, only length is indicated. The region around L = 50 in. has been enlarged and replotted on a linear scale in the upper right-hand corner to show that there is a smooth change, as the *minimum* pressure is reached, at a length of approximately 52 in. or an $L/D \approx 17$. For a value of $L/D > 17$ the pressure will remain essentially constant and the shell may be considered infinite in length. It is assumed that this value of $L/D \approx 17$ holds for all the materials studied.

In like manner, the effects of variations of diameter and thickness on the values of pressure were determined.

Using these relationships, a semi-graphical method was developed for determining the critical incident pressure required to cause failure of a cylindrical shell in the lateral loading orientation. The necessary curves are shown in Figures 4.3 to 4.6. The solid lines indicate the range of data and the dashed lines are extrapolations.

Figure 4.4 shows plots of the pressure ratio, F_W, vs. charge-weight, W. For a given shell configuration and material the pressure required for failure will decrease with an increase in charge weight. If the pressure required for a 1-pound charge is used as a standard, then

$$F_W = p_W / p_{W_o} \leq 1$$

where p_W is the pressure required at weight = W and p_{W_o} is the pressure required at weight = 1 lb.

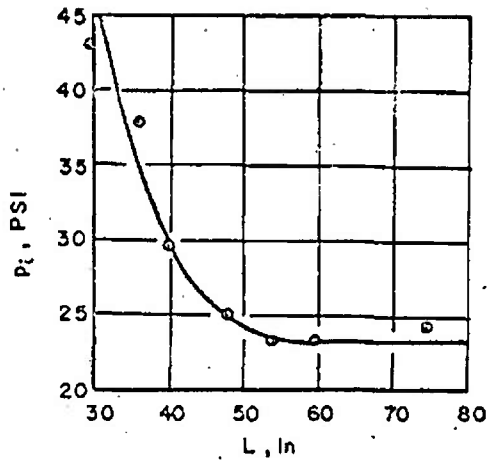

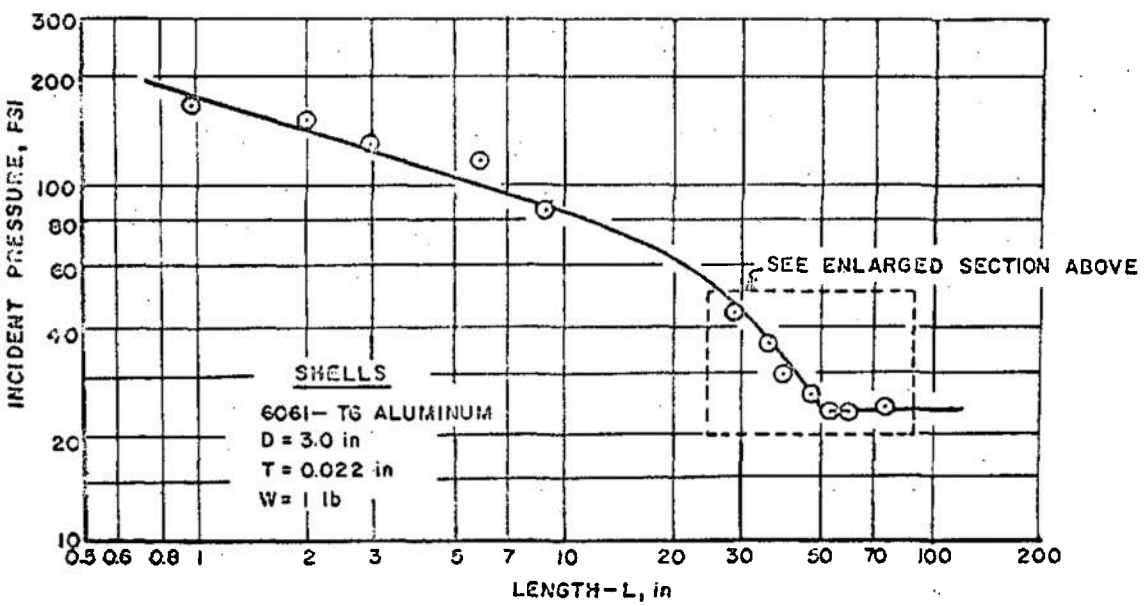

Fig. 1.2 Incident Pressure vs. Length

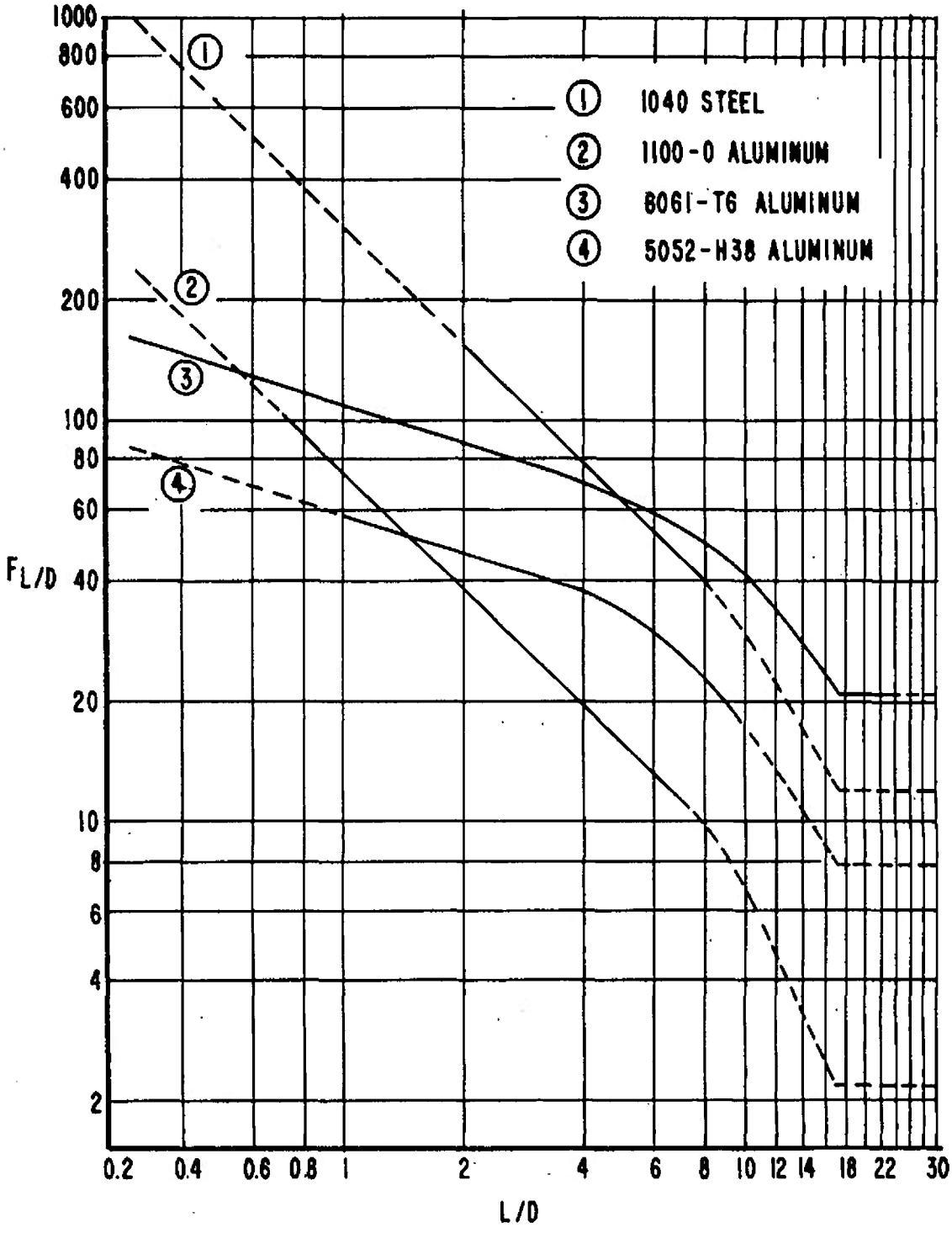

FIGURE 4.3 LENGTH-TO-DIAMETER RATIO FACTOR, $F_{L/D}$

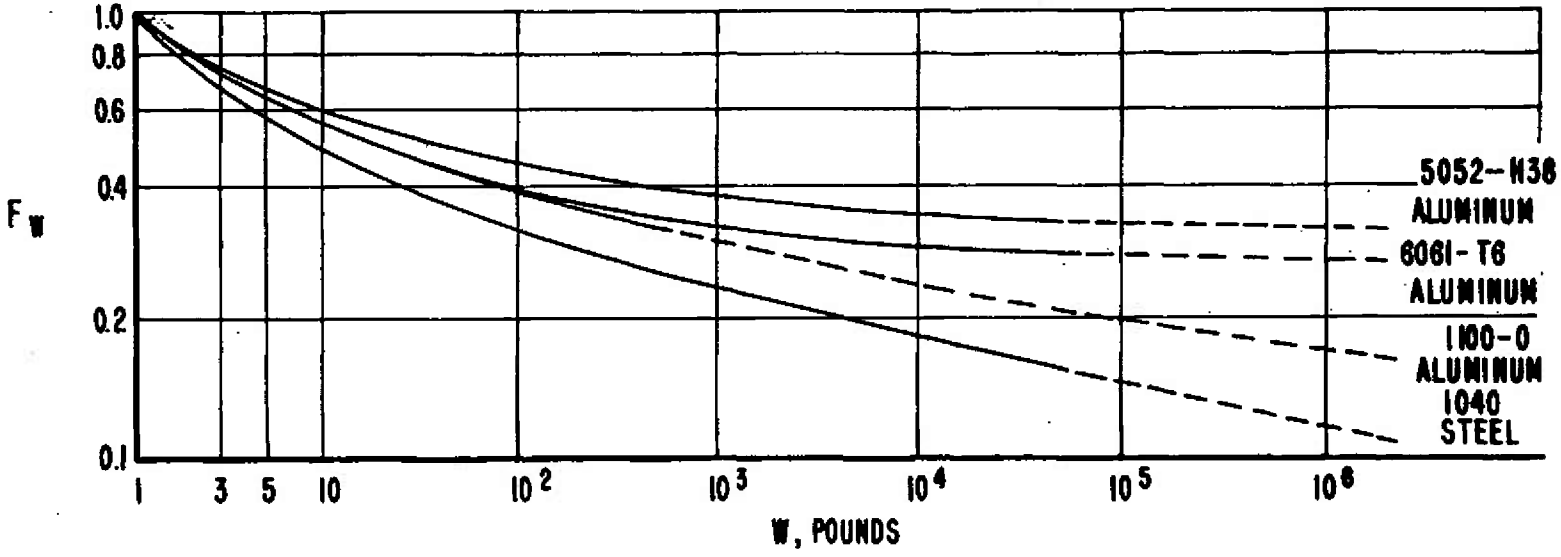

FIGURE 4.4 CHARGE WEIGHT FACTOR, F_W

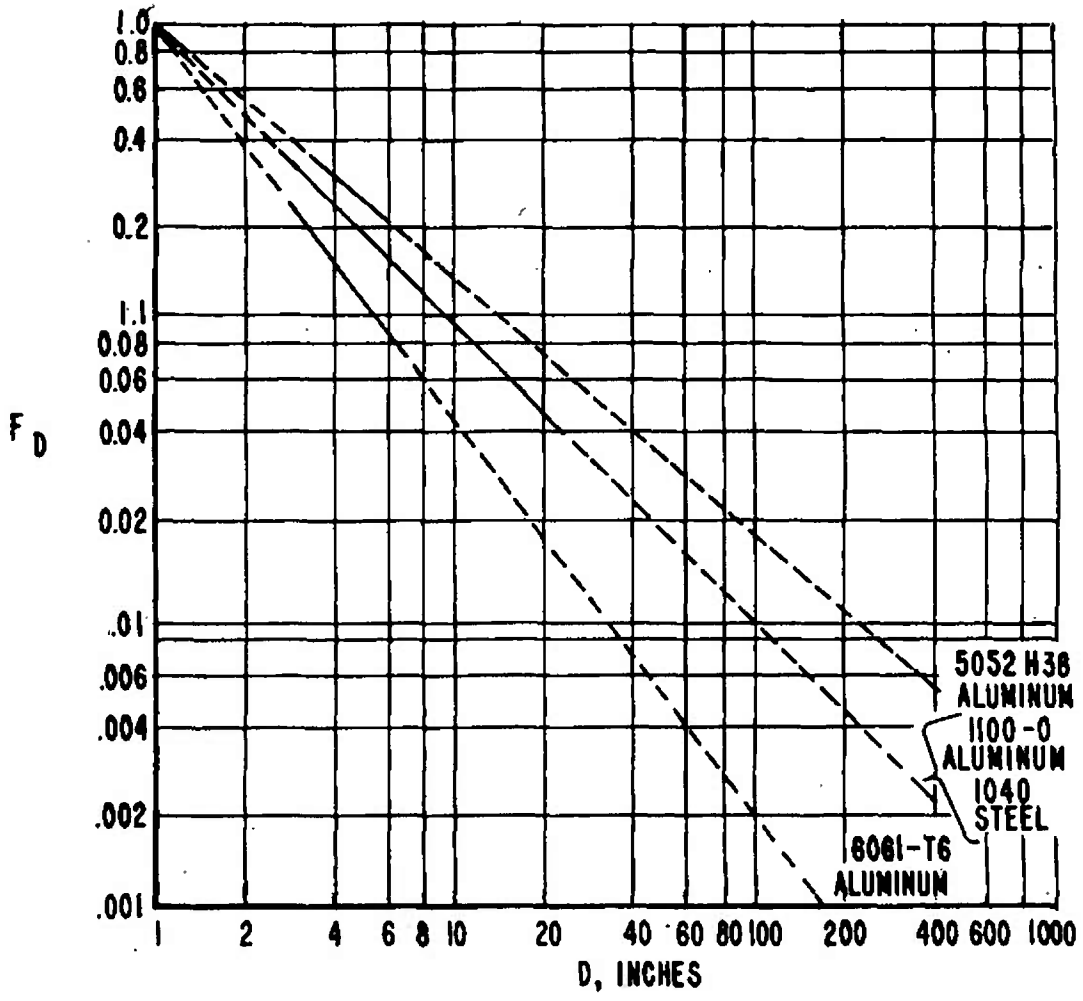

FIGURE 4.5 DIAMETER FACTOR, F_D

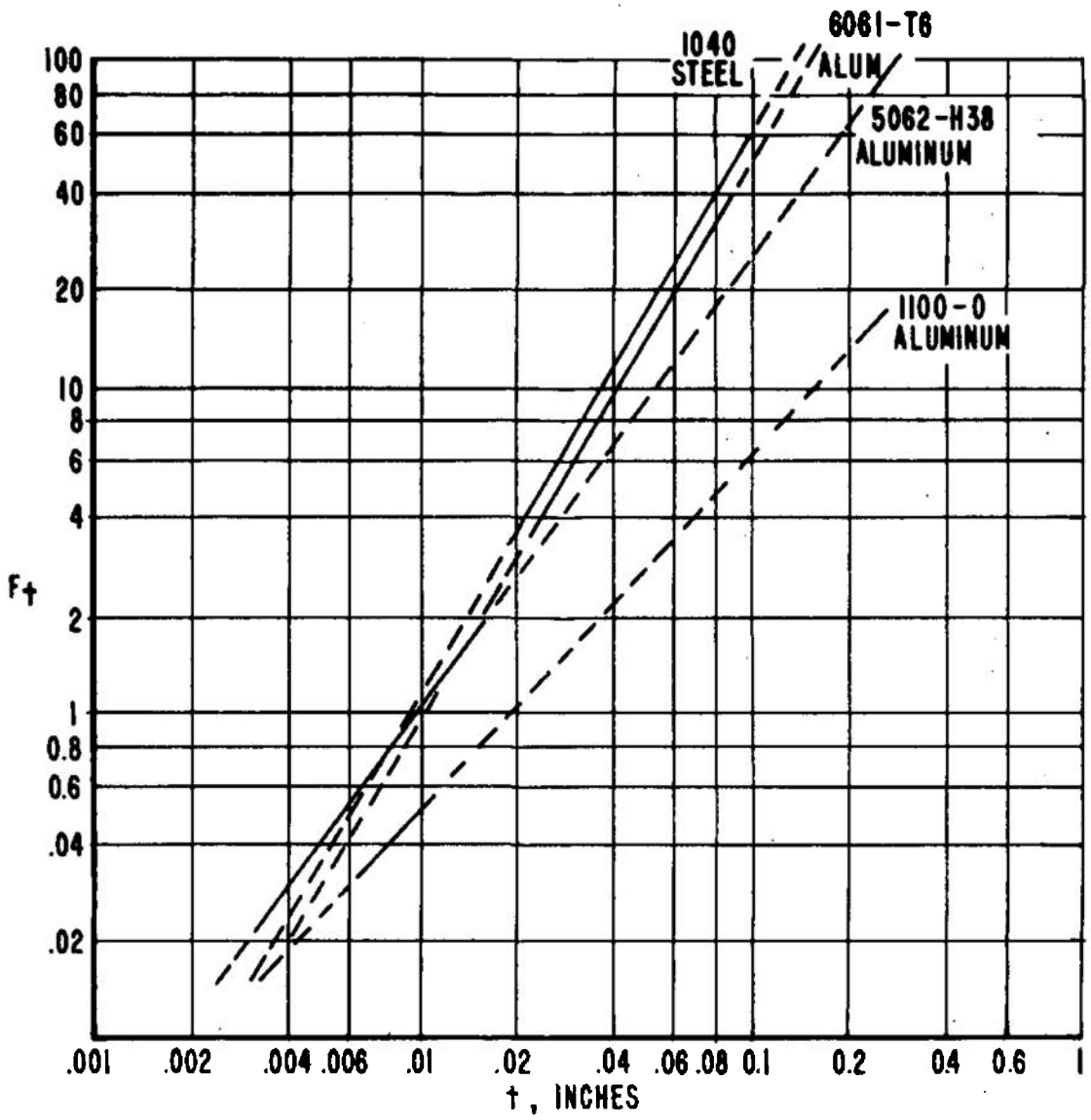

FIGURE 4.6 THICKNESS FACTOR F_t

The curves in Figures 4.5 and 4.6 are plots of the pressure ratios F_D and F_t vs. Diameter, D, the Thickness, t, respectively. In Figure 4.5 the standard diameter is 1 inch and

$$F_D = p_D/p_{D_o} \leq 1 \quad .$$

where p_D is the pressure required at diameter = D and p_{D_o} is the pressure required at diameter = 1 inch. The pressure required decreases as the diameter increases. In Figure 4.6 the standard thickness is 0.01 inch for 3 materials and 0.02 inch for the 1100-0 aluminum alloys and the values of F_t may be equal to, greater than, or less than one.

The curves in Figure 4.3 are plots of the pressure ratio, $F_{L/D}$, vs. length-to-diameter ratio, L/D, for standard values of charge weight, diameter and thickness, and a unit atmospheric pressure. These curves have the same shape as shown in Figure 4.2 but have been adjusted so that the product of these four factors ($F_{L/D}$, F_W, F_D, F_t) and the ambient pressure, p_o, will yield a critical pressure, p_{cr}, that best fits the data. If a different set of standard values had been chosen, the curves of Figure 4.3 would have been shifted appropriately. The standard value of thickness for the 1100-0 aluminum was purposely set at 0.02 inch in order to shift the $F_{L/D}$ curve to a more convenient position. The factors $F_{L/D}$, F_w, F_D, and F_t are dimensionless pressure ratios and p_o is the ambient pressure in psi so that

$$p_{cr} = p_o F_{L/D} F_w F_D F_t$$

for laterally loaded shells.

As an example, consider shell 112. It is 5052-H38 aluminum foil with the following dimension: L = 18.0 inches, D = 6.0 inches and t = 0.003 inch. The charge weight was 1.1 lbs. The ambient pressure was 14.7 psi. Then

$p_o = 14.7$, $F_{L/D} = 60$, $F_w = 0.98$, $F_D = 0.21$, $F_t = 0.20$

and

$$p_{cr} = p_o F_{L/D} F_w F_D F_t$$

$$= (14.7)(4.08)(0.98)(0.21)(0.20)$$

$$p_{cr} = 2.47 \text{ psi}$$

The actual pressure was $p_i = 2.50$ psi. Therefore the deviation of the calculated value from the actual value is -1.2 percent.

In the longitudinal orientation the shells require higher values of pressure for failure deformation. The data available indicate that the critical pressure may be determined by the following relationships:

$$\bar{p}_{cr} = p_{cr} \psi$$

where $\bar{p}_{cr}$ is the critical pressure for longitudinal loading, p_{cr} is the critical pressure for lateral loading, and ψ is the mulitplying factor ≈ 6.0 for steel, ≈ 2.0 for aluminum.

The curves in Figures 4.3 to 4.6 indicate the expected extrapolations for these non-dimensional factors for changes of the shell parameters of length, diameter and thickness and for changes of explosive charge weight. These extrapolations are shown as dashed lines. However, the changes in materials are represented as separate curves and therefore a separate set of curves must be determined for each new material. This means that some testing would be required for each material, but not to the extent presented here for these four materials. Further investigation is required to determine relationship between the blast parameters and the material properties.

The relationships just stated have been based on an arbitrary, but realistic, failure criterion that defines a certain amount of permanent deformation. If the failure criterion should be changed and a different amount of deformation selected the above relations could be easily adjusted. A few tests for each material would establish the ratio of pressure required

for the new criterion to the pressure already found. This ratio would establish a multiplying factor to amend the relationships to satisfy the new criterion.

4.3 Comparison of Calculated and Actual Pressures

Critical pressures have been computed for all the shells using the above relations and Figures 4.3 to 4.6. These values are listed along with the actual pressures in Table B.4, Appendix B. Percentage deviations between the calculated and actual pressures have also been listed for those shells that sustained approximately failure level permanent deformations. The average deviation for 159 points is 14 percent, with a spread of ± 40 percent (except for 4 points that were greater than 50 percent.) Over 70 percent of these data had a deviation of less than 20 percent.

There are many sources of error that help to generate this spread of ± 40 percent. Not all deformations fall within the defined 5 to 10 percent of the original diameter. Some deformations are greater and some are less. Time and economy precluded the refiring of many of these so that the required deformation levels might be obtained. In other cases the required value of deformation was "straddled" by two firings and the one closest was used.

The nominal thickness of the steel sheet was quite good, but the thickness variations of the drawn tubing and foil were approximately ± 10 percent. No check was made of the roundness of the finished shells. In working with the foil shells, which were rolled by hand, deviations are expected.

A large source of error is in the values of the "actual" pressures and impulses. The values should not vary on the average more than 5 to 10 percent from the true value but individual values could be off by as much as 20 percent.

If a number of "identical" shells are placed equidistant from one charge the deformation would vary ± 20 percent from the average value.

Considering these possible sources of error, the agreement is quite good, since there was an average deviation of 14 percent with over 70 percent of the points having a deviation of less than 20 percent.

4.4 Discussion of Theoretical Analyses

The theoretical analyses of Greenspon[17-19] are the only complete analyses for the response of a three-dimensional shell exposed to blast loading. In this section the analyses will be discussed in some detail and a comparison with the experimental data will be made in the following section.

If the energy absorbed by the shell is plotted against the lateral deflection in both the elastic and plastic regions, then there can be a region of instability in the elastic region which corresponds to snap buckling of the structure. If no instabilities occur in the elastic region, when the structure becomes plastic there could be a plastic instability point. If this point does not exist, and the structure is loaded further, then there should be a point at which a slight increase in energy will correspond to a relatively large increase in deflection. This should happen when the structure is about to collapse.

The initial kinetic energy can be determined in terms of the applied impulse. It will be assumed that all the kinetic energy that is imparted to the shell by the impulse goes into energy of deformation. The final deformation will occur when the shell comes to rest so that the final kinetic energy is zero.

As indicated in Section 3 there are two types of asymmetric deformation: a collapse mode with a failure hinge and buckling mode with a number of lobes. The problem is to determine which pattern will be produced before the energy can be computed. Fortunately the experimental data along with static elastic stress analysis indicate the following: if the static buckling load is less than the static yield load the shell should buckle under dynamic load, and if the yield load is less than the buckling load the shell should collapse. The static analysis only tells which pattern the shell will assume under dynamic loading.

A series of static buckling curves were obtained by Greenspon[19] for the case of a nonuniform consine distribution of lateral pressure where $\bar{p}$ is maximum static pressure and S_o is the yield stress in tension. Assuming that the membrane theory holds and using the VonMises yield condition, a series of collapse curves were also obtained. These two sets of curves, as shown in Figure 4.7, may now be used to predict whether a shell will first collapse or yield.

The deformation energy (or work done by the internal forces) per unit volume of an elastic-plastic body can be written[17]

$$V_o = \int_o^{e_i} S_i de_i + \frac{\bar{K}\theta^2}{2} \tag{1}$$

where

$$S_i = \frac{\sqrt{2}}{2}\left[(S_x - S_y)^2 + (S_y - S_z)^2 + (S_z - S_x)^2 + 6(\tau_{xy}^2 + \tau_{yz}^2 + \tau_{zx}^2)\right]^{1/2}$$

$$e_i = \frac{\sqrt{2}}{3}\left[(e_x - e_y)^2 + (e_y - e_z)^2 + (e_z - e_x)^2 + \frac{3}{2}(\gamma_{xy}^2 + \gamma_{yz}^2 + \gamma_{zx}^2)\right]^{1/2}$$

and

$$\theta = e_x + e_y + e_z \qquad \bar{K} = \text{bulk modulus} \ .$$

Assuming an incompressible material ($\theta = 0$) and a thin shell, Equation (1) becomes

$$V = \int_{VoL}\left[\int_o^{e_i} S_i de_i\right] dVoL \tag{2}$$

$$S_i = \left[S_x^2 - S_x S_y + S_y^2 + 3\tau_{xy}^2\right]^{1/2} \ ,$$

$$e_i = \frac{2}{\sqrt{3}}\left[e_x^2 + e_x e_y + e_y^2 + \frac{1}{4}\gamma_{xy}^2\right]^{1/2} \ .$$

Strain equations for e_x, e_y, e_z can be written in terms of the midsurface strains, the curvatures and twist. If all terms in the strains which contain u and v are neglected (assuming that they are

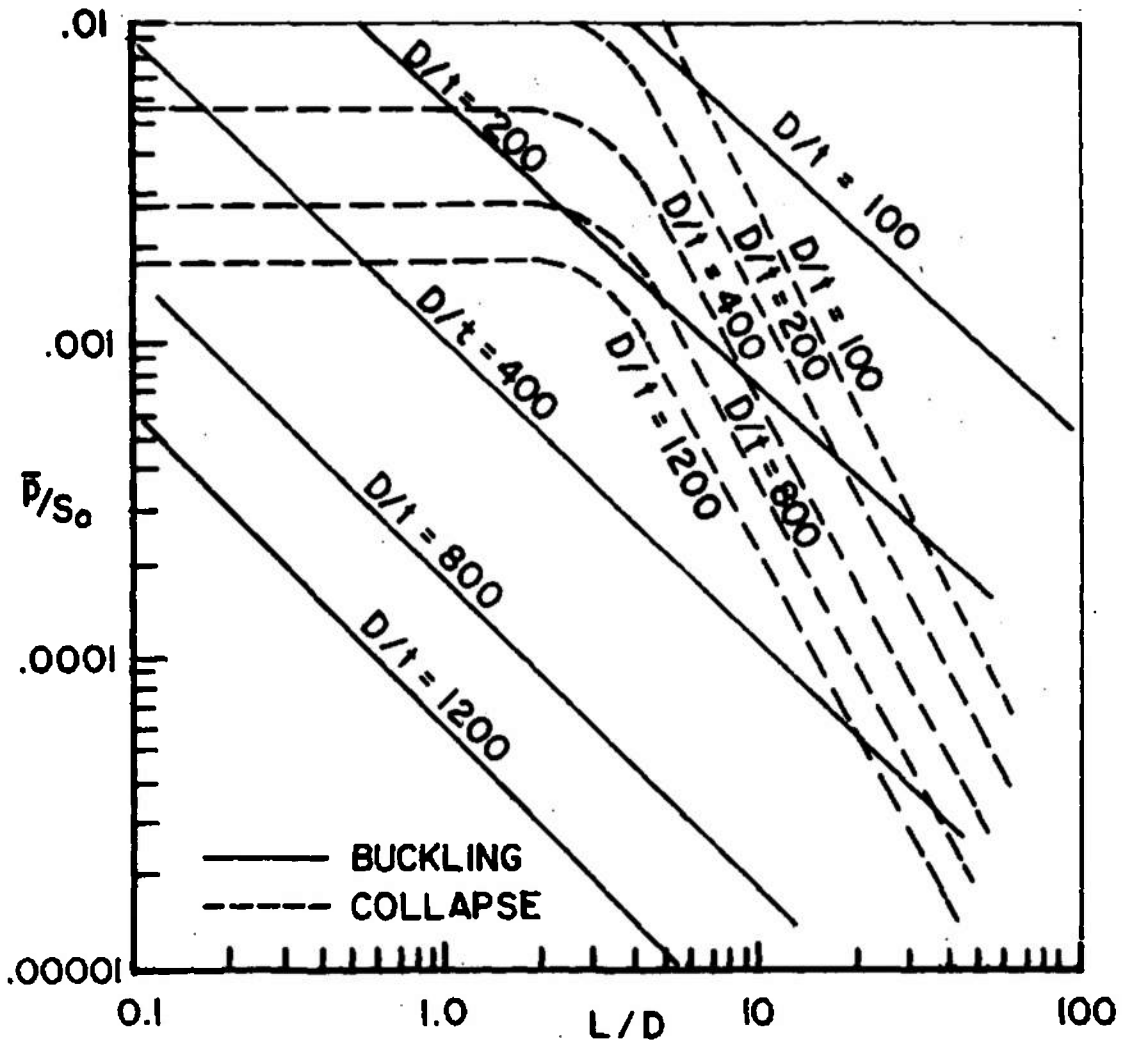

FROM GREENSPON (REF. 19)

FIGURE 4.7 BUCKLING AND COLLAPSE LOADS

small compared to w and its derivatives), then the strain equations are written as

$$e_x = \frac{1}{2}\left(\frac{\partial w}{\partial x}\right)^2 - r\,\frac{\partial^2 w}{\partial x^2}$$

$$e_y = \frac{1}{2}\left(\frac{\partial w}{a\partial \phi}\right)^2 - \frac{w}{a} - \frac{r}{a^2}\,\frac{\partial^2 w}{\partial \phi^2}$$

$$\gamma_{xy} = \frac{\partial w}{\partial x}\,\frac{\partial w}{a\partial \phi} - 2\,\frac{r}{a}\,\frac{\partial^2 w}{\partial x \partial \phi} \qquad (3)$$

where a = mean radius

x, θ = cylindrical coordinates

w = displacement in radial direction

r = radial distance from the midsurface to any element within the shell thickness

Assuming a Poissons ratio of 1/2, a general deformation type elastic-plastic stress-strain law can be written as

$$S_x = \frac{4}{3}\,\frac{S_i}{e_i}\,(e_x + \frac{1}{2}\,e_y)$$

$$S_y = \frac{4}{3}\,\frac{S_i}{e_i}\,(e_y + \frac{1}{2}\,e_x)$$

$$\tau_{xy} = \frac{1}{3}\,\frac{S_i}{e_i}\,\gamma_{xy} \qquad (4)$$

where

$$\frac{S_i}{e_i} = E\left[1 - w(e_i)\right] .$$

Consider an elastic-linear, strain hardening, incompressible material with

$$E = \frac{S_o}{e_o} \qquad (5)$$

where S_o is the yield stress in tension and e_o is the yield strain in tension.

Then for the Elastic Case $w(e_i) = 0$ for $e_i < e_o$

and for the Plastic Case $w(e_i) = \lambda(1 - \frac{e_o}{e_i})$ for $e_i > e_o$ (6)

where

$$\lambda = 1 - \frac{1}{E}\frac{dS_i}{de_i} \quad .$$

Substituting in the stress-strain law of Equation (6) the expression for e_i from Equation (2), and the strain values from Equation (3) in Equation (2) and integrating with respect to r,

$$V = \int_o^L \int_o^{2\pi} \left\{\frac{2}{3} E(1 - \lambda)[t\xi(x,\phi)] + \frac{2\lambda E e_o}{\sqrt{3}} t\sqrt{\xi(x,\phi)}\right\} a d\phi dx \quad . \quad (7)$$

The bending strains are neglected in obtaining Equation (7).

Similar expressions can be obtained for perfectly plastic materials ($\lambda = 1$) in the plastic region and for elastic materials ($\lambda = 0$) in the elastic region.

If a new variable $x' = x/L$ is defined and $w = w_o f(x',\phi)$ then the two integrals for the plastic and elastic cases can be combined as follows:

$$V = \frac{E(1 - \lambda)taL}{2(1 - \nu^2)} \int_o^1 \int_o^{2\pi} \alpha dx' d\phi + \frac{E(1 - \lambda)taL}{6(1 - \nu^2)} \int_o^1 \int_o^{2\pi} \beta dx' d\phi$$

$$+ \frac{\lambda E e_o taL}{\sqrt{3}} \int_o^1 \int_o^{2\pi} \left\{\left[\frac{(2\beta + \gamma)\sqrt{\alpha + \gamma + \beta}}{4\beta}\right.\right.$$

$$+ \frac{(4\alpha\beta - \gamma^2)}{8\beta} \frac{1}{\sqrt{\beta}} \sinh^{-1}\left(\frac{2\beta + \gamma}{\sqrt{4\alpha\beta - \gamma^2}}\right)\Bigg] - \left[\frac{(\gamma - 2\beta)\sqrt{\alpha - \gamma + \beta}}{4\beta}\right.$$

$$\left.\left. + \frac{(4\alpha\beta - \gamma^2)}{8\beta} \frac{1}{\sqrt{\beta}} \sinh^{-1}\left(\frac{\gamma - 2\beta}{\sqrt{4\alpha\beta - \gamma^2}}\right)\right]\right\} dx' d\phi \quad (8)$$

where

$$\alpha(x,\phi) = \frac{1}{4}\left(\frac{w_o}{a}\right)^4\left(\frac{a}{L}\right)^4\left(\frac{\partial f}{\partial x'}\right)^4 + \frac{1}{2}\left(\frac{w_o}{a}\right)^4\left(\frac{a}{L}\right)^2\left(\frac{\partial f}{\partial x'}\right)^2\left(\frac{\partial f}{\partial \phi}\right)^2 - \nu\left(\frac{w_o}{a}\right)^3\left(\frac{a}{L}\right)^2 f\left(\frac{\partial f}{\partial x'}\right)^2$$

$$+ \frac{1}{4}\left(\frac{w_o}{a}\right)^4\left(\frac{\partial f}{\partial \phi}\right)^4 - \left(\frac{w_o}{a}\right)^3 f\left(\frac{\partial f}{\partial \phi}\right)^2 + \left(\frac{w_o}{a}\right)^2 f^2$$

$$\gamma(x,\phi) = -\left(\frac{w_o}{a}\right)^3\left(\frac{a}{L}\right)^4\left(\frac{t}{2a}\right)\left(\frac{\partial^2 f}{\partial x'^2}\right)\left(\frac{\partial f}{\partial x'}\right)^2 - \left(\frac{w_o}{a}\right)^3\left(\frac{t}{2a}\right)\left(\frac{\partial^2 f}{\partial \phi^2}\right)\left(\frac{\partial f}{\partial \phi}\right)^2$$

$$+ 2\left(\frac{w_o}{a}\right)^2\left(\frac{t}{2a}\right)\left(\frac{\partial^2 f}{\partial \phi^2}\right) f - \nu\left(\frac{w_o}{a}\right)^3\left(\frac{a}{L}\right)^2\left(\frac{t}{2a}\right)\left(\frac{\partial f}{\partial x'}\right)^2\left(\frac{\partial^2 f}{\partial \phi^2}\right)$$

$$- \nu\left(\frac{w_o}{a}\right)^3\left(\frac{a}{L}\right)\left(\frac{t}{2a}\right)\left(\frac{\partial^2 f}{\partial x'^2}\right)\left(\frac{\partial f}{\partial \phi}\right)^2 + 2\nu\left(\frac{w_o}{a}\right)^2\left(\frac{a}{L}\right)^2\left(\frac{t}{2a}\right) f\left(\frac{\partial^2 f}{\partial x'^2}\right)$$

$$- 2(1-\nu)\left(\frac{w_o}{a}\right)^3\left(\frac{a}{L}\right)^2\left(\frac{t}{2a}\right)\left(\frac{\partial^2 f}{\partial x' \partial \phi}\right)\left(\frac{\partial f}{\partial x'}\right)\left(\frac{\partial f}{\partial \phi}\right)$$

$$\beta(x,\phi) = \left(\frac{w_o}{a}\right)^2\left(\frac{a}{L}\right)^4\left(\frac{t}{2a}\right)^2\left(\frac{\partial^2 f}{\partial x'^2}\right)^2 + 2\nu\left(\frac{w_o}{a}\right)^2\left(\frac{t}{2a}\right)^2\left(\frac{a}{L}\right)^2\left(\frac{\partial^2 f}{\partial x'^2}\right)\left(\frac{\partial^2 f}{\partial \phi^2}\right)$$

$$+ \left(\frac{w_o}{a}\right)^2\left(\frac{t}{2a}\right)^2\left(\frac{\partial^2 f}{\partial \phi^2}\right)^2 + 2(1-\nu)\left(\frac{w_o}{a}\right)^2\left(\frac{a}{L}\right)^2\left(\frac{t}{2a}\right)^2\left(\frac{\partial^2 f}{\partial x' \partial \phi}\right)^2 .$$

The integrals are dimensionless quantities which are functions of the dimensionless ratios w_o/a, a/L, $t/2a$. Equation (8) has been programmed on the U. S. Army Ballistic Research Laboratory computer. The deformation energy depends on a given shape $f(x',\phi)$, the given parameters a/L and $t/2a$ and a series of values of w_o/a.

To develop the impulse-energy relation, let I be the impulse per unit mass applied to the shell. Then the impulse momentum relation for an elemental mass dm can be written

$$\dot{w}\, dm = I\, dm \qquad (9)$$

where $\dot{w}$ is the lateral velocity imparted to the mass by the impulse. If $\dot{u}$ and $\dot{v}$ are neglected,

$$\dot{w} = I \quad .$$

The kinetic energy imparted to the shell is

$$T_E = \int_A \frac{1}{2} \rho t \dot{w}^2 dA = \frac{1}{2} \int_A \rho t I^2 dA \qquad (10)$$

where ρt is the mass per unit area and dA is an elemental area. For a variable impulse over the surface of the shell

$$I(x,y) = I_o f(x,y) \qquad (11)$$

where $y = a\phi$.

Equating the initial kinetic energy to the energy of deformation absorbed by the shell, the total impulse becomes

$$I_t = \int_A I_o \rho t f(x,y) dA = \int_A \sqrt{V \frac{2\rho t}{\int_A f^2(x,y) dA}} f(x,y) dA \qquad (12)$$

4.5 Comparison of Experimental Data with Theoretical Analyses

Collapse Mode. A few typical cases of collapse load determinations will be worked out and compared with experimental values.

Assume 1. The shell is made of perfectly plastic material;

2. The radius of the shell is considerably smaller than the length;

3. The deflection of the shell is much smaller than the radius;

4. $\frac{w_o}{\sqrt{3}} \gg e_o \frac{a}{2}$.

With these assumptions the energy Equation (8) is greatly simplified. The deflection pattern for collapse is shown in Figure 4.8 and from geometrical considerations can be expressed as

$$W(x,\phi) = a \cos\phi - \sqrt{a^2 - \frac{1}{4}\left[D_o - \frac{D_o}{L/2} x\right]^2} \quad . \qquad (13)$$

Let $x' = x/L$.

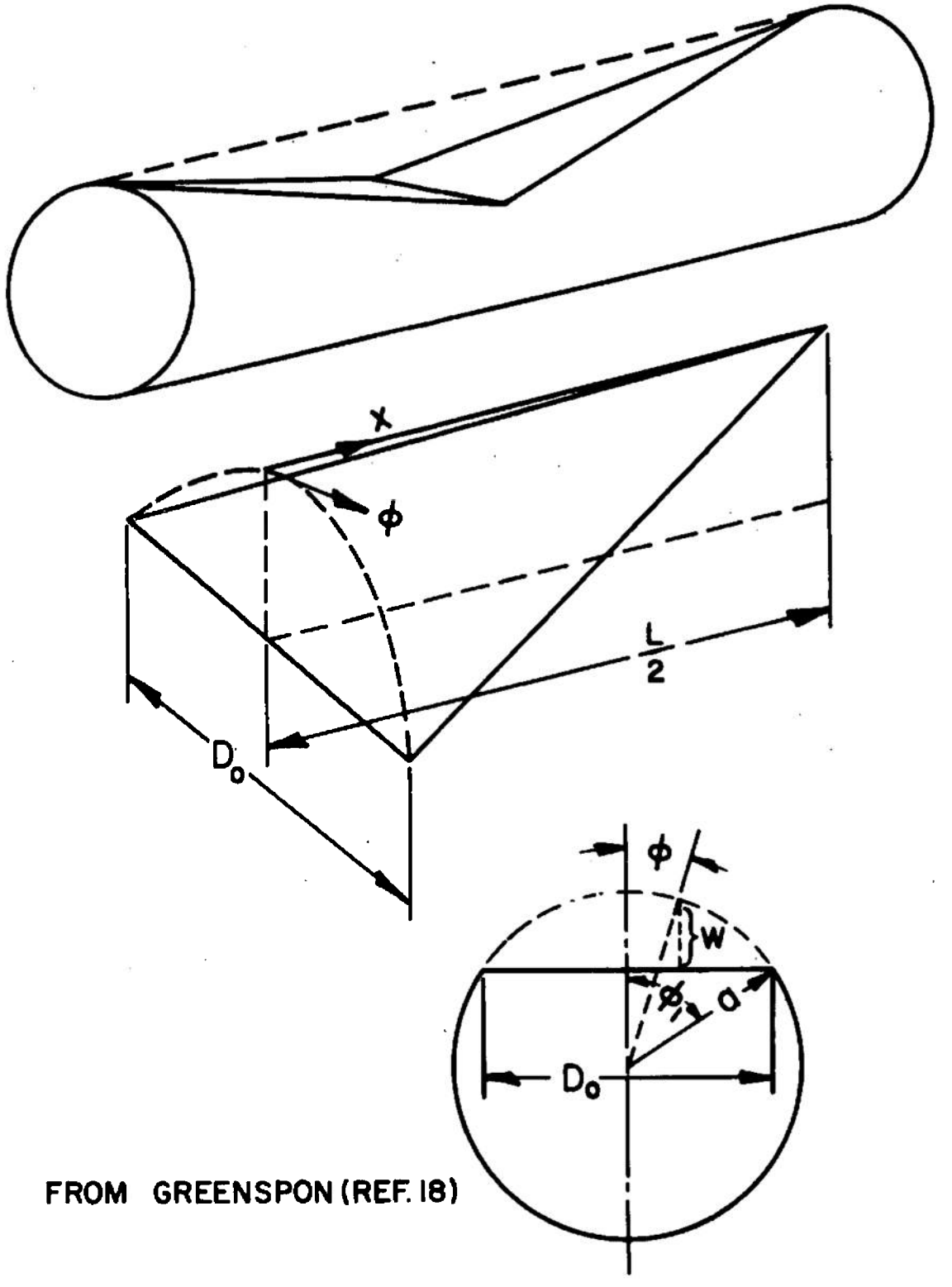

FROM GREENSPON (REF. 18)

FIGURE 4.8 COLLAPSE PATTERN

Then

$$w(x',\phi) = a\cos\phi - \sqrt{a^2 - \frac{D_o}{4}[1 - 2x']^2} \qquad \text{for} \qquad o < x' < \frac{1}{2}$$

$$w(x',\phi) = a\cos\phi - \sqrt{a^2 - \frac{D_o}{4}[1 + 2x']^2} \qquad \text{for} \qquad -\frac{1}{2} < x' < 0 \tag{14}$$

where D_o is the width of the hinge line. The deformation expressions in Equation (14) are put in the simplified form of Equation (8). Then using Equation (12) and assuming that

$$f(x,y) = f(x,\phi) = e^{-2\phi}$$

the relation between the impulse and deformation can be written as

$$I_t = 2tLD\sqrt{\Sigma}\sqrt{\frac{S_o\rho}{\sqrt{3}}} \tag{15}$$

where

$$\Sigma = \frac{D}{D_o}\left[\frac{3}{4}\left(\frac{D_o}{D}\right)^2 - \frac{\bar{\phi}}{4}^2 - \frac{\bar{\phi}D_o}{2D}\sqrt{1 - \left(\frac{D_o}{D}\right)^2}\right]$$

$$\bar{\phi} = \sin^{-1}\frac{D_o}{D} \quad .$$

The total impulse may also be expressed in terms of the impulse per unti area, I_A as follows:

$$I_t = 2\int_o^L \int_o^\pi I_A e^{-2\phi} a\,d\phi\,dx$$

$$I_A \approx 2\frac{I_t}{DL}$$

$$I_A \approx 4t\sqrt{\Sigma}\sqrt{\frac{S_o\rho}{\sqrt{3}}} \quad . \tag{16}$$

Equation (16) predicts the impulse per unit area which will produce a given D_o/D. Unfortunately the exact value of experimental impulse is not known but values of incident impulse per unit area and reflected impulse per unit area were determined. The actual impulse applied to the shell will be somewhere between these two values. For eight steel shells that were tested, Equation (16) specified values of impulse that fall between the two experimental values in five cases and are slightly higher than the reflected impulse in the other three cases. These values are given in Table 4.2. Use of the more accurate relations should yield even better results.

Buckling Mode. A typical case of buckling will be worked out and compared with experimental data.

Assume a deflection pattern of the form

$$w(x', \phi) = \sin \pi x' e^{-k\phi} \cos n\phi \qquad 0 < \phi < \pi$$

$$w(x', \phi) = \sin \pi x' e^{-k(2\pi - \phi)} \cos n(2\pi - \phi) \qquad \pi < \phi < 2\pi \; . \tag{16}$$

The general Equation (8) must mow be used. For an aluminum shell the theory predicted that 5 lobes would be formed with $w_o/a \approx 0.5$ and would require an impulse of 21 psi-milliseconds. The experiment showed that for an incident impulse of 21 psi-milliseconds and a reflected impulse of 46.8 psi-msec, the deflection was $w_o/a \approx 0.5$ with 5 lobes.

Post failure collapse and buckling curves are given in Figure 4.9 for typical cases. It can be seen from the curves that very thin, short shells will buckle before they collapse and longer thicker shells will collapse first.

It is felt that the comparison between the analyses of Greenspon and the experimental data presented here is quite good. More exact details of loading in terms of the actual values of the impulse that load the shell will greatly aid the analyses.

TABLE 4.2

Comparison of Theoretical and Experimental Values of Impulse for Shell Collapse

Shell Dimensions			Impulse (psi-millisec)		
Length (in.)	Diameter (in.)	Thickness (in.)	Theoretical*	Experimental	
				Incident	Reflected
6.0	3.0	0.019	123	89	299
8.62	3.0	0.019	82	15.5	69.5
8.62	3.0	0.019	71.5	48	160
11.62	3.0	0.019	71.5	14.5	56.1
11.62	3.0	0.019	71.5	25	83
18.0	3.0	0.019	123	68	190
18.0	6.0	0.019	71.5	22	67
17.5	6.0	0.035	143	64	200

* Reference (18)

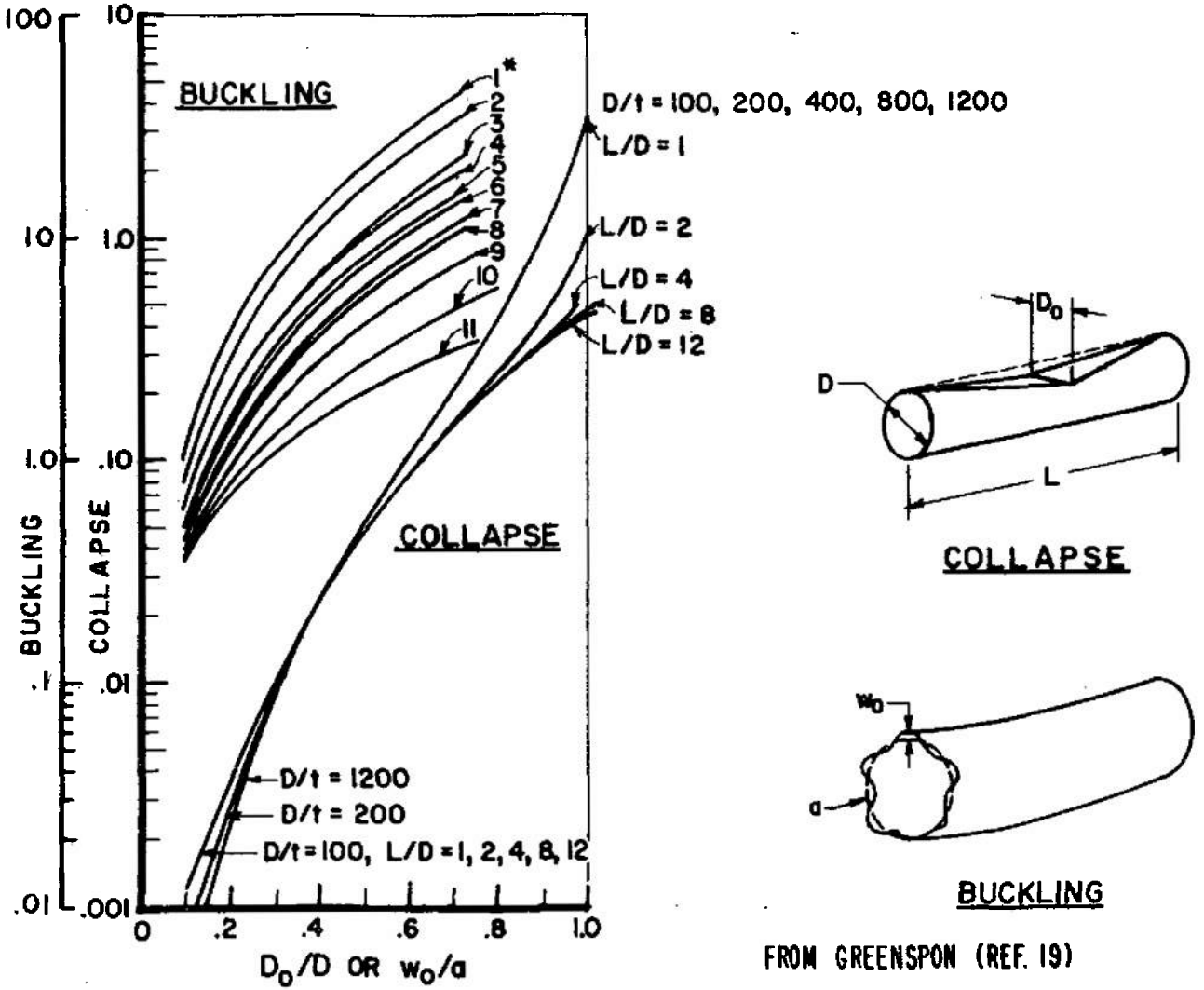

FROM GREENSPON (REF. 19)

BUCKLING

CURVE NO.*	D/t	L/D
1	1200	1
2	800	1
3	400	1
4	1200	2
5	200	1
6	800	2
7	100	1
8	1200	4
	800	4
	400	2
9	1200	8
	400	4
	200	2
	100	2
10	800	8
	400	8
	200	4
	100	4
11	800	12
	400	12
	200	8
	100	12

FIGURE 4.9-POST FAILURE COLLAPSE AND BUCKLING CURVES

5. SUMMARY AND CONCLUSIONS

5.1 Statement of the Problem

The general problem tested in this report is an experimental investigation of the response of cylindrical shells to blast loading. Comparisons with theory are also made.

It was assumed that a given level of deformation of the shell would constitute failure. The level of deformation or failure criterion chosen was a radial permanent deformation approximately 5 to 10 percent of the original diameter for thin-walled, right-circular, cylindrical shells exposed to external blast from charges of high explosive.

The specific problm may now be stated as follows:

> Determine the relationships between the shell and blast parameters that will predict a deformation to determine whether failure has occurred according to a specified failure criterion. The relationships should be sufficiently general to be adaptable to variations in the magnitudes of the deformation defined by the failure criterion.

5.2 Origin and Importance of the Problem

This problem was prompted by the need for a clearly defined failure criterion for a wide spectrum of aerospace vehicles, when exposed to blast from a nuclear environment, that could be satisfied in terms of the vehicle geometry and blast parameters. Since these vehicles are predominantly of a cylindrical shell configuration, a failure criterion for simple shells would make a realistic first order approximation to the actual structure. The failure criterion chosen was based on previous experience in determining the vulnerability of actual missiles.

5.3 Procedure of the Investigation

Thin-walled cylindrical shells were fabricated from 1040 steel and 6061-T6, 5052-H38 and 1100-0 aluminum. The shell diameters varied from 3 to 24 inches, the lengths from 1 to 75 inches and the thicknesses from 0.003 to 0.136 inches. The shells had length-to-diameter ratios of 0.3 to 25 and diameter-to-thickness ratios of 60 to 2,000. A few were instrumented with strain gages.

The shells were fastened to heavy end caps and mounted on stands. These stands were positioned about charges of high explosive ranging in weight from 1 pound to 500 tons. The shells were oriented so that the blast impinged on the shells either along a line perpendicular to the longitudinal axis (lateral loading) or along an extension of the longitudinal axis (longitudinal loading). A nose cone was added to the shell for the longitudinal loading orientation to minimize the distrubance of the flow.

The shells were positioned about the explosive charge at various distances such that the blast parameter values would be below those required to cause failure. The shells were then repositioned in increments until failure was obtained.

Tests were conducted at the U. S. Army Ballistic Research Laboratories, Aberdeen Proving Ground, Maryland; Yuma Proving Ground, Yuma, Arizona and Suffield Experimental Station, Ralston, Alberta, Canada.

5.4 Results

A total of 204 data points were obtained from 316 firings on 299 shells. The data were presented as iso-damage curves for each material. These iso-damage curves represent the combinations of pressure and impulse that cause failure of a given shell geometry as the charge weight changes. These curves are boundaries between the safe and failure regimes.

Two distinct deformation patterns were observed for the lateral loading orientation. For the collapse mode, a single plastic hinge line was formed. For the buckling mode, one or more longitudinal lobes were formed. In each case the maximum deflection occurs approximately in the center of the shell at the point closest to the explosive charge.

An axisymmetric type of buckling mode was produced by the longitudinal loading. The maximum deflection does not occur at the mid-length of the shell but closer to the forward end cap. The shells were stronger in the longitudinal loading orientation.

It was found that shells may be considered infinite in length when the length-to-diameter ratio, $L/_D \approx 17$. For greater values of $L/_D$ the critical pressure, p_{cr}, remains constant.

A semi-graphical formulation of the failure criterion relating the critical incident blast pressure to shell parameters and charge weight is presented. The comparison of calculated and actual pressures for 159 shells is given. The average deviation between these values is 14 percent with a spread of ± 40 percent (except for 4 points that were greater than 50 percent). Over 70 percent of these data had a deviation of less than 20 percent.

The theoretical analyses of Greenspon are the only complete analyses for both the asymmetric and axisymmetric response of three-dimensional shells exposed to blast loading. An energy method is used to predict the final degree of deformation. This method consists of equating the total kinetic energy imparted to the shell by the applied loading to the energy absorbed by the structure during deformation. The kinetic energy can be determined in terms of the impulse generated by the charge detonation. The energy absorbed by the shell will depend on its mode of failure.

Eight typical cases of collapse-load determinations were worked out and compared with experimental data. Unfortunately, the exact value of experimental impulse is not known, but values of incident impulse per unit area and reflected impulse per unit area were determined. The actual impulse applied to shell will be somewhere between these two values. Simplified relations were used and the impulse values obtained fell between the two experimental values in five cases and were slightly higher than the reflected impulse in the other three cases. Use of the more accurate theoretical expressions should yield even better correlation.

A typical case of buckling was worked out and compared with experimental data. Theory predicted an impulse of 21 psi-milliseconds compared to an experimental value of incident impulse of 21 psi-milliseconds. Theory and experiment agreed that the deformation pattern would consist of five lobes.

The theoretical analyses show good correlation with the experimental data.

Some strain data were also obtained and is presented in two tables. These were exploratory firings to check the system. The reproducibility of the strain readings was quite good. There is no correlation of these strain values with theory as the only theoretical analyses presently available do not give details of elastic response for finite shells.

5.5 Conclusions

The scope of this report is unique and presents for the first time relationships between shell and blast parameters that are based on the effects of a real blast against real, three-dimensional cylindrical shells with clamped ends. Furthermore, the results are in reasonable agreement with a failure criterion. The relationships obtained should provide vehicle designers with a reasonable failure criteria in a form that is very simple and immediately useful.

The relationships are sufficiently flexible so that they could be easily modified to satisfy other failure criteria based on permanent deformation values. The relationship between blast parameters and material properties remains to be determined.

The comparison with the theoretical analyses of Greenspon indicate good agreement. More exact details of loading in terms of the actual values of the impulse that load the shell will greatly aid the analyses.

5.6 Suggestions for Further Research

It is felt that sufficient data exist so that extensive testing would not be required to develop relations for other materials of interest such as stainless steel and titanium. The author is planning to study such materials. In addition, firings are presently being conducted using a series of more realistic models. These include water or gas filled shells, stiffened shells, pre-heated shells, pre-loaded shells (torsion, compression, bending), freely supported shells, and composite shells. The latter are constructed of concentric shells of dissimilar materials, thicknesses and radii.

Attempts were made to measure details of loading by determining the pressure-time history of the impinging blast at a number of points on the shell surface. A non-responding shell was instrumented with flush-mounted pressure transducers. However, the transducers did not function properly and require further development.

ACKNOWLEDGEMENTS

This report gives the results of a research program conducted primarily at the U. S. Army Ballistic Research Laboratories. Portions of the program were also conducted at the Yuma Proving Ground, Yuma, Arizona, and the Suffield Experimental Station, Ralston, Alberta, Canada.

The auther gratefully acknowledges the contributions of many individuals and groups during the conduct of this investigation. The basic data were obtained with the assistance of H. Goldstein, M. Lampson, M. Hayashi and the members of the Ballistic Research Laboratories' field crew. The data from Project Big Bird were obtained with the assistance of R. Mayerhofer and Lt E. Rosicky and the Personnel of the Yuma Proving Ground. The data from Operation Snow Ball were obtained with the assistance of O. Johnson, W. Ewing, G. Watson, J. Caudill and the personnel of the Suffield Experimental Station.

The research reported was accepted by the Pennsylvania State University as satisfying partial requirements for the Doctor of Philosophy Degree. Doctor Norman Davids, Department of Engineering Mechanics acted as advisor and made many helpful suggestions concerning the planning of the tests and the preparation of the report.

The original manuscript of the doctoral thesis, which was prepared by Mrs. W. J. Schuman, Jr. has been modified slightly for this report.

WILLIAM J. SCHUMAN, JR.

BIBLIOGRAPHY

1. Abrahamson, G. R. Techniques for Simulating X-Ray Impulses on ReEntry Vehicles (U). U. S. Air Force Special Weapons Center AFSWC-TR-61-26, March, 1961. (SECRET-RD)

2. Abrahamson, G. R. Investigation of Response of Simplified ICBM-Type Structures to Impulsive Loading. Air Force Special Weapons Center Technical Report No. AFSWC-TDR-62-94, Vol. II, December, 1962.

3. Abrahamson, G. R Supplementary Report - Estimated Bounds on the Ultimate Achievable Structural Hardness of Re-Entry Vehicles (U). Stanford Research Institute Report SRI-3-2483, October, 1963. (SECRET-RD)

4. Abrahamson, G. R. and Florence, A. L. Investigation of Response of Simplified ICBM-Type Structures to Impulsive Loading (U). Air Force Special Weapons Center Report No. AFSWC-TDR-62-94, Vol. 1 November, 1962. (SECRET-RD)

5. Abrahamson, G. R. and Goodier, J. N. Dynamic Plastic Flow Buckling of a Cylindrical Shell From Uniform Radial Impulse. Stanford Research Institute Technical Report 001-62, June, 1962.

6. Baker, W. E., Ewing W. O. and Hanna, J. W. Laws for Large Elastic Response and Permanent Deformation of Model Structures Subjected to Blast Loading. U. S. Army Ballistic Research Laboratories Report No. 1060, December, 1958.

7. Baker, W. E. and Schuman, W. J. Air Blast Data for Correlation with Moving Airfoil Tests. U. S. Army Ballistic Research Laboratories Technical Note No. 1421, 1961.

8. Balmer, H. and Witmer, E. Theoretical-Experimental Correlation of Large Dynamic and Permanent Deformations of Impulsively-Loaded Simple Structures. Air Force Flight Dynamics Laboratory Technical Documentary Report No. FDL-TDR-64-108, July, 1964.

9. Baron, M. L. and Bleich, H. H. Further Studies of a Cylindrical Shell to a Transverse Shock Wave. Columbia University Technical Report No. 10, December, 1953.

10. Bleich, H. H. and DiMaggio, F. L. Dynamic Buckling of Submerged Plates and Shells. Columbia University Technical Report No. 12, September, 1954.

11. Cole, R. H. Underwater Explosions. Princeton University Press, 1948.

12. Courant, R. and Friederichs, K. O. Supersonic Flow and Shock Waves. Interscience Publishers, Inc., New York, 1948.

13. DeHart, R. C. and Basdekas, N. L. Response of Aircraft Fuselages and Missile Bodies to Blast Loading. Air Force Flight Dynamics Laboratory Technical Documentary Report ASD-TDR-62-458, January, 1963.

14. DeHart, R. C., Rastrelli, L. U., Basdekas, N. L., Minor, J. and Pape, B. Structural Vulnerability of Pre-Launch Missiles to Nuclear Weapon Effects (U). USAF Flight Dynamic Laboratory Report FDL-TDR-64-45, July, 1964. (CONFIDENTIAL)

15. Glasstone, S. The Effects of Nuclear Weapons. U. S. Atomic Energy Commission, April, 1962.

16. Goodman, H. J. Compiled Free-Air Blast Data on Bare Spherical Pentolite. U. S. Army Ballistic Research Laboratories Report No. 1092, February, 1960.

17. Greenspon, J. E. Elastic and Plastic Behavior of Cylindrical Shells Under Dynamic Loads Based on Energy Criteria. J. G. Engineering Research Associate Technical Report No. 3, February 1963.

18. Greenspon, J. E. Collapse, Buckling and Post Failure of Cylindrical Shells. J. G. Engineering Research Associates Technical Report No. 4, December, 1963.

19. Greenspon, J. E. Post Failure Deflections of Cylindrical Shells Under Dynamic Lateral Loads. J. G. Engineering Research Associates Technical Report No. 5, August, 1964.

20. Hodge, P. G., Jr. Impact Pressure Loading of Rigid-Plastic Cylindrical Shells. Polytechnic Institute of Brooklyn Pibal Report No. 255, May, 1954.

21. Hodge, P. G., Jr. Ultimate Dynamic Load of a Circular Cylindrical Shell. Polytechnic Institute of Brooklyn Pibal Report No. 265 November, 1954.

22. Hodge, P. G., Jr. The Influence of Blast Characteristics on the Final Deformation of Circular Cylindrical Shells. Polytechnic Institute of Brooklyn Pibal Report No. 266, December, 1954.

23. Hoover, C. H. Comparison Tests of British and American Self-Recording Pressure-Time Gages. U. S. Army Ballistic Research Laboratories Memorandum Report No. 1221, July, 1959.

24. Iliouchine. Plasticite. Edition Eyrolles, 1956.

25. Kinney, G. F. Explosive Shocks in Air. The MacMillan Company, 1962.

26. Laing, F. J. Report NR/85/01. The Directorate of Artillery Research and Development War Office, London, May 1961. (SECRET)

27. Leech, J., Pian, T. H. H., Witmer, E., and Herrmann, W. Dynamic Response of Shells to Externally-Applied Dynamic Loads. Air Force Flight Dynamics Laboratory Technical Documentary Report No. ASD-TDR-62-610 November, 1962.

28. Lindberg, H. E. Buckling of a Very Thin Cylindrical Shell Due to an Impulsive Pressure. Journal of Applied Mechanics, Pages 267-272, June, 1964.

29. Mindlin, R. D. and Bleich, H. H. Response of an Elastic Cylindrical Shell to a Transverse Step Shock Wave. Columbia University Technical Report No. 3, March, 1952.

30. Nash, W. A. Bibliography on Shells and Shell-Like Structures. U. S. Navy Department David W. Taylor Model Basin Report No. 863, November, 1954.

31. Pian, T. H. On Large Dynamic Deformations of General Shells. Air Force Flight Dynamics Laboratory Technical Documentary Report No. RTD-TDR-63-4271, January, 1964.

32. Radkowski, P. P., Humphreys, J. S., Bodner, S. R., Payton, R. G., and Budiansky, B. Studies on the Dynamic Response of Shell Structures and Materials to a Pressure Pulse. Air Force Special Weapons Center Report AFSWC-TR-61-31 (II), July, 1961.

33. Rosendorf, L. and Kintish, I. Status Report-Research for Determination of Blast Effects on Re-Entry Vehicle Structures. Picatinny Arsenal Technical Memorandum 1152, March, 1963.

34. Rosendorf, L. Response of Simple Geometric Shells to Impulsive Loading. Picatinny Arsenal Technical Memorandum 1227, July, 1963.

35. Rosendorf, L. Blast Effects Tests on Simple Instrumented Shells. Picatinny Arsenal Technical Memorandum 1420, February, 1964.

36. Rosendorf, L. Preliminary Report: Operation Snow Ball (U). Vol 1 DASA Data Center Report DASA 1550-1, October, 1964. (CONFIDENTIAL)

37. Sachs, R. G. The Dependence of Blast on Ambient Pressure and Impulse. U. S. Army Ballistic Research Laboratories, Report No. 466, 1944.

38. Sankaranarayanan, R. Dynamic Response of Plastic Circular Cylindrical Shells Under Lateral and Hydrostatic Pressures. Polytechnic Institute of Brooklyn Pibal Report No. 573, June, 1961.

39. Schuman, W. J. Response of Cylindrical Shells Exposed to External Blast Loading. Proceedings of Army Conference on Dynamic Behavior of Materials and Structures, Army Research Office - Durham, 1962.

40. Schuman, W. J. The Response of Cylindrical Shells to External Blast Loading. U. S. Army Ballistic Research Laboratories Memorandum Report No. 1461 March, 1963.

41. Schuman, W. J. The Response of Cylindrical Shells to External Blast Loading, Part II. U. S. Army Ballistic Research Laboratories Memorandum Report No. 1560, May, 1964.

42. Schuman, W. J. Vulnerability of Simulated Missile Bodies to Blast. Proceedings of Conference on Nuclear Effects on Re-Entry Vehicles and Interceptor Missiles, Defense Atomic Support Agency December, 1964.

43. Sevin, E. Test on the Loading of Horizontal Cylindrical Shapes. Wright Air Development Center Report No. WADC-TR-55-420, October, 1955.

44. Thomas, L. H. Note on Becker's Theory of the Shock Front. Journal Chemistry and Physics Vol. 12, 1949, pp. 449-457.

45. Wah, Rastrelli, L. U., Basdekas, N. L. and DeHart, R. C. Response of Missile Structures to Impulse Loading. Air Force Aeronautical Systems Division Report ASD-TDR-62-475, March, 1963.

46. Witmer, E., Herrmann, W., Leech, J. W. and Pian, T. H. H. Responses of Plates and Shells to Intense External Loads of Short Duration. Wright Air Development Division WADD Technical Report 60-433, April, 1960.

47. Witmer, E. A., Balmer, H. A., Leech, J. W. and Pian, T. H. H. Large Dynamic Deformations of Beams, Circular Rings, Circular Plates and Shells. AIAA Launch and Space Vehicles Shell Structures Conference, April, 1963.

48. British Ordnance Board Minutes 13565, 1915.

49. Final Report on Buckling of Shells Under Dynamic Loads. Space Technology Laboratories Report No. 8622-0001-RU-000, October, 1961.

50. Scientific Observations on the Explosion of a 20 Ton TNT Charge, Volume 1, General Information and Measurements. Suffield Experiment Station Report No. 203.

APPENDIX A

FIRING AREAS AND INSTRUMENTATION

Intentionally Left Blank.

Fig. A.1 Field Arrangement at Ballistic Research Laboratories

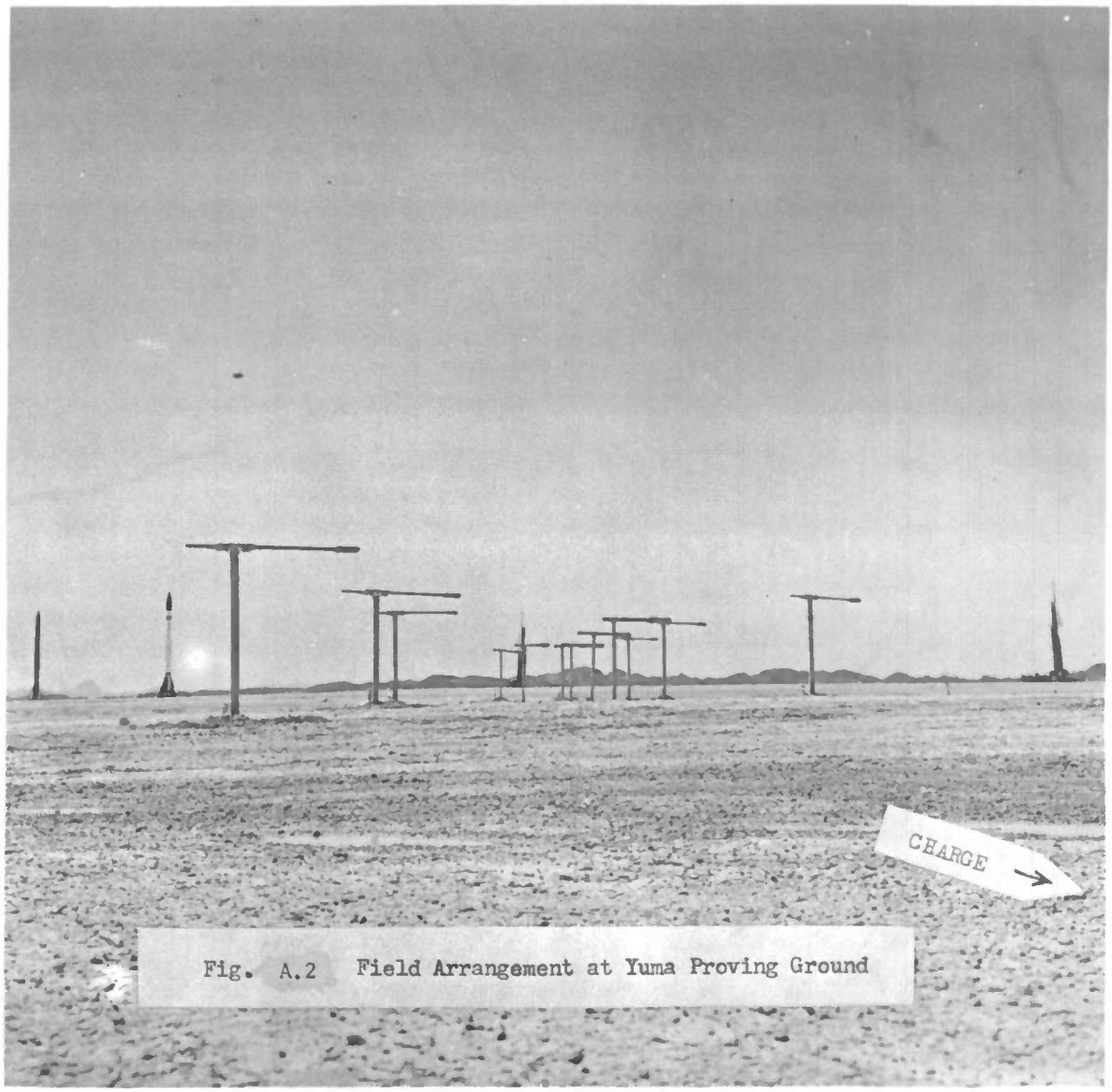

Fig. A.2 Field Arrangement at Yuma Proving Ground

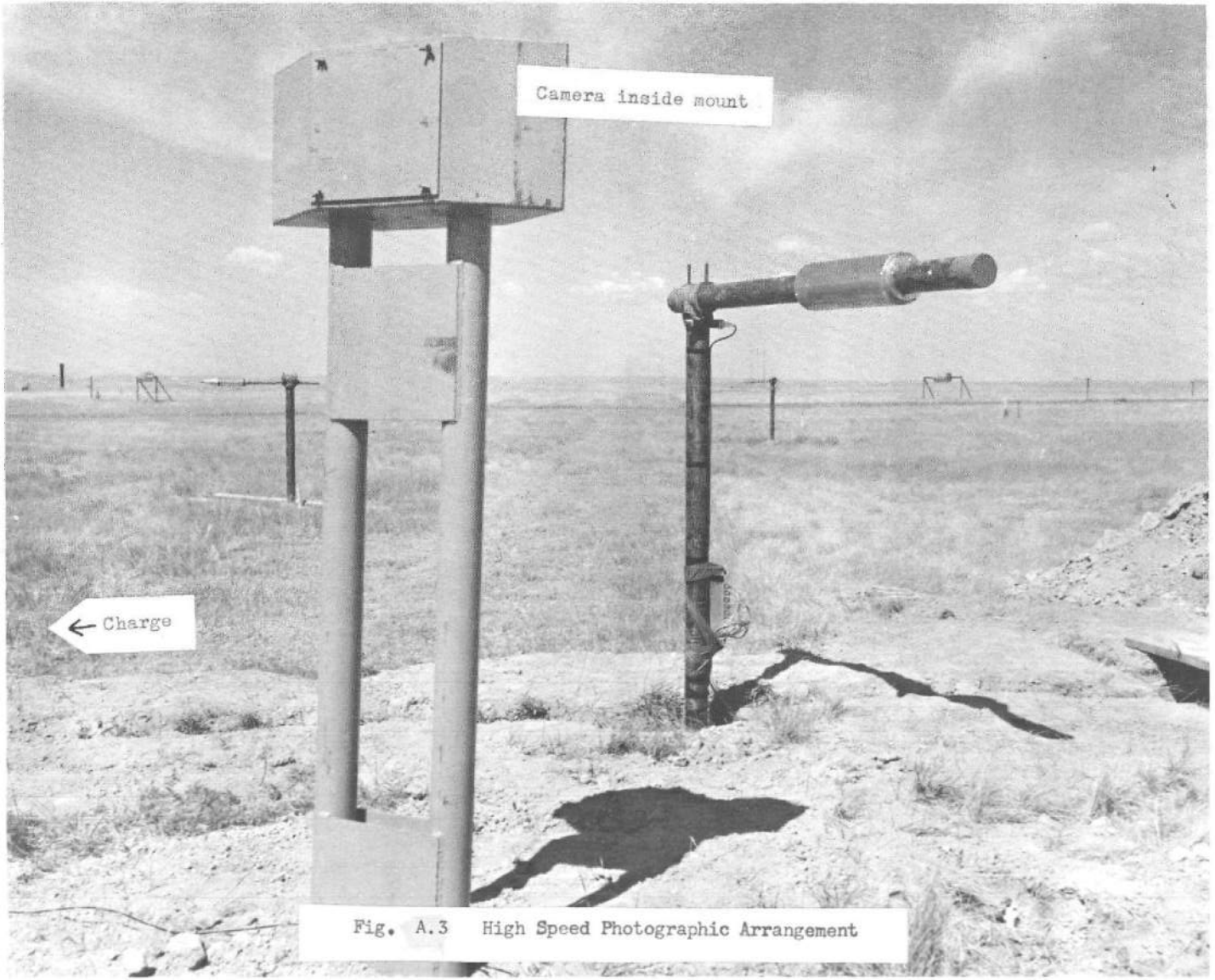

Fig. A.3 High Speed Photographic Arrangement

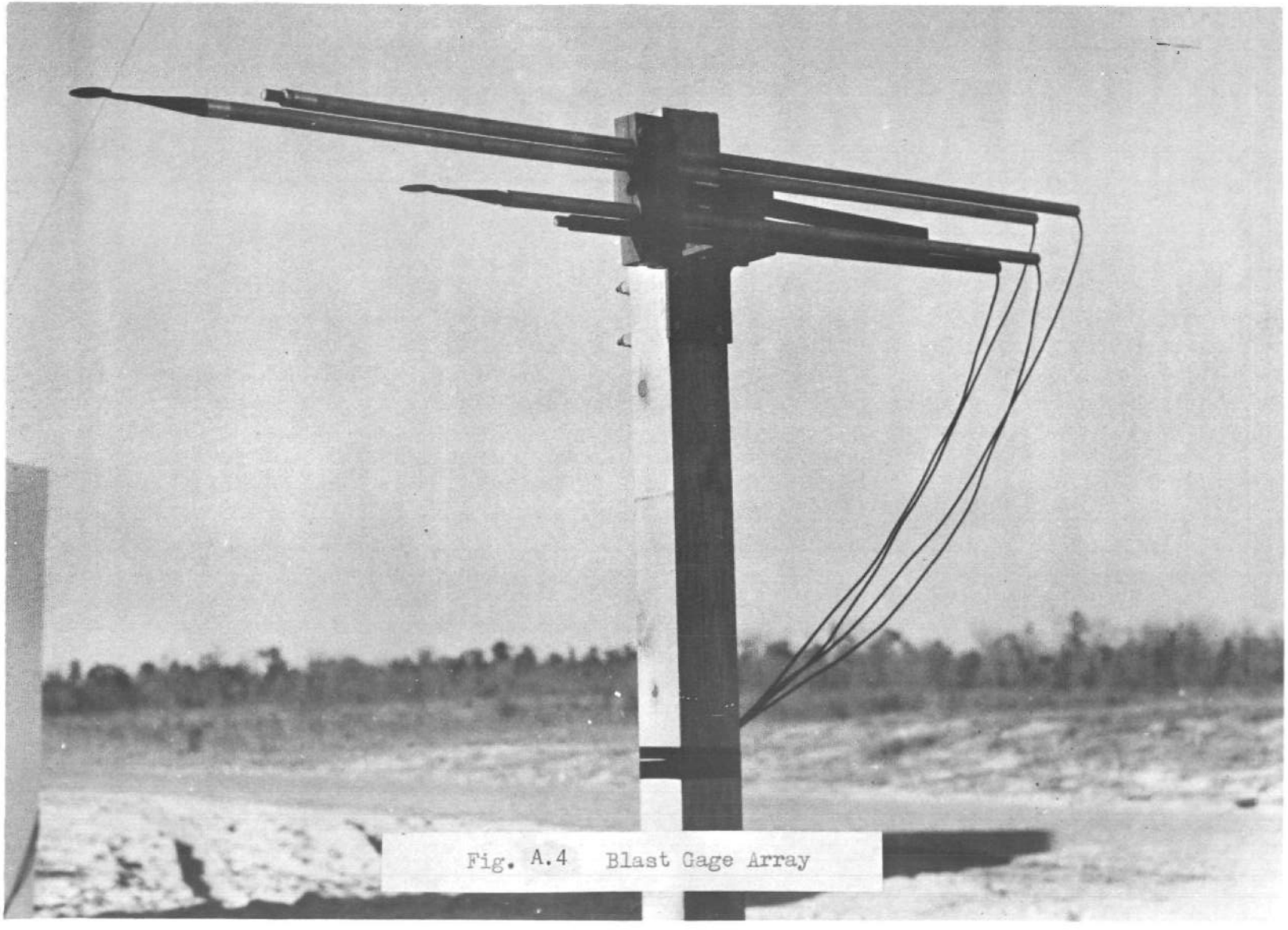

Fig. A.4 Blast Gage Array

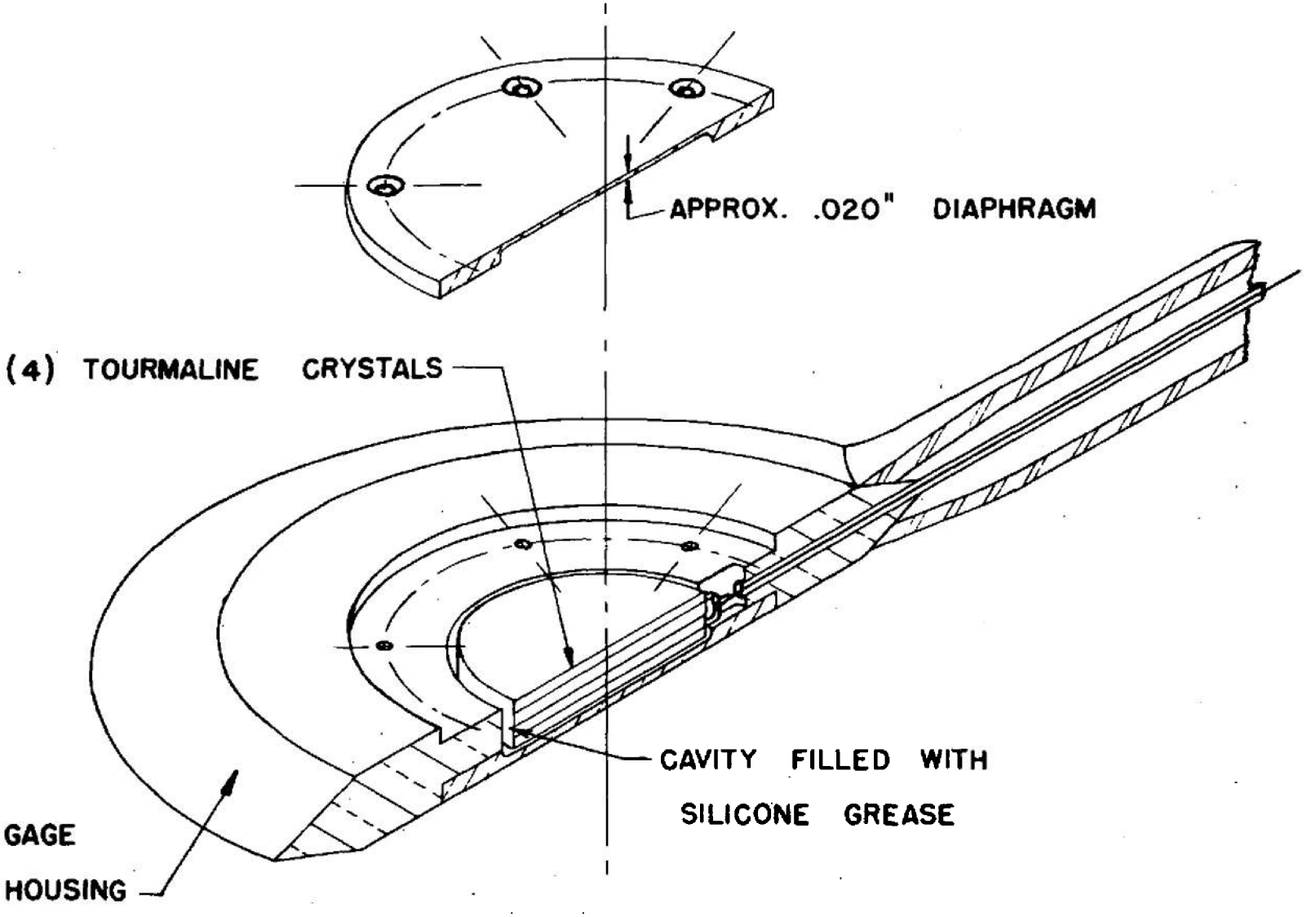

Fig. A.5 Piezoelectric Blast Gage

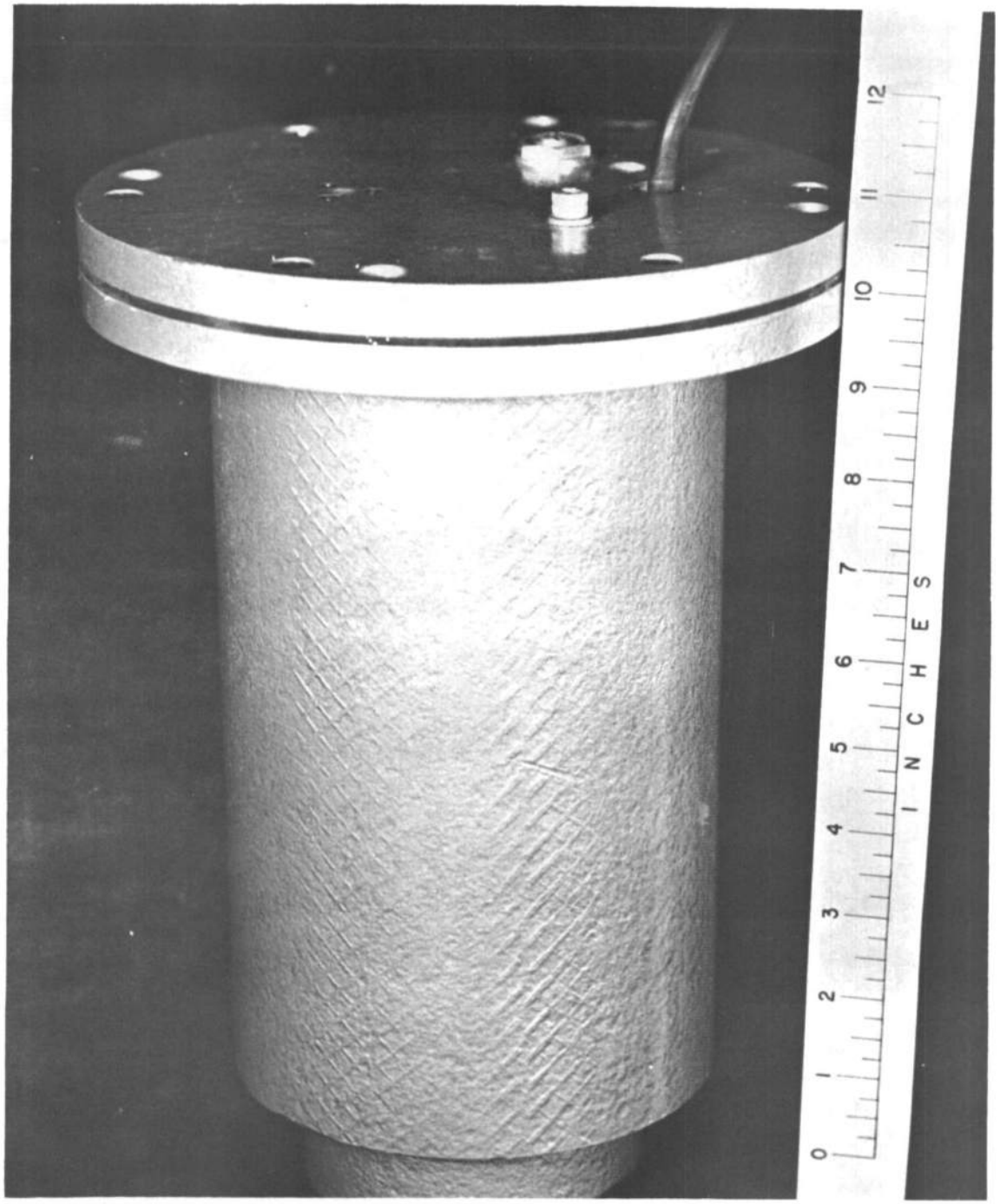

Fig. A.6 Self-Recording Gage

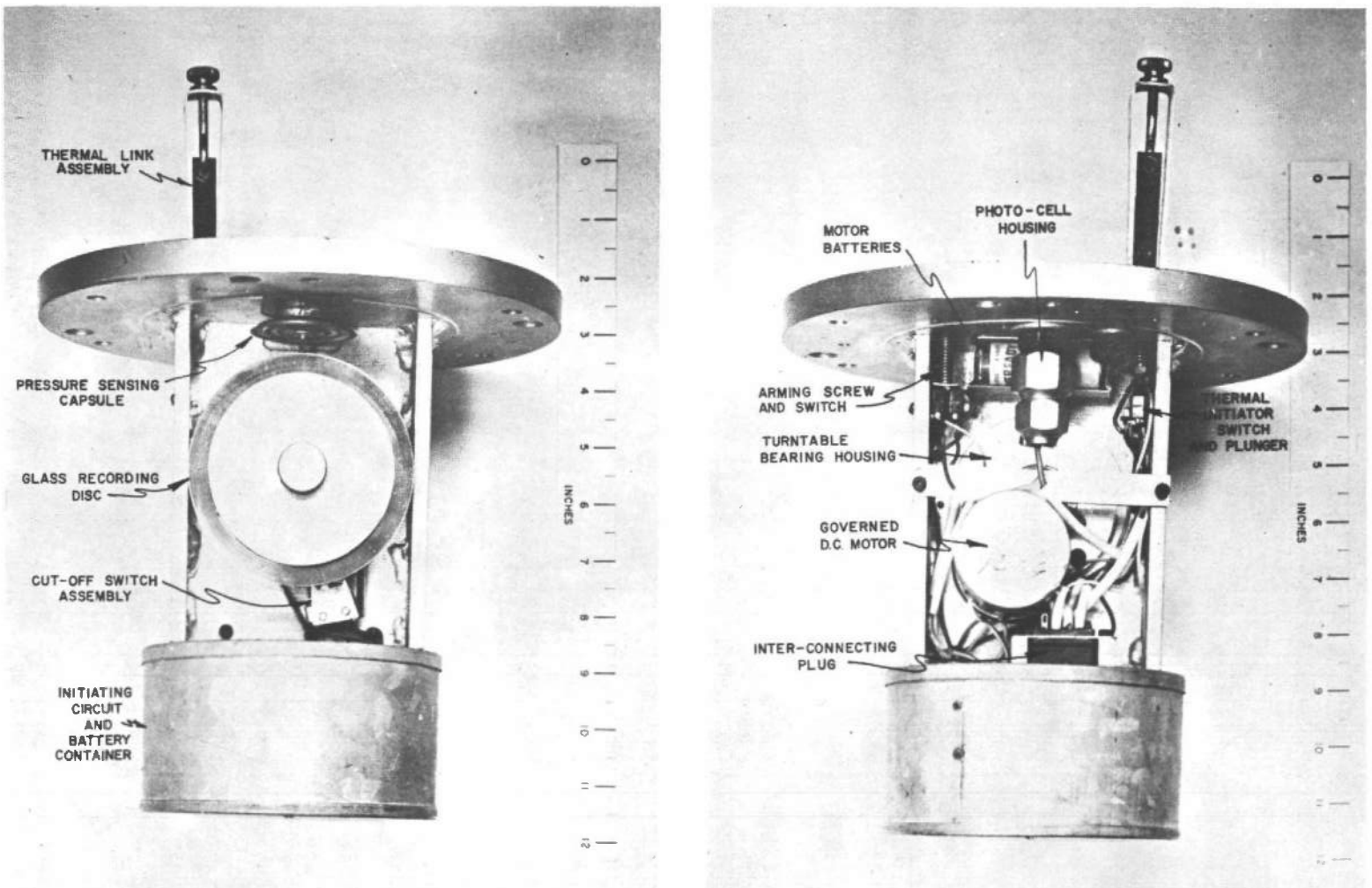

Fig. A.7 Details of Self-Recording Gage

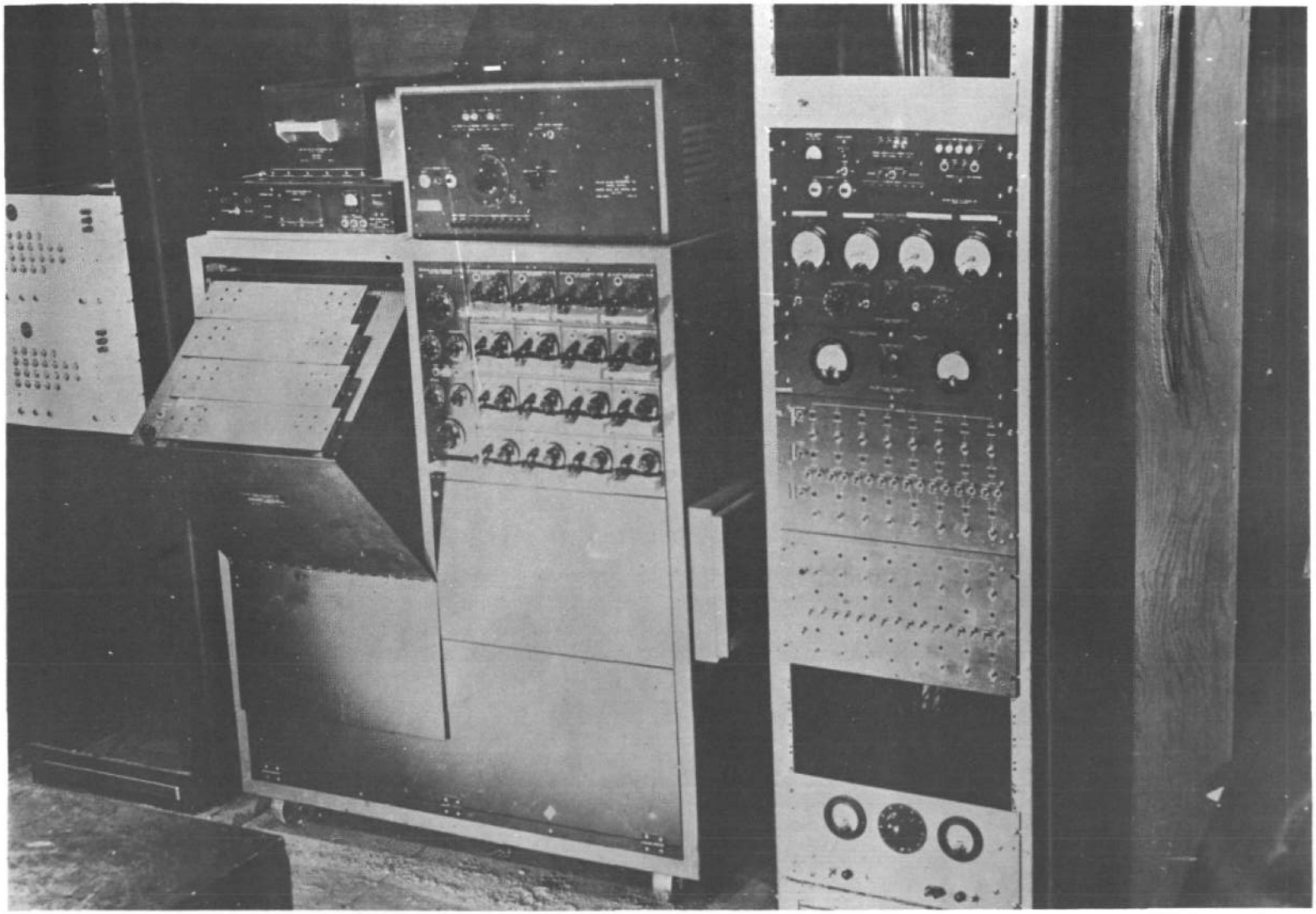

Fig. A.8 Pressure Recording Equipment

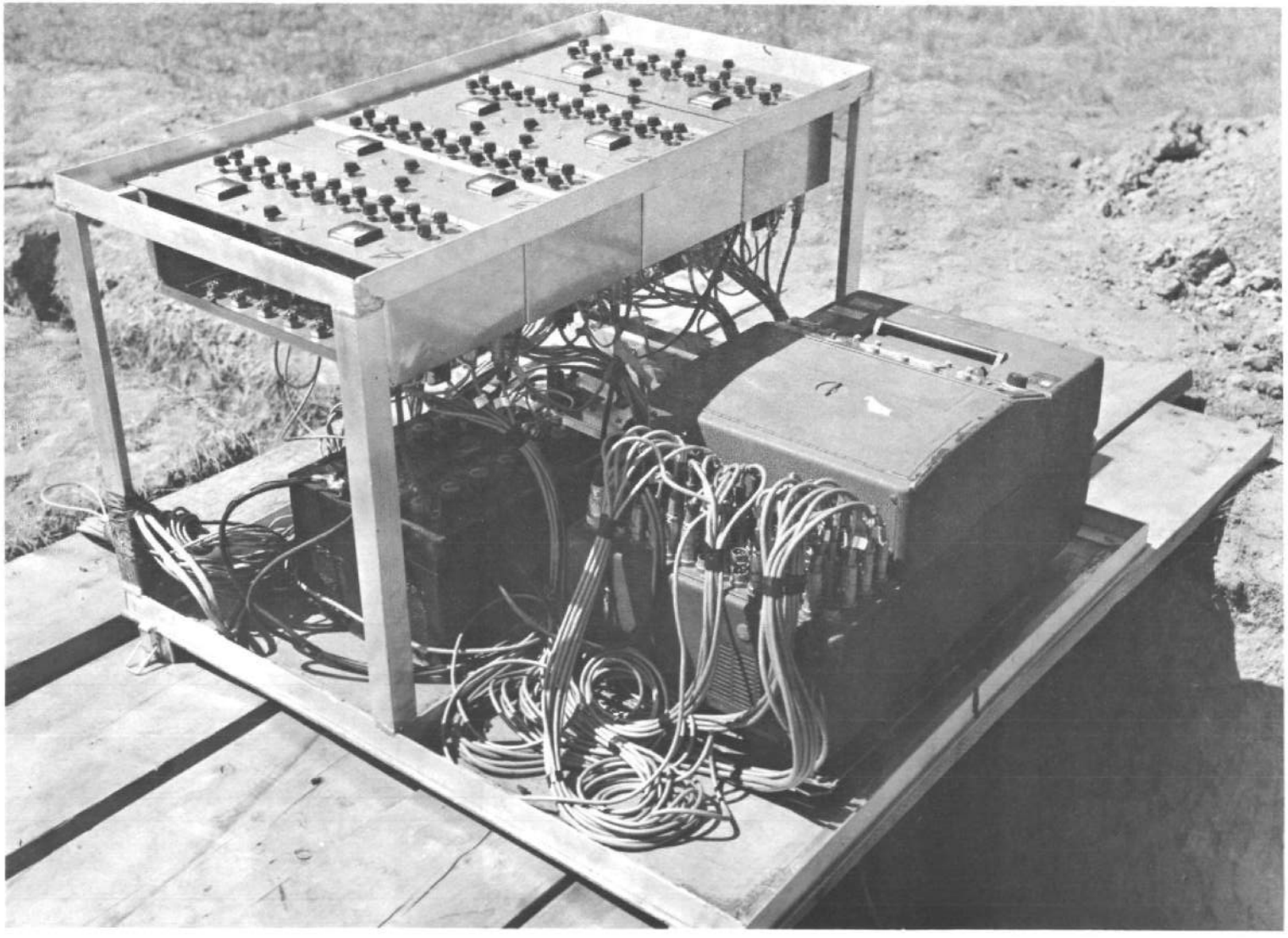

Fig. A.9 Strain Recording Equipment

Intentionally Left Blank.

APPENDIX B

TABLES OF DATA

Intentionally Left Blank.

TABLE B.1

Blast Parameters for Shells

Shell No.	Explosive Weight W (lbs.)	Explosive Distance R (ft.)	Pressure Incident p_i (psi)	Pressure Reflected p_r (psi)	Impulse Incident I_i (psi-msec)	Impulse Reflected I_r (psi-msec)
1	8.4	6.0	117.	662	28.8	112
2	389	29.0	60.3	198	89.0	299
3	1.1	2.5	159	1,070	15.5	69.5
4	8.4	7.0	82.4	331	26.9	95.8
5	64	16.0	58	185	48.8	160
6*	1.1	1.5**	448	3,600	17.0	119
7*	8.3	3.0	463	3,680	35.5	254
8	389	33.8	39.7	112	83.2	250
9	900	45.0	36.7	109	103	310
10	2,200	60.0	40.2	150	140	423
11	22,800	130**	41.5	157	310	937
12	54,500	215	25.2	81.0	350	969
13	1.4×10^6	800	14.5	---	950	---
14*	2,200	30**	197	1,180	204	1,010
15	22,800	70**	172	1,000	434	2,020
16	54,500	85	215	1,300	608	3,100
17	1.1	3.0	118	625	14.5	56.1
18	8.4	8.0	60.3	199	25.4	83.2
19	1.1	3.5	82.4	331	13.4	47.9
20	8.3	9.0	44.8	129	21.6	72.7
21	8.4	10.0	36.0	97.0	22.8	67.3
22	389	46.0	19.8	46.3	68.4	190
23	900	55.0	25.0	61.8	88.5	245
24	8.4	11.0	27.9	70.6	20.3	59.9
25	389	128**	2.9	5.95	23.4	50.4
26	8.4	4.5	213	1,590	32.6	153
27	64	10.0	166	1,160	60.8	268
28	389	23.9	96.7	419	98.5	380
29	2,200	44.0	84.5	400	170	618
30	22,800	90.0	99.0	490	369	1,460
31	54,500	130**	83.0	387	498	1,790
32	8.4	5.4	172	1,240	31.1	138
33	8.4	10.0	36.0	97.0	22.8	67.3
34	389	44.0	21.8	320	69.4	182
35	900	70.0	14.4	33.8	72.6	186
36	54,500	315	10.9	28.0	256	627
37	1.4×10^6	1,060	8.50	---	740	---
38*	1.4×10^6	630	25.0	---	1,150	---
39	8.4	5.8	130	706	29.6	116
40	64	13.0	91.3	419	64.0	200
41	389	28.0	63.6	213	92.0	307

TABLE B.1 (Cont'd.)

Shell No.	Explosive Weight W (lbs.)	Explosive Distance R (ft.)	Pressure Incident p_i (psi)	Pressure Reflected p_r (psi)	Impulse Incident I_i (psi-msec)	Impulse Reflected I_r (psi-msec)
42	2,200	59.0	42.0	160	142	433
43	22,800	130**	41.5	157	310	937
44	54,500	185	35.8	128	388	1,200
45	8.4	3.0	463	3,680	35.5	254
46	64	9.0**	209	1,600	64.0	304
47	389	18.0	174	1,205	119	489
48	1.4×10^6	960	10.0	---	805	---
49	389	25.0	83.7	338	98.8	344
50*	66	5.5**	544	4,260	71.9	566
51*	389	9.0**	617	5,000	130	1,200
52	389	15.0	257	1.985	118	592
53	1.4×10^6	1,250	6.30	---	635	---
54	1.4×10^6	690	20.5	---	1,070	---
55	115	15.0	107	544	68.5	266
56	389	25.0**	83.7	338	98.8	344
57*	389	11.0**	404	3,010	124	73.0
58	78,000	245	24.5	62.5	390	1,090
59	389	178	1.87	3.75	17.5	32.3
60	1.0	12.5	5.05	10.4	4.6	10.8
61	8.4	35.0	3.04	6.17	7.55	14.7
62	389	200	1.62	3.20	16.1	28.6
63	115	114	1.98	4.25	12.7	26.4
64	900	250	1.72	3.53	22.7	40.6
65	2,200	350**	1.66	3.48	29.6	59.8
66	22,800	810	1.53	3.23	60.5	126
67	54,500	1,150**	1.42	2.98	76.8	133
68	389	197	1.65	3.26	16.2	29.2
69	1.1	10.5	7.12	15.1	5.62	13.4
70	8.6	26.0	4.84	10.0	9.41	21.2
71	115	70.0	4.08	8.24	20.2	45.1
72	8.4	35.0	3.05	6.17	7.10	15.3
73	115	90.0	2.75	5.59	15.9	34.1
74	1.1	7.0	16.6	39.7	8.27	21.3
75	1.1	8.0	12.5	28.4	7.33	18.3
76	1.0	8.0	12.1	27.8	7.3	19.0
77	8.5	20.0	7.94	17.2	12.0	30.2
78	115	58.0	5.48	12.6	23.8	54.2
79	389	106	4.26	7.94	29.2	65.7
80	900	150	3.53	7.20	36.7	79.8
81	2,200	245	2.62	5.75	41.3	87.8
82	22,800	500**	2.90	6.40	96.6	206
83	54,500	650**	3.06	6.65	133	286
84	1.4×10^6	1,850	3.30	---	425	---
85	389	128**	2.94	5.95	24.1	51.1
86	389	285**	1.06	2.19	11.6	18.2

TABLE B.1 (Cont'd.)

Shell No.	Explosive Weight W (lbs.)	Explosive Distance R (ft.)	Pressure Incident p_i (psi)	Pressure Reflected p_r (psi)	Impulse Incident I_i (psi-msec)	Impulse Reflected I_r (psi-msec)
87	1.1	11.0	6.80	14.1	5.54	12.8
88	389	172	2.0	3.97	18.2	35.0
89	1.1	6.5	19.7	47.0	8.72	23.3
90	8.6	16.0	12.3	27.9	14.5	36.2
91	115	44.0	9.41	20.6	31.1	75.2
92	1.1	7.0	16.6	39.7	8.21	21.3
93	8.5	22.0	6.53	13.2	11.0	25.4
94	115	48.0	7.82	17.1	28.6	67.8
95	1.1	6.5	19.7	47.0	8.72	23.3
96	8.2	18.0	9.40	20.6	12.8	31.0
97	1.0	6.0	22.1	54.4	9.4	26.0
98	8.4	15.0	13.5	33.8	15.4	40.6
99	115	35.0	15.3	34.6	37.4	97.0
100	389	59.6	11.5	25.9	51.1	131
101	900	70.0	14.4	33.8	72.6	186
102	2,200	110	10.3	26.8	86.4	211
103	22,800	270	8.20	20.3	170	400
104	54,500	350	8.79	21.7	233	559
105	1.0	4.0	58.8	176	12.5	40.0
106	8.4	9.0	45.6	135.2	23.4	73.5
107	115	20.0	55.8	172	57.6	185
108	389	35.8	35.0	97.0	81.8	230
109	2,200	55.0	44.5	198	150	464
110	22,800	125**	45.0	173	318	971
111	54,500	150**	59.0	247	456	1,500
112	1.1	20.0	2.50	5.07	2.99	6.19
113	8.4	60.0	1.5	2.94	5.08	7.30
114	115	150	1.41	2.87	9.85	16.9
115	389	350	0.82	1.73	9.60	13.9
116*	389	180	1.84	37.0	17.5	32.8
117	2,200	575	0.91	1.88	18.2	35.1
118	22,800	1,200	0.94	1.98	41.8	80.9
119	54,500	1,800	0.84	1.74	49.4	72.2
120	22,800	300**	6.78	16.3	155	358
121	8.5	48.0	1.94	3.89	5.23	10.8
122	115	90.0	2.75	5.59	15.9	34.1
123	1.1	10.0	7.94	17.2	6.02	15.1
124	8.3	25.0	5.14	10.7	9.54	22.1
125	389	150	2.47	4.78	21.2	40.2
126	2,200	260	2.43	5.28	39.0	82.6
127	22,800	640	2.05	4.44	76.1	159
128	54,500	850	2.10	4.46	103	215
129	1.4×10^6	1,550	4.35	---	508	---
130*	1.4×10^6	880	12.0	---	865	---
131	54,500	225**	22.7	71.0	338	923

TABLE B.1 (Cont'd.)

Shell No.	Explosive Weight W (lbs.)	Explosive Distance R (ft.)	Pressure Incident p_i (psi)	Pressure Reflected p_r (psi)	Impulse Incident I_i (psi-msec)	Impulse Reflected I_r (psi-msec)
132	1.1	12.5	5.32	10.7	4.95	11.2
133	8.5	48.0	1.97	3.90	5.27	11.0
134	115	95.0	2.55	5.15	15.1	32.2
135	1.1	2.5	177	1,030	15.7	73.7
136	1.1	2.67	153	850	15.3	67.6
137	1.1	2.9	130	765	15.0	62.5
138	1.1	3.0	119	675	14.7	59.6
139	1.1	3.5	85.2	346	13.6	48.9
140	8.5	9.0	45.6	135	23.4	73.5
141	115	26.0	29.6	96.0	47.9	137
142	900	45.0	36.7	109	103	310
143	2,200	60.0	40.2	150	140	422
144	22,800	160	25.5	82.0	264	730
145	54,500	220	23.9	76.0	344	950
146	1.1	4.6	43.0	160	11.0	34.2
147	1.1	5.0	35.3	125	10.5	31.0
148	1.1	5.4	29.5	100	9.92	28.3
149	1.1	5.8	25.0	80.0	9.30	26.0
150	1.1	6.0	23.1	73.0	9.13	25.0
151	1.1	6.0	23.1	73.0	9.13	25.0
152	1.1	5.83	24.5	78.0	9.31	25.7
153	1.0	2.0	264	2,060	16.5	84
154	8.4	6.0	116	625	28.4	1.10
155	115	17.0	80.8	720	64.3	229
156	2,200	44.0	84.5	400	170	618
157	54,500	130	80.4	387	498	1,790
158	1.0	3.0	112	588	14.2	55.0
159	8.5	8.0	57.5	184	24.0	80.0
160	115	22.0	45.6	130	54.2	167
161	900	55.0	25.0	61.8	88.5	245
162	2,200	70.0	28.5	94.0	126	354
163	22,800	150	29.5	102	277	790
164	54,500	215	25.5	81.0	350	969
165	1.4×10^6	690	20.5	---	1,070	---
166	1.1	1.8	346	2,330	17.3	116
167	389	25.0	83.7	338	98.8	344
168	389	16.0	218	1,660	118	562
169	1.4×10^6	640	24.0	---	1,130	---
170	1.0	8.0	12.4	27.9	7.55	19.6
171	1.1	10.0	7.80	16.2	5.92	14.8
172	1.1	10.0	7.80	16.2	5.92	14.8
173	1.1	15.0	3.97	7.95	4.08	8.77
174	1.1	16.0	3.53	7.05	3.90	8.20
175	15.0	60.0	1.91	3.75	5.93	11.4
176	8.3	16.0	11.9	27.2	14.7	39.2

TABLE B.1 (Cont'd)

Shell No.	Explosive Weight W (lbs.)	Explosive Distance R (ft.)	Pressure Incident p_i (psi)	Pressure Reflected p_r (psi)	Impulse Incident I_i (psi-msec)	Impulse Reflected I_r (psi-msec)
177	66	40.0	7.65	16.5	23.4	58.5
178	115	70.0	4.18	8.66	21.1	46.8
179	389	275	1.07	2.28	11.7	19.0
180*	1.1	4.5	46.3	132	11.8	36.8
181*	64	20.0	34.5	91.0	42.5	130
182	1.0	20.0	2.57	5.80	3.06	6.22
183	1.1	13.0	4.85	10.2	4.60	10.4
184	8.4	40.0	2.50	5.0	5.84	12.9
185	1.1	25.0	1.91	3.82	2.90	4.70
186	1.1	10.0	7.80	16.2	5.92	14.8
187	8.2	24.0	5.68	11.5	9.66	23.2
188	15.0	40.7	3.24	6.48	8.58	18.1
189	15.0	20.0**	11.5	25.7	17.7	44.7
190	389	65.0	9.4	20.85	49.64	125.8
191	1.1	8.0**	12.4	27.9	7.55	19.6
192	15.0	25.0**	7.35	15.7	13.8	34.4
193	389	75.0	7.20	15.42	43.8	105.8
194	1.1	10.0	7.80	16.2	5.92	14.8
195	8.2	20.0	7.65	16.3	11.7	28.8
196	15.0	35.2	3.97	8.10	10.0	22.1
197	389	160**	2.16	4.30	19.7	38.0
198	14.8	75.5	1.40	2.79	4.66	8.08
199	15.0	70.1	1.54	3.10	5.05	9.10
200	389	150**	2.32	4.73	21.2	42.3
201	389	160**	2.16	4.30	19.7	38.0
202	15.0	30.0	5.28	11.0	11.8	26.6
203	15.0	30.0	5.28	11.0	11.8	26.6
204	389	200	1.76	3.23	15.7	29.2

* Shells loaded longitudinally, all others loaded laterally.

** No permanent deformation at this distance.

TABLE B.2

Strain Data for Shells at Ballistic Research Laboratories

Round No.	106	107	109	110	111
Explosive Wt. (lb.)	1.06	1.06	1.07	8.19	8.19
Explosive Dist. (ft.)	3.75	3.75	3.5	8.0	8.0
Press. p_i (psi)	69.2	69.2	82.4	58.8	58.8
Gage Position	Maximum Strain (μ in/in)				
1L	603	551	611	--	--
1C	1,635	1,281	1,749	1,923	--
2L	559	536	752	581	633
2C	790	752	1,112	656	894
3L	909	668	1,308	726	983
3C	1,065	663	646	1,749	1,543
4L	577	574	745	612	656
4C	641	514	790	734	1,013

Shell Dimensions - Diameter - 3", Length - 9", Thickness - .019"

Material - Steel

TABLE B.3

Strain Data for Shells at Suffield Experimental Station

Shell No.	37	48	165	169
Diameter (D)	6.0	12.0	6.0	9.0
Length (L)	18.0	36.0	18.0	27.0
Thickness (t)	0.035	0.035	0.042	0.065
Material	Steel	Steel	Aluminum Tubing	Aluminum Tubing
Pressure (p_i)	8.50	10.0	20.5	24.0
Gage Position	Maximum Strain (μ in/in)			
1L	--	302	438	--
1C	--	837	550	4,493
2L	422	897	692	1,405
2C	227	761	1,425	--
3L	--	747	396	--
3C	--	1,505	2,970	4,589
4L	--	883	533	--
4C	427	2,030	2,159	1,360

TABLE B.4

Comparison of Actual and Calculated Pressures for Failure Deformation

Shell No.	Incident Pressure* p_i (psi)	Calculated Critical Pressure p_{cr} (psi)	Deviation %	Remarks
1	117	117	0	
2	48.5	59.7	+23.1	
3	159	160	+ 0.6	
4	82.4	83.3	+ 1.1	
5	58	55.3	- 4.7	
6**	448	960***	-	No Deformation
7**	463	500***	+ 8.0	
8	39.7	42.4	+ 6.8	
9	36.7	36.7	0	
10	40.2	33.7	-16.1	
11	41.5	26.0	-	No Deformation
12	25.2	23.7	- 6.0	
13	14.5	18.6	+22.1	
14**	197	223***	-	No Deformation
15**	172	172***	-	No Deformation
16**	215	157***	-	Excess Deformation
17	118	118	0	
18	60.3	61.4	+ 1.8	
19	82.4	95.0	+15.3	
20	44.8	49.4	+10.3	
21	36.0	40.0	+11.1	
22	17.4	20.4	+17.2	
23	25.0	18.5	-26.0	
24	27.9	30.2	+ 8.2	
25	2.9	15.4	-	No Deformation
26	213	232	+ 8.9	
27	166	154	-	No Deformation
28	96.7	113	+16.8	
29	84.5	93.5	+10.7	
30	99.0	72.2	-27.1	
31	82.0	65.8	-	No Deformation
32	172	112	-34.9	
33	36.0	38.9	+ 8.0	
34	21.8	19.8	- 9.2	
35	14.4	17.9	+24.4	
36	10.9	11.6	+ 6.4	
37	8.50	9.00	+ 5.6	
38**	25.0	54.0	+53.7	
39	130	113	-13.1	
40	91.3	74.6	-29.3	
41	63.6	55.6	-12.6	

TABLE B.4 (Cont'd.)

Shell No.	Incident Pressure* p_i (psi)	Calculated Critical Pressure p_{cr} (psi)	Deviation %	Remarks
42	42.0	46.1	+ 9.8	
43	41.5	35.6	-	No Deformation
44	35.8	32.4	- 9.5	
45	463	416	-10.1	
46	209	276	-	No Deformation
47	174	204	+17.2	
48	10.0	12.6	+20.6	
49	83.7	102	+21.9	
50*	544	800	-	No Deformation
51**	617	612	-	No Deformation
52	257	276	+ 7.3	
53	6.30	9.08	+30.6	
54	20.5	34.1	+39.9	
55	107	226	+52.7	
56	83.7	199	-	No Deformation
57**	404	1,200	-	No Deformation
58	24.5	136	-	No Deformation
59	1.87	2.16	+15.5	
60	5.05	4.62	- 8.5	
61	3.04	2.92	- 4.0	
62	1.62	1.91	+17.9	
63	1.98	2.10	+ 6.1	
64	1.72	1.80	+ 4.7	
65	1.66	1.73	+ 4.2	
66	1.53	1.60	+ 4.6	
67	1.42	1.54	-	No Deformation
68	1.65	1.60	- 3.0	
69	7.12	7.46	+ 4.6	
70	4.84	4.85	+ 0.2	
71	4.08	3.47	-17.6	
72	3.05	4.21	+27.6	
73	2.75	3.01	+ 8.6	
74	16.6	15.9	- 4.2	
75	12.5	13.1	+ 4.8	
76	12.1	11.5	- 5.0	
77	7.94	7.27	- 8.5	
78	5.48	5.26	- 4.0	
79	4.26	4.76	+11.7	
80	3.53	4.50	+27.5	
81	2.62	4.33	+65.3	
82	2.90	3.98	-	No Deformation
83	3.06	3.87	-	No Deformation
84	3.30	3.70	+10.8	

TABLE B.4 (Cont'd.)

Shell No.	Incident Pressure* p_i (psi)	Calculated Critical Pressure p_{cr} (psi)	Deviation %	Remarks
85	2.94	3.98	-	No Deformation
86	1.06	2.88	-	No Deformation
87	6.80	6.75	- 0.7	
88	2.0	2.02	+ 1.0	
89	19.7	18.8	- 4.7	
90	12.3	12.2	- 0.8	
91	9.41	8.72	- 7.9	
92	16.6	16.5	- 0.6	
93	6.53	10.6	+38.4	
94	7.82	7.60	- 2.9	
95	19.9	22.4	+12.1	
96	9.40	14.5	+35.2	
97	22.1	29.0	+31.2	
98	13.5	18.1	+34.1	
99	15.3	13.3	-13.1	
100	11.5	11.8	+ 2.6	
101	14.4	11.2	-22.2	
102	10.3	10.9	+ 5.8	
103	8.20	10.0	+21.9	
104	8.79	9.72	+10.6	
105	58.8	74.0	+25.8	
106	45.6	46.6	+ 2.2	
107	55.8	33.7	-39.6	
108	35.0	30.3	-13.4	
109	44.5	27.8	-37.5	
110	45.0	25.5	-	No Deformation
111	59.0	24.9	-	No Deformation
112	2.50	2.47	- 1.2	
113	1.50	1.54	+ 2.7	
114	1.41	1.14	-19.1	
115	0.82	1.03	+25.6	
116**	1.84	2.06***	+12.0	
117	0.91	0.94	+ 3.3	
118	0.94	0.87	- 7.4	
119	0.84	0.85	+ 1.2	
120**	6.78	1.94***	-	No Deformation
121	1.94	2.30	+15.6	
122	2.75	1.65	-66.7	
123	7.94	6.30	-20.7	
124	5.14	3.97	-22.8	
125	2.47	2.58	+ 4.4	
126	2.43	2.36	- 2.9	
127	2.05	2.17	+ 5.9	

TABLE B.4 (Cont'd.)

Shell No.	Incident Pressure* p_i (psi)	Calculated Critical Pressure p_{cr} (psi)	Deviation %	Remarks
128	2.10	2.12	+ 1.0	
129	4.35	5.17	+16.1	
130**	12.0	10.3	-16.5	
131	22.7	11.4	-	No Deformation
132	5.32	4.72	-12.7	
133	1.97	3.06	+35.6	
134	2.55	2.19	-16.4	
135	177	176	- 0.6	
136	153	142	- 7.2	
137	130	126	- 3.1	
138	119	99.4	-16.5	
139	85.2	88.0	+ 3.3	
140	45.6	51.9	+13.8	
141	29.6	34.3	+15.6	
142	36.7	29.1	-20.8	
143	40.2	27.6	-31.4	
144	25.5	25.6	+ 0.4	
145	23.9	25.1	+ 5.0	
146	43.0	46.0	+ 7.0	
147	35.3	37.9	+ 7.4	
148	29.5	33.1	+12.2	
149	25.0	25.7	+ 2.8	
150	23.1	23.0	- 0.4	
151	23.1	23.0	- 0.4	
152	24.5	23.0	- 6.1	
153	264	256	- 3.0	
154	116	149	+28.4	
155	80.8	101	+25.0	
156	84.5	80.8	- 4.4	
157	80.4	73.0	- 9.2	
158	112	99.3	-11.3	
159	57.5	58.8	+ 2.3	
160	45.6	38.6	-15.3	
161	25.0	32.8	+31.2	
162	28.5	31.2	+ 9.5	
163	29.5	28.7	- 2.7	
164	25.2	28.4	+12.7	
165	20.5	25.7	+20.1	
166	346	306	-11.6	
167	83.7	73.5	-12.2	
168	218	226	+ 3.7	
169	24.0	32.3	+25.7	
170	12.4	15.3	-	Excess Deformation

TABLE B.4 (Cont'd.)

Shell No.	Incident Pressure* p_i (psi)	Calculated Critical Pressure p_{cr} (psi)	Deviation %	Remarks
171	7.80	10.5	-	Excess Deformation
172	7.80	6.36	-	Excess Deformation
173	3.97	5.32	+34.0	
174	3.53	3.62	+ 2.5	
175	1.91	1.89	- 1.0	
176	11.9	2.15	-	Excess Deformation
177	7.65	1.53	-	Excess Deformation
178	4.18	1.40	-	Excess Deformation
179	1.07	1.08	+ 0.9	
180**	46.3	7.18***	-	Excess Deformation
181**	34.5	3.04***	-	Excess Deformation
182	2.57	2.71	+ 9.0	
183	4.85	2.16	-	Excess Deformation
184	2.50	1.30	-	Excess Deformation
185	1.91	1.45	-24.1	
186	7.80	6.19	-20.6	
187	5.68	3.71	-34.7	
188	3.24	3.22	- 0.6	
189	11.5	16.6	-	No Deformation
190	9.40	9.60	+ 2.1	
191	12.4	21.8	-	No Deformation
192	7.35	11.3	-	No Deformation
193	7.20	6.60	- 8.3	
194	7.80	7.50	- 3.8	
195	7.65	4.46	-	Excess Deformation
196	3.97	3.90	- 1.8	
197	2.16	2.25	-	No Deformation
198	1.40	1.80	+28.6	
199	1.54	1.48	- 3.9	
200	2.32	4.69	-	No Deformation
201	2.16	4.09	-	No Deformation
202	5.28	3.72	-	Excess Deformation
203	5.28	3.05	-	Excess Deformation
204	1.76	1.76	0.0	

* From Table B.1

** Longitudinal Loading Orientation (all others are lateral loading orientation)

*** Calculated Critical Pressures for Lateral Loading Orientation have been multiplied by 6.0 for Steel, 2.0 for Aluminum

APPENDIX C

TYPICAL DEFORMATION PATTERNS OF SHELLS

Intentionally Left Blank.

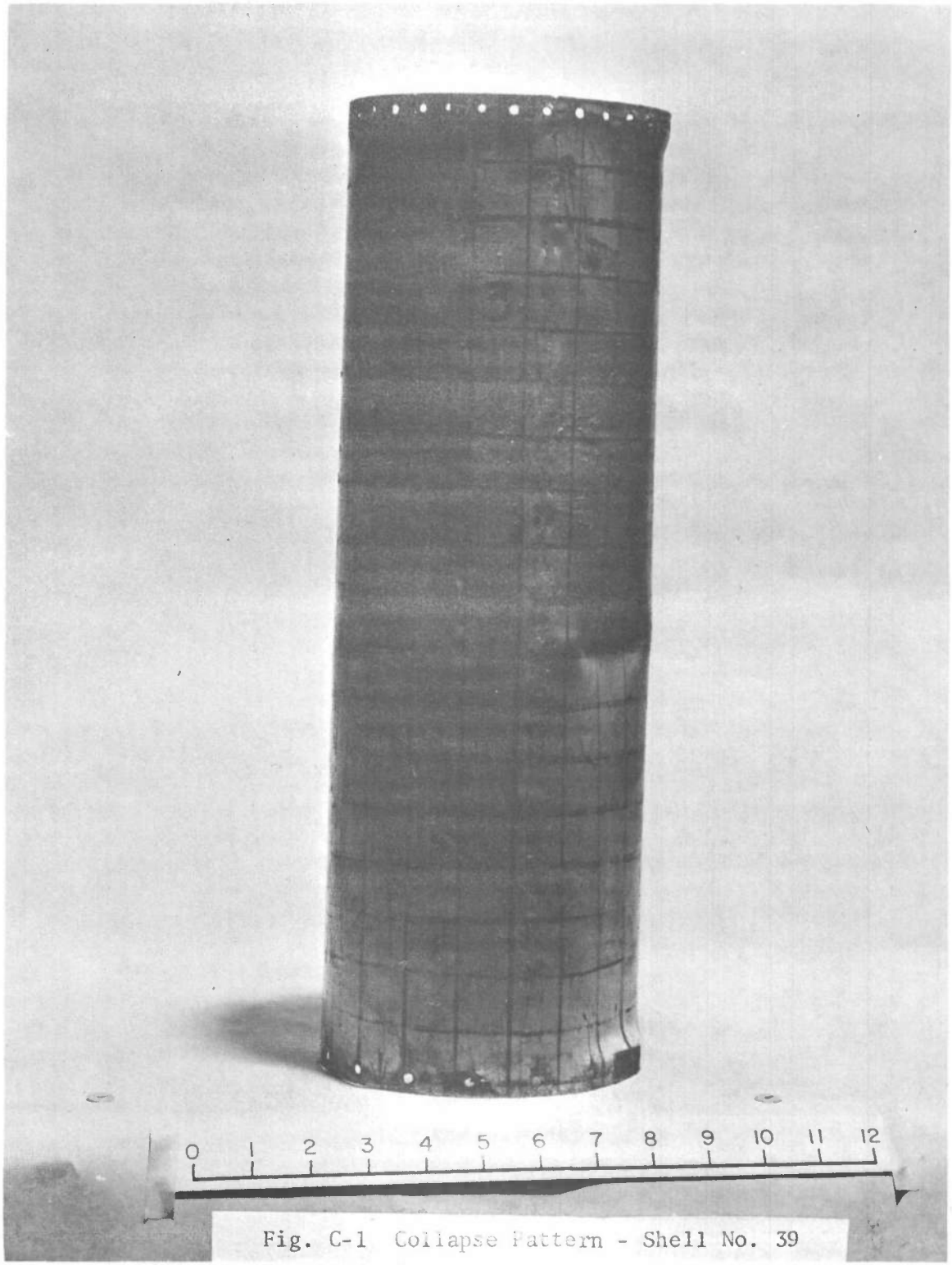

Fig. C-1 Collapse Pattern - Shell No. 39

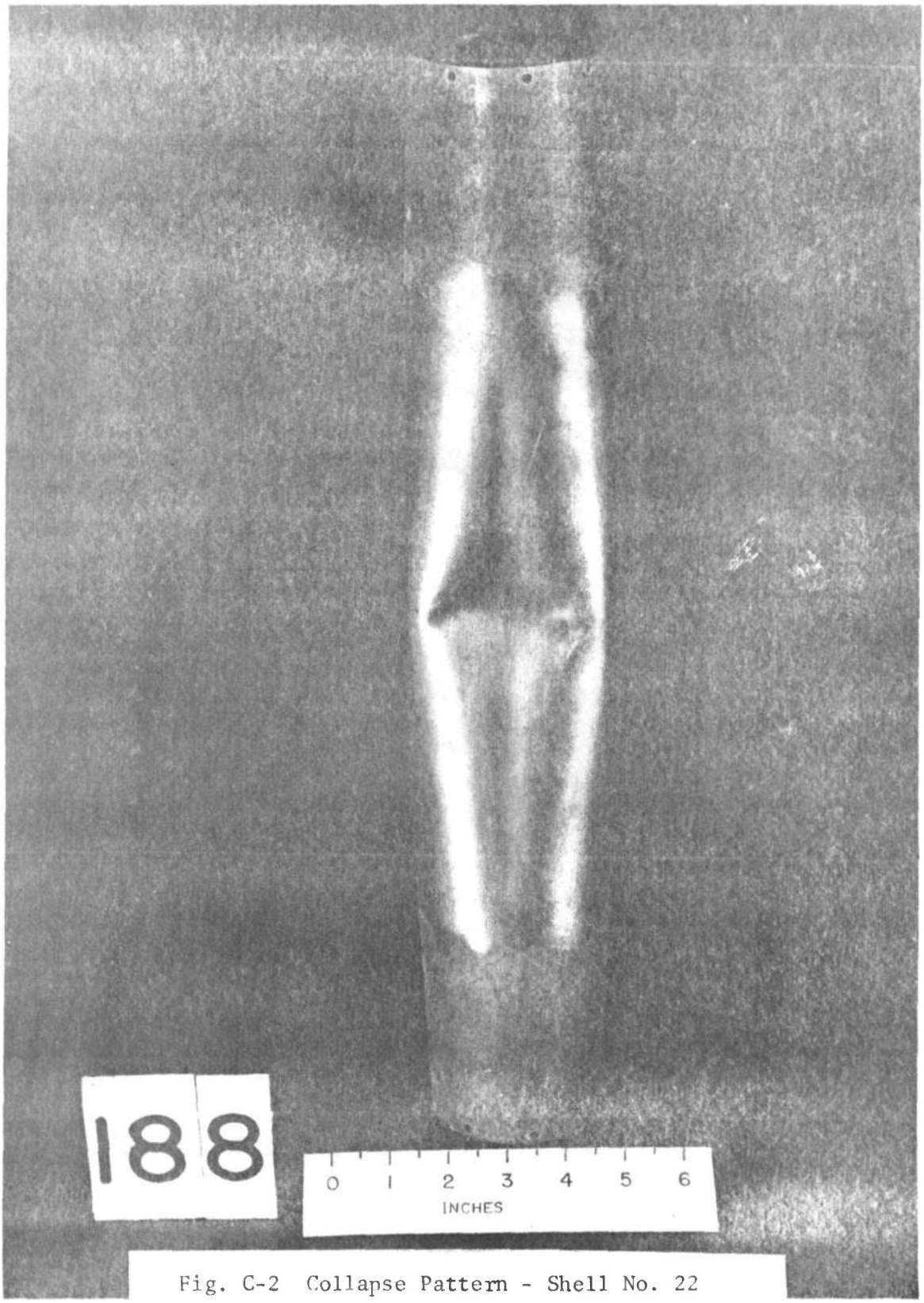

Fig. C-2 Collapse Pattern - Shell No. 22

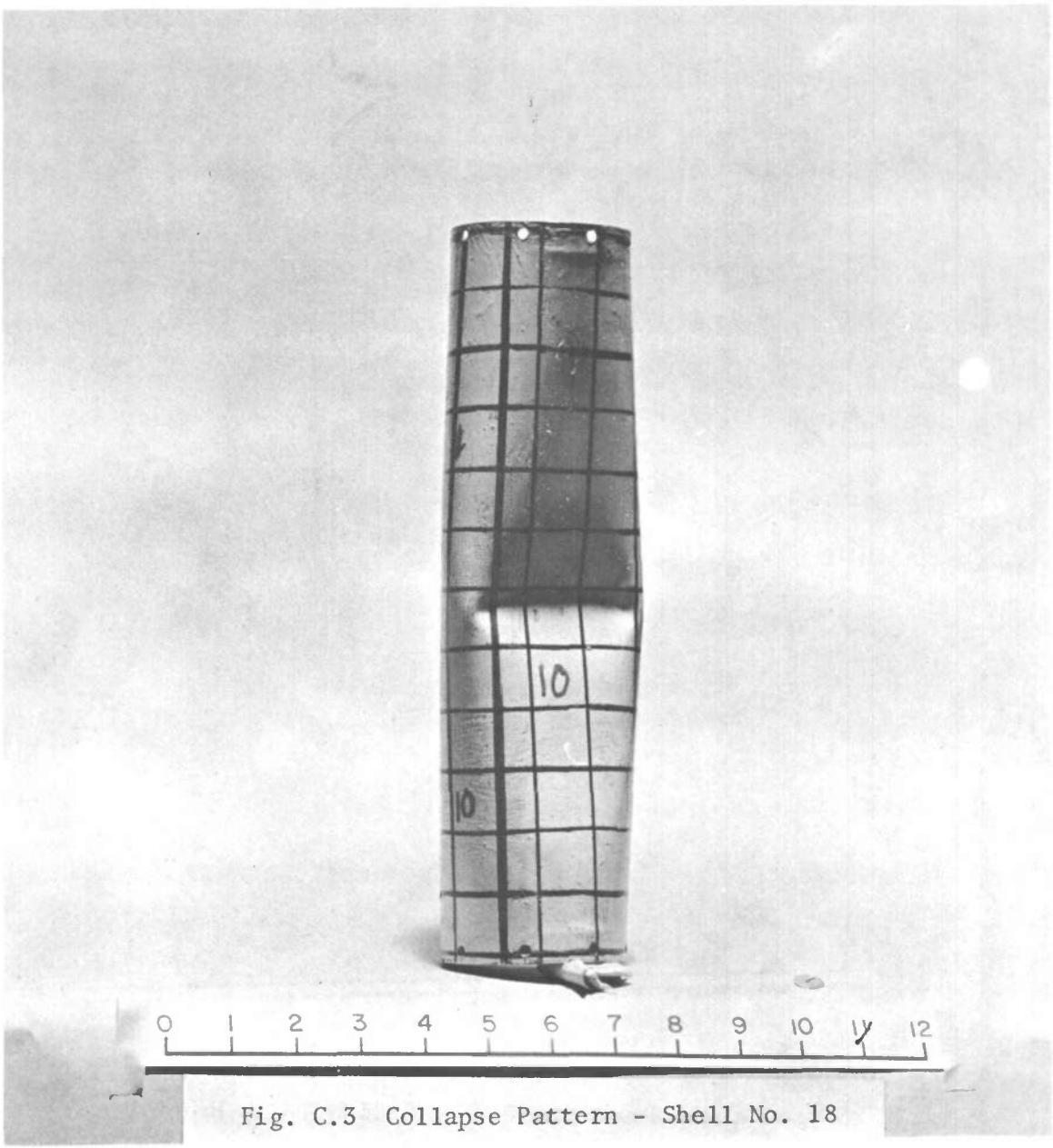

Fig. C.3 Collapse Pattern - Shell No. 18

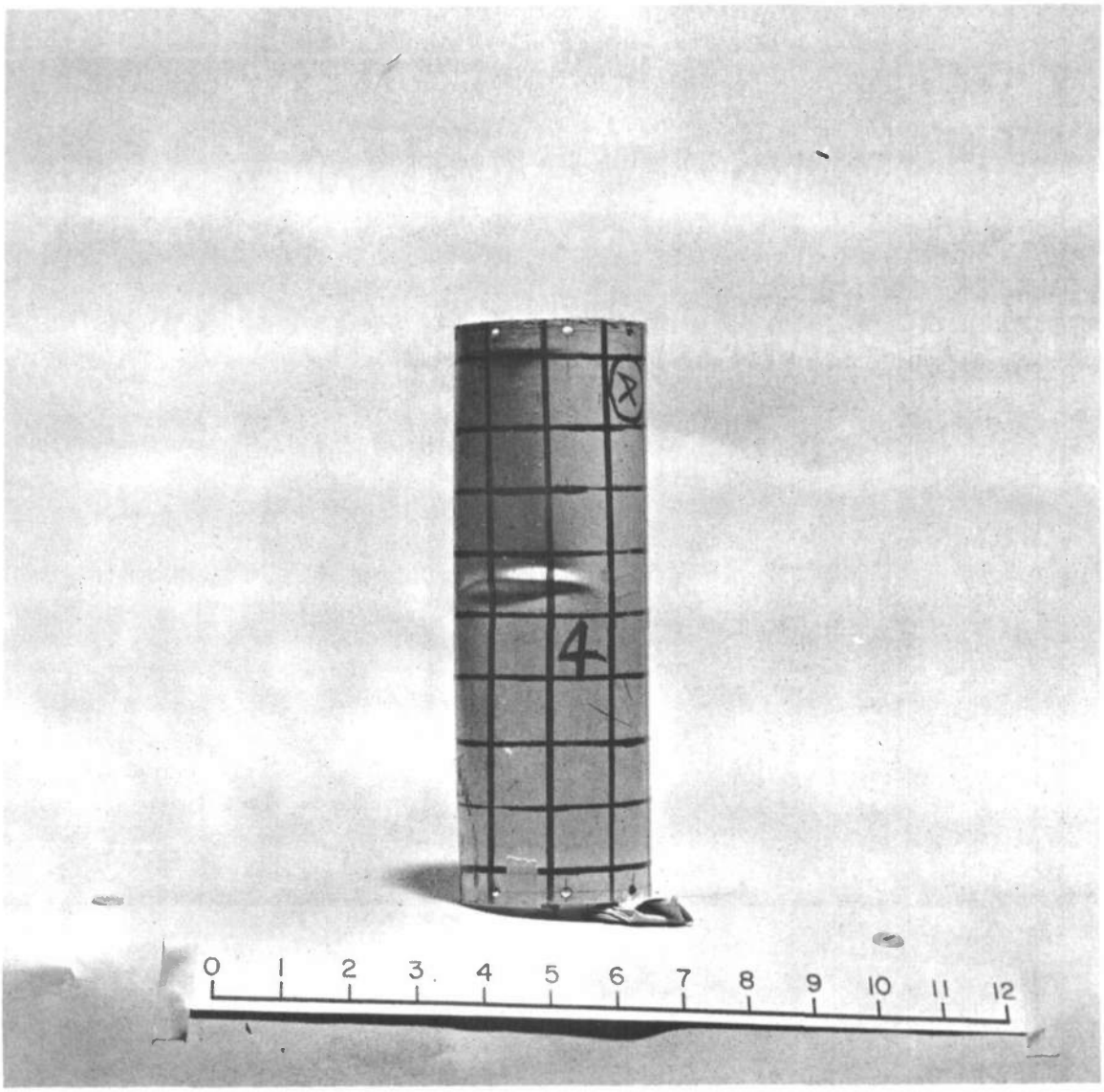

Fig. C.4 Special Collapse Pattern - Shell No. 4 - Front View

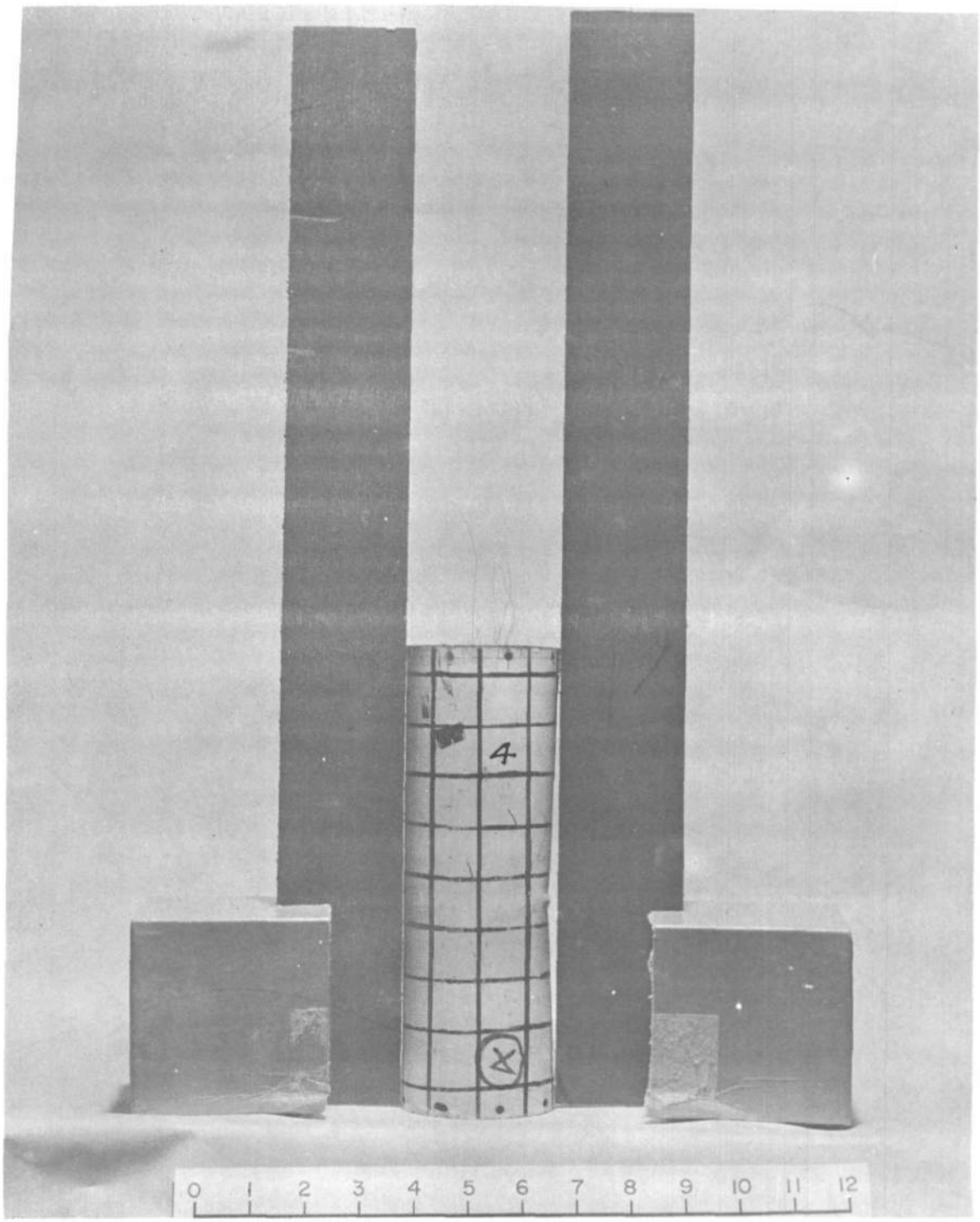

Fig. C.5 Special Collapse Pattern - Shell No. 4 - Side View

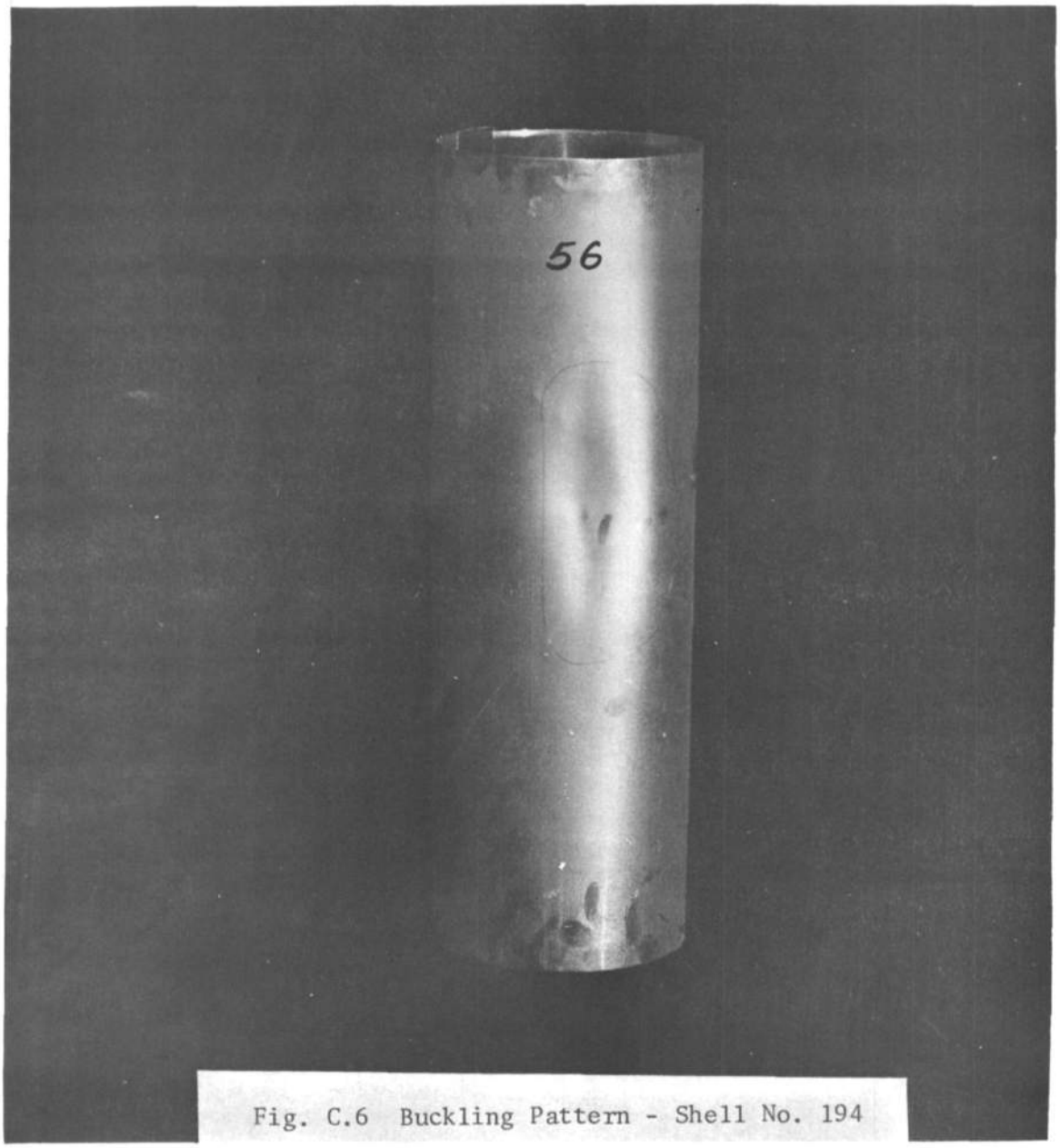

Fig. C.6 Buckling Pattern - Shell No. 194

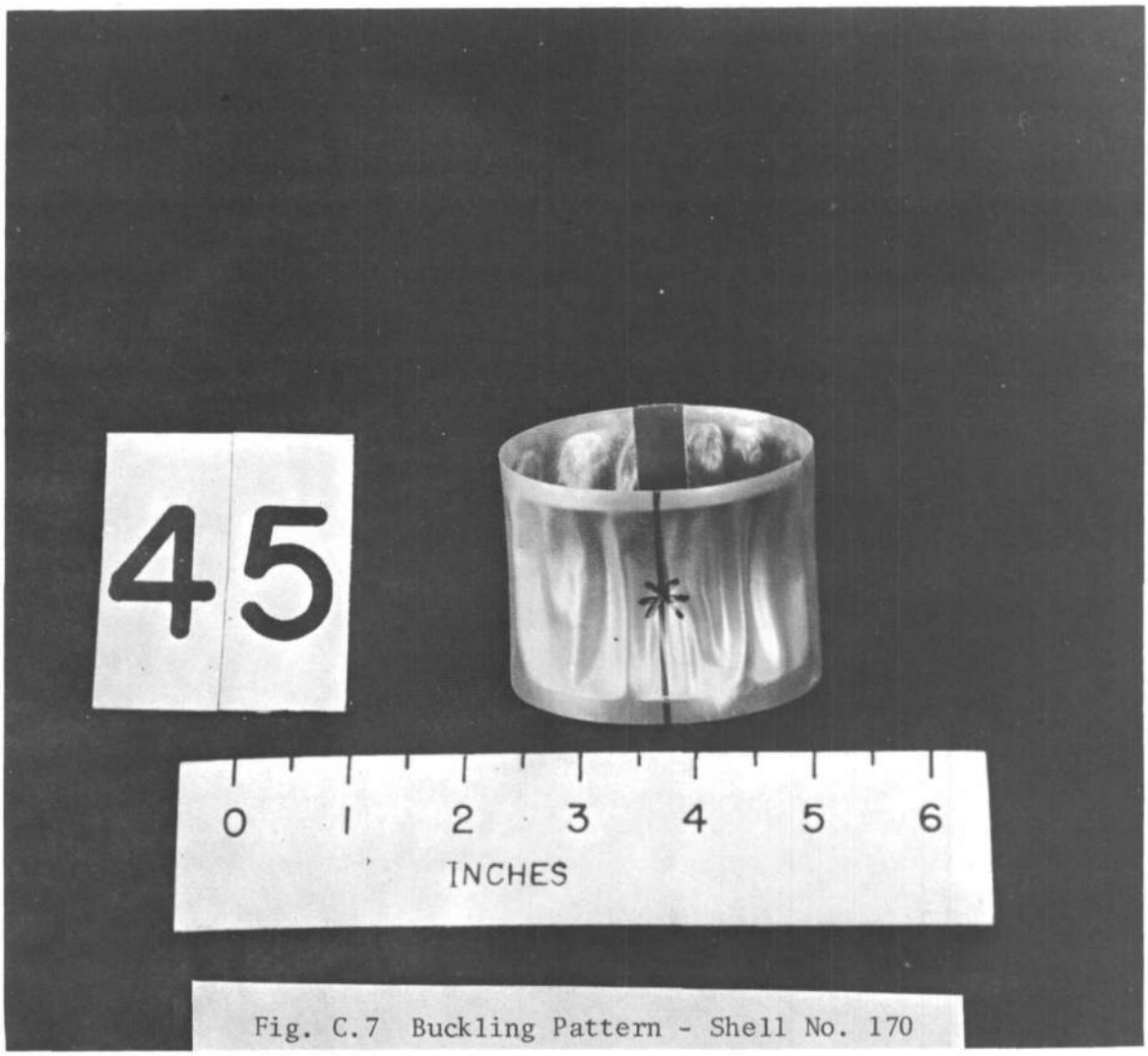

Fig. C.7 Buckling Pattern - Shell No. 170

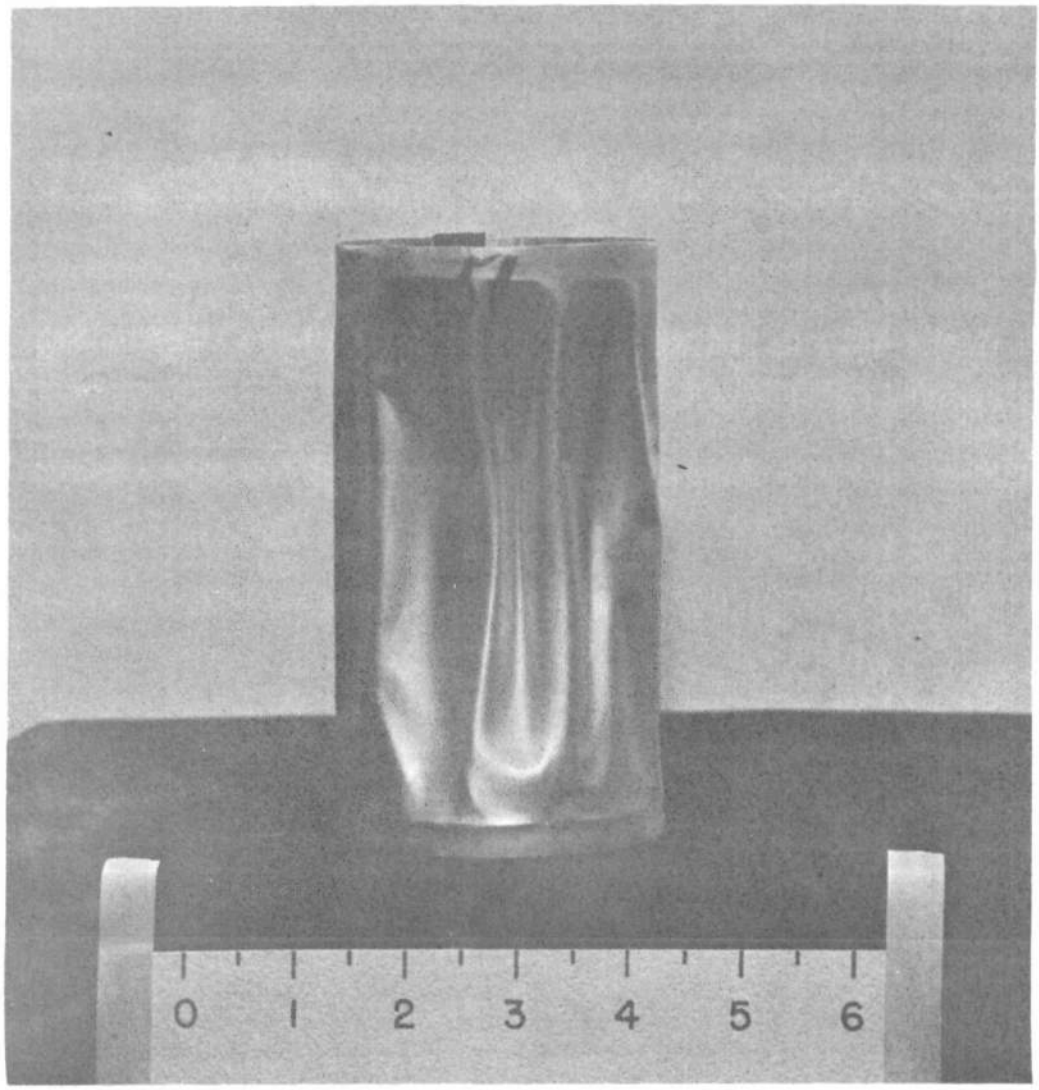

Fig. C.8 Buckling Pattern - Shell No. 172

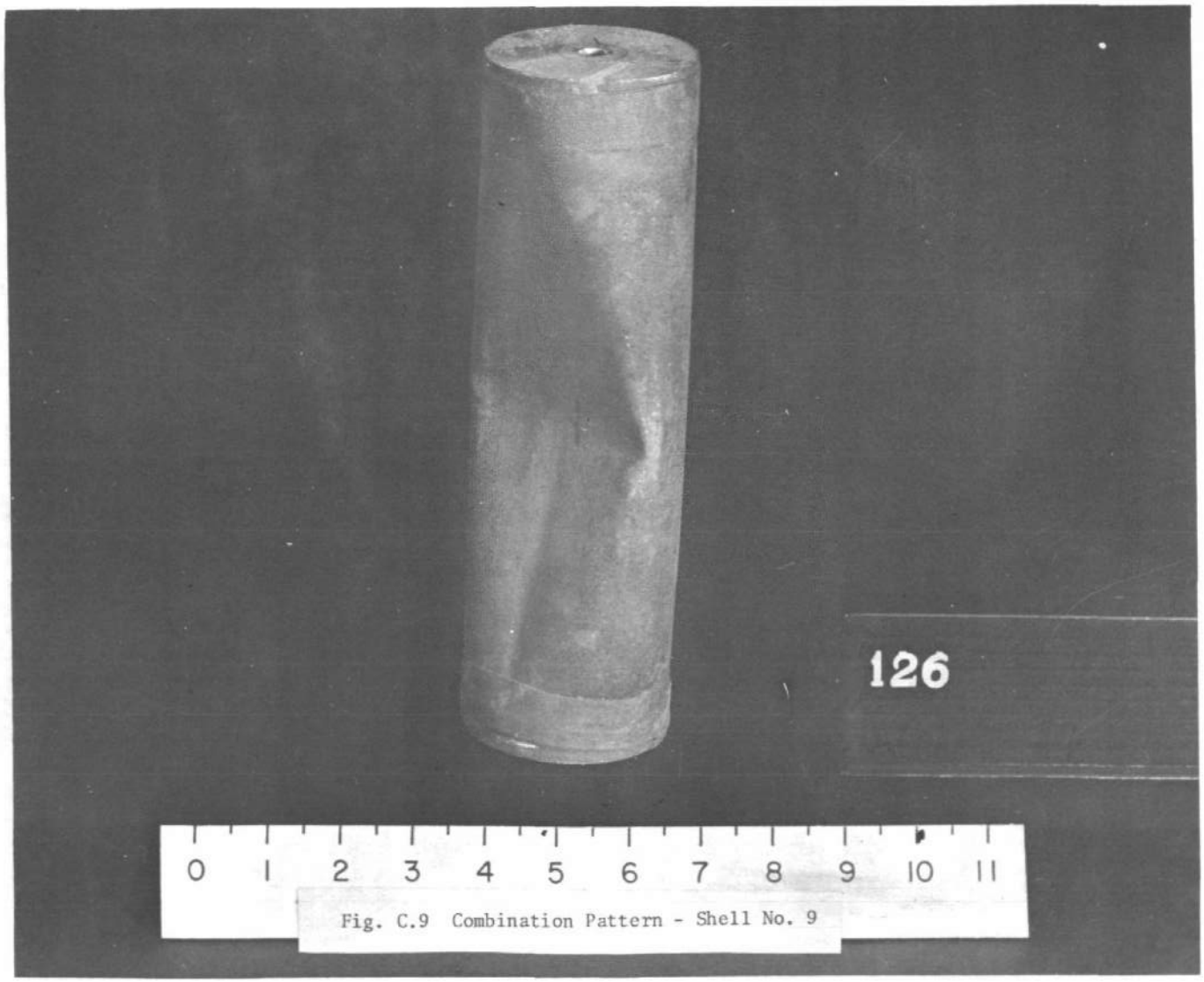

Fig. C.9 Combination Pattern - Shell No. 9

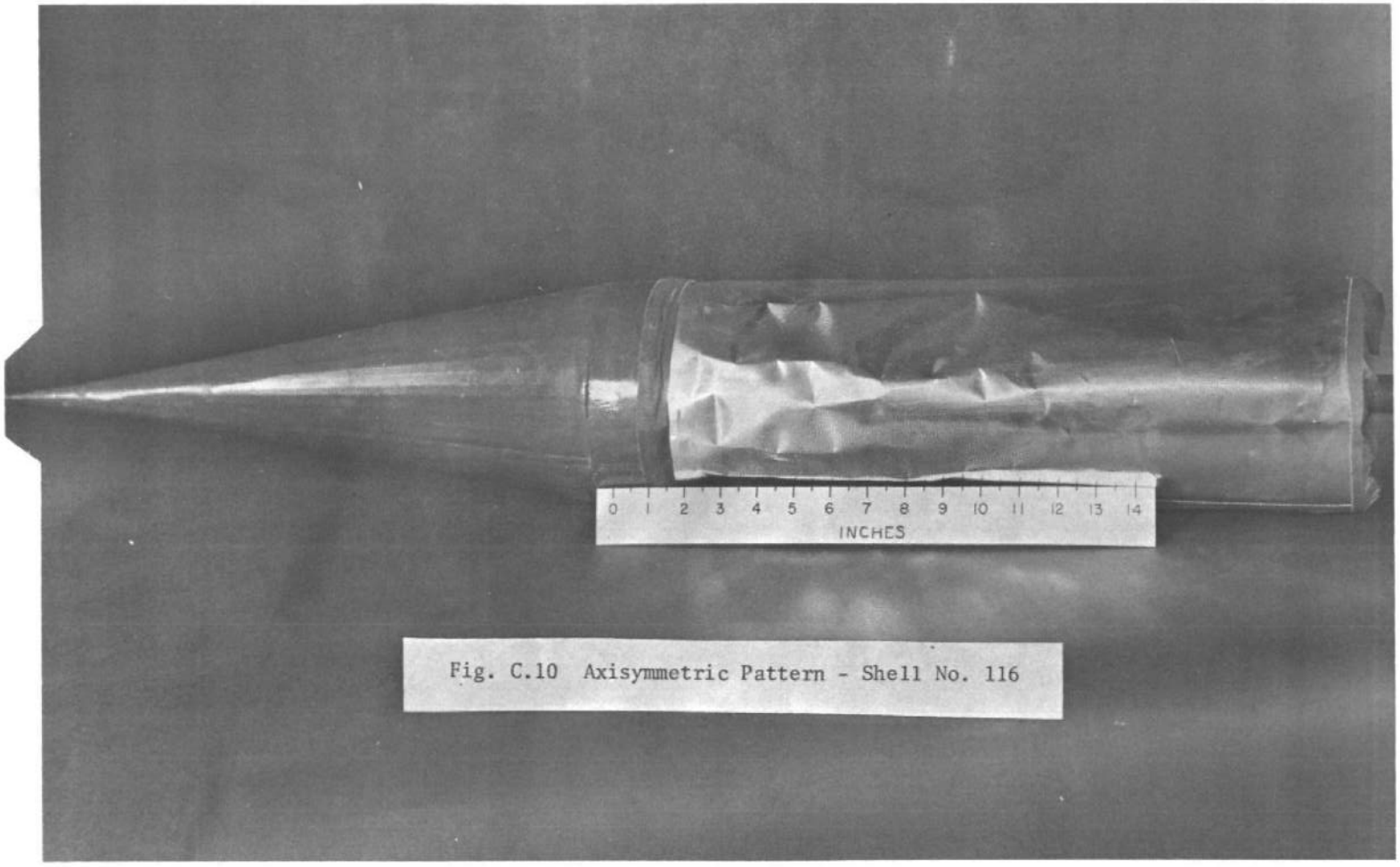

Fig. C.10 Axisymmetric Pattern - Shell No. 116

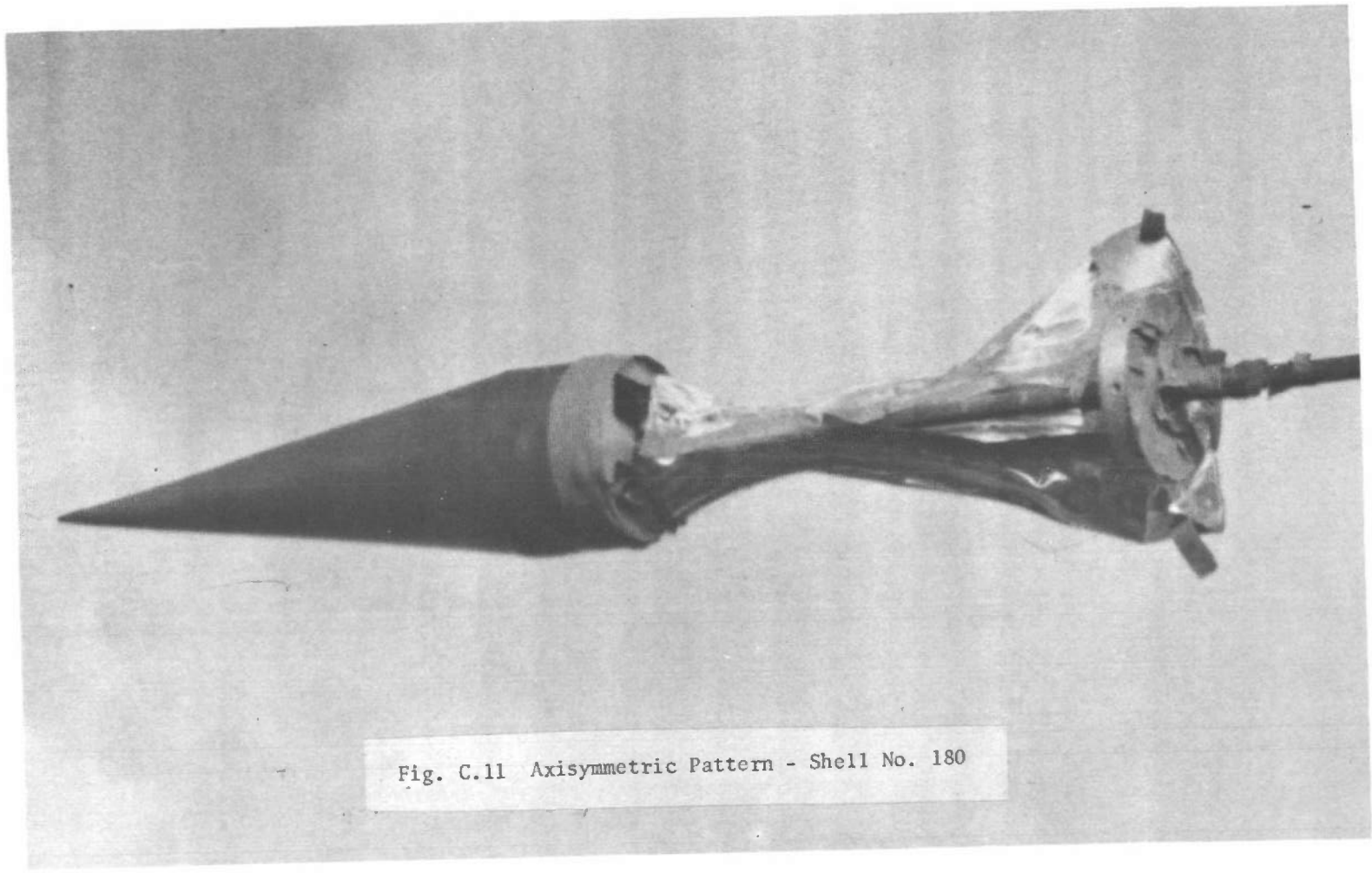

Fig. C.11 Axisymmetric Pattern - Shell No. 180

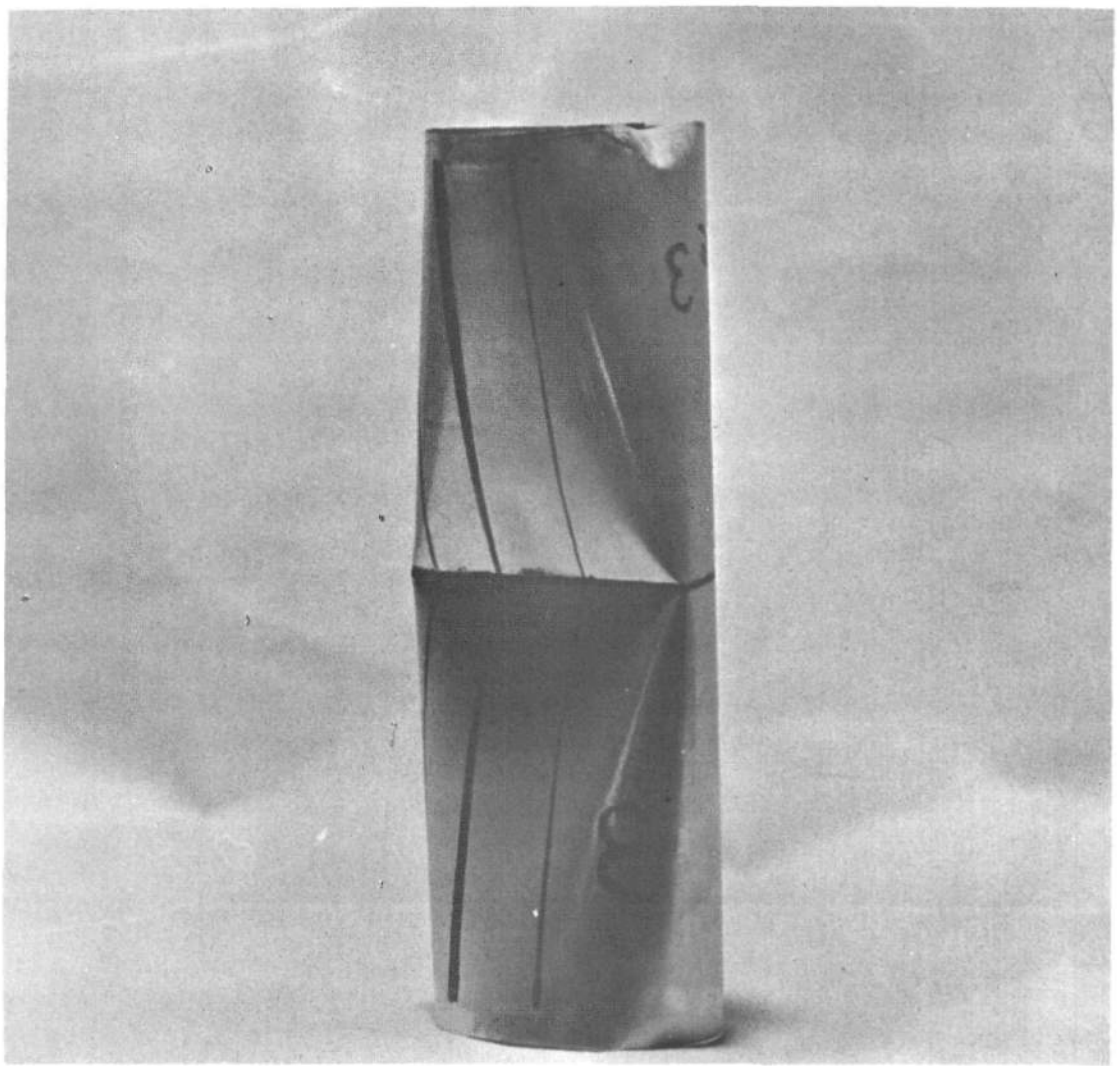

Fig. C.12 Static Deformation Pattern

DISTRIBUTION LIST

No. of Copies	Organization
20	Commander Defense Documentation Center ATTN: TIPCR Cameron Station Alexandria, Virginia 22314
2	Director Defense Atomic Support Agency ATTN: Blast and Shock Division Washington, D. C. 20301
1	Commander, Field Command Defense Atomic Support Agency Sandia Base P. O. Box 5100 Albuquerque, New Mexico 87115
1	Director Defense Research & Engineering (OSD) Washington, D. C. 20301
1	Institute for Defense Analyses 400 Army-Navy Drive Arlington, Virginia 22202
1	Director Defense Intelligence Agency ATTN: AP1(K2), Mr. White Washington, D. C. 20301
1	Commanding General U. S. Army Materiel Command ATTN: AMCRD-RP-B Washington, D. C. 20315
4	Commanding General U. S. Army Missile Command ATTN: AMCPM-NXE AMCPM-ZE AMCPM-MB AMSMI-RSD Redstone Arsenal, Ala. 35809
5	Commanding General U. S. Army Missile Command ATTN: AMCPM-MA AMCPM-SE AMCPM-HA AMCPM-HE AMCPM-PE Redstone Arsenal, Ala. 35809
1	Commanding General U. S. Army Engineering Research & Development Laboratories ATTN: STINFO Branch Fort Belvoir, Virginia 22060
5	Commanding Officer Picatinny Arsenal ATTN: Mr. L. Rosendorf Mr. G. Demitrack Mr. W. Benson Mr. J. Chernoff Dover, New Jersey 07801
1	Commanding General White Sands Missile Range ATTN: AMTED-E-NEL New Mexico 88002
1	Commanding General U. S. Army Weapons Command Rock Island, Illinois 61202
1	Commanding Officer Harry Diamond Laboratories ATTN: Mr. Seijo Washington, D. C. 20438
1	Commanding Officer Watertown Arsenal ATTN: Technical Information Section Watertown, Massachusetts 02172

DISTRIBUTION LIST

No. of Copies	Organization
2	Commanding Officer U. S. Army Research Office (Durham) Box CM, Duke Station Durham, North Carolina 27706
3	Chief, Bureau of Naval Weapons ATTN: DLI-3 Department of the Navy Washington, D. C. 20360
2	Commander U. S. Naval Ordnance Laboratory White Oak Silver Spring, Maryland 20910
5	Commanding Officer U. S. Naval Ordnance Laboratory ATTN: Dr. Brown S. G. Plentzas (2 cys) Corona, California 91720 Of Interest to: Mr. Richard L. Higuera, Code 552 (2 cys)
1	Commander U. S. Naval Ordnance Test Station ATTN: Code 4057 China Lake, California 93557
1	Commander U. S. Naval Ordnance Test Station 3202 E. Foothill Boulevard Pasadena, California 91108
1	Superintendent U. S. Naval Postgraduate School ATTN: Director of Libraries Monterey, California 93940
2	Director U. S. Naval Research Laboratory ATTN: Code 5367 Washington, D. C. 20390
3	Commander U. S. Naval Weapons Laboratory ATTN: D. W. Culbertson (Code TEV) Dr. W. G. Soper Dahlgren, Virginia 22448
2	Commanding Officer U. S. Naval Air Development Center Johnsville, Pennsylvania 18974
1	Commander U. S. Naval Missile Center Point Mugu, California 93041
1	Chief of Naval Research ATTN: ONR: 439: N. Perrone Washington, D. C. 20360
1	Commanding Officer & Director David W. Taylor Model Basin ATTN: Technical Library, Code 42 Washington, D. C. 20007
1	Inspector of Naval Material 428 South Warren Street Syracuse, New York 13202
2	Hq, USAF (AFRST) Washington, D. C. 20330
1	RADC Griffis AFB Rome, New York 13442
2	AFWL (WLL) Kirtland AFB New Mexico 87117

DISTRIBUTION LIST

No. of Copies	Organization
4	BSD (BSBKA, BSTBK, BSQK, BSTAK) Norton AFB California 92409
2	AFETR (ETX - Col W. H. Lee, MPORS - L. J. Ullian) Patrick AFB, Florida 32925
4	AFFDL (FDT) Wright-Patterson AFB Ohio 45433
2	AFIT (Library; Mechanics Dept) Wright-Patterson AFB Ohio 45433
1	FTD Wright-Patterson AFB Ohio 45433
1	SEG (SEF) Wright-Patterson AFB Ohio 45433
1	Director National Aeronautics & Space Administration Washington, D. C. 20546
2	Director John F. Kennedy Space Center, NASA ATTN: KN-ES-3 KN-ES-34 Cocoa Beach, Florida 32931
1	Jet Propulsion Laboratory 4800 Oak Grove Drive Pasadena, California 91103
4	Director National Aeronautics & Space Administration Langley Research Center ATTN: Mr. Harold B. Pierce Atmospheric Input Section Langley Station Hampton, Virginia 23365
2	Director National Aeronautics & Space Administration Manned Spacecraft Center ATTN: Library Houston, Texas 77058
1	Director National Aeronautics & Space Administration George C. Marshall Space Flight Center ATTN: Claude Grain/M-P&VE-SD Redstone Arsenal, Ala. 35812
2	Applied Physics Laboratory ATTN: Dr. Hill Document Library 8621 Georgia Avenue Silver Spring, Maryland 20910
4	Aerospace Corporation ATTN: R. M. Cooper P. O. Box 95085 Los Angeles, California 90045
3	Aerospace Corporation ATTN: P. P. Radkowski D. B. Singer Dr. P. W. Peterson San Bernardino, California 92400
2	Aircraft Armaments, Inc. Cockeysville, Maryland 21030

DISTRIBUTION LIST

No. of Copies	Organization
1	Allied Research Associates, Inc. ATTN: Mr. Sapowith Virginia Road Concord, Massachusetts 01742
2	Aluminum Company of America ATTN: F. D. Buggie Two Penn Center Plaza Philadelphia, Pa. 19102
2	AVCO Corporation Research and Advanced Development Division ATTN: Mr. J. R. Henry Mr. John S. Humphreys 201 Lowell Street Wilmington, Massachusetts 02149
1	Barry Research & Development ATTN: Mr. Jerome E. Ruzicky 700 Pleasant Street Watertown, Massachusetts 02172
4	Boeing Company ATTN: R. W. Hager 51-72 J. W. Flick, Jr. 51-72 R. Elam R. Murakami Seattle, Washington 98124
1	Cornell Aeronautical Laboratory P. O. Box 235 Buffalo, New York 14221
2	Douglas Aircraft Company, Inc. Advance Missile Technology ATTN: Eugene A. Fitzgerald, A-263 3000 Ocean Park Boulevard Santa Monica, California 90405
2	Douglas Aircraft Company ATTN: William Kindel, Field Representative 1100 17th Street, N. W. Washington, D. C.
1	Falcon Research & Development Co. Denver, Colorado 80218
1	General Electric Company ATTN: Mr. T. L. Brewer, V & H Systems Engineering 3198 Chestnut Street Philadelphia, Pennsylvania 19101
1	General Motors Corporation Defense Research Laboratories ATTN: J. W. Gehring Santa Barbara, California 93100
2	J. G. Engineering Research Associates 3831 Menlo Drive Baltimore, Maryland 21215
2	Kaman-Avidyne ATTN: Dr. N. P. Hobbs R. D'Amato 76 Cambridge Street Burlington, Massachusetts 01801
3	Kaman-Nuclear ATTN: D. C. Sachs L. Bothell R. Keefe Garden of Gods Road Colorado Springs, Colorado 80900
2	Lockheed Aircraft Corporation Lockheed Nuclear Products ATTN: B. H. Little, Jr. Georgia Division Marietta, Georgia 30060
1	Lockheed Missile & Space Division P. O. Box 504 Sunnyvale, California 94086
1	The Martin Company Baltimore, Maryland 21203

DISTRIBUTION LIST

No. of Copies	Organization
1	The Martin Company ATTN: Tech Development Section Denver, Colorado 80201
2	The Martin Company ATTN: H. R. Fuehrer, MP-109 R. Dudley, MP-492 Orlando, Florida 32800
1	North American Aviation, Inc. ATTN: James Sheng Downey, California 91242
1	Raytheon Company Mail No. 550 Hartwell Road Bedford, Massachusetts 01730
1	Republic Aviation Corporation ATTN: Sup. Eng. Library Farmingdale, Long Island New York 11735
3	Southwest Research Institute Department of Mechanical Sciences ATTN: Dr. H. N. Abramson Dr. W. H. Chu Dr. W. E. Baker 8500 Culebra Road San Antonio, Texas 78228
2	Sperry Utah Company ATTN: AMCPM-SEU Salt Lake City, Utah 84116
2	Stanford Research Institute Poulter Laboratories ATTN: Dr. G. Abrahamson Dr. H. Lindberg Menlo Park, California 94025
4	TRW Space Technology Laboratories ATTN: Dr. J. D. Wood Mr. Kenneth Mann (3 cys) One Space Park Redondo Beach, California 90278
1	Brown University Providence, Rhode Island 02912
1	Columbia University ATTN: G. Harrison New York, New York 11200
1	IIT Research Institute ATTN: P. G. Hodge, Jr. Chicago, Illinois 60616
3	Massachusetts Institute of Technology ATTN: Dr. E. A. Witmer Dr. J. R. Ruetenik J. Percy Cambridge, Massachusetts 02139
1	Polytechnic Institute of Brooklyn ATTN: J. Kemper Brooklyn, New York 11200
1	Stanford University ATTN: N. J. Hoff Stanford, California 94300
1	University of California College of Engineering Los Angeles, California 90024
1	University of Florida ATTN: W. A. Nash Gainesville, Florida
1	University of Minnesota ATTN: C. N. DeSilva Minneapolis, Minnesota 55414

DISTRIBUTION LIST

No. of Copies	Organization
2	Professor N. Davids The Pennsylvania State University Department of Engineering Mechanics University Park, Pa. 16802
	Aberdeen Proving Ground
	Chief, Tech Lib
	Air Force Ln Ofc Marine Corps Ln Ofc Navy Ln Ofc CDC Ln Ofc

Unclassified
Security Classification

DOCUMENT CONTROL DATA - R&D

(Security classification of title, body of abstract and indexing annotation must be entered when the overall report is classified)

1. ORIGINATING ACTIVITY *(Corporate author)*
U. S. Army Ballistic Research Laboratories
Aberdeen Proving Ground, Maryland

2a. REPORT SECURITY CLASSIFICATION
Unclassified

2b. GROUP

3. REPORT TITLE
A FAILURE CRITERION FOR BLAST LOADED CYLINDRICAL SHELLS

4. DESCRIPTIVE NOTES *(Type of report and inclusive dates)*

5. AUTHOR(S) *(Last name, first name, initial)*
Schuman, William J., Jr.

6. REPORT DATE	7a. TOTAL NO. OF PAGES	7b. NO. OF REFS
May 1965	128	50

8a. CONTRACT OR GRANT NO.

b. PROJECT NO.
1P014501A33E

c.

d.

9a. ORIGINATOR'S REPORT NUMBER(S)
Report No. 1292

9b. OTHER REPORT NO(S) *(Any other numbers that may be assigned this report)*

10. AVAILABILITY/LIMITATION NOTICES
Distribution of this document is unlimited.

11. SUPPLEMENTARY NOTES

12. SPONSORING MILITARY ACTIVITY
U. S. Army Materiel Command
Washington, D. C.

13. ABSTRACT

The results of an extensive experimental program to study the plastic response of thin-walled, unstiffened cylindrical shells to external blast loading are presented. Empirical relations between the shell and blast parameters that satisfy a failure criterion based on a given level of plastic deformation are given.

A comparison of calculated and actual overpressure values for 159 shells that had responses satisfying the failure criterion (permament deformation in the radial direction - 5 percent to 10 percent of the original diameter) is made. The average deviation between these values is 14 percent.

DD FORM 1 JAN 64 1473

Unclassified
Security Classification

14. KEY WORDS	LINK A		LINK B		LINK C	
	ROLE	WT	ROLE	WT	ROLE	WT
Shell Response						
Dynamic Response						
Blast Response						
Blast Loading						
Simulated Missiles						
Plastic Failure of Shells						
Failure Criterion						
Shell Deformation						
Cylindrical Shells						
Structural Dynamics						
Shell Dynamics						

INSTRUCTIONS

1. ORIGINATING ACTIVITY: Enter the name and addreas of the contractor, subcontractor, grantee, Department of Defenae activity or other organization *(corporate author)* issuing the report.

2a. REPORT SECURITY CLASSIFICATION: Enter the overall security classification of the report. Indicate whether "Restricted Data" is included. Marking ia to be in accordance with appropriate security regulations.

2b. GROUP: Automatic downgrading is specified in DoD Directive 5200.10 and Armed Forcea Industrial Manual. Enter the group number. Alao, when applicable, show that optional markings have been used for Group 3 and Group 4 as authorized.

3. REPORT TITLE: Enter the complete report title in all capital letters. Titles in all casea ahould be unclassified. If a meaningful title cannot be selected without classification, show title classification in all capitals in parenthesis immediately following the title.

4. DESCRIPTIVE NOTES: If appropriate, enter the type of report, e.g., interim, progress, summary, annual, or final. Give the inclusive dates when a specific reporting period is covered.

5. AUTHOR(S): Enter the name(s) of author(s) as shown on or in the report. Enter last name, first name, middle initial. If military, show rank and branch of aervice. The name of the principal author is an absolute minimum requirement.

6. REPORT DATE: Enter the date of the report as day, month, year; or month, year. If more than one date appears on the report, use date of publication.

7a. TOTAL NUMBER OF PAGES: The total page count should follow normal pagination procedures, i.e., enter the number of pages containing information.

7b. NUMBER OF REFERENCES: Enter the total number of referencea cited in the report.

8a. CONTRACT OR GRANT NUMBER: If appropriate, enter the applicable number of the contract or grant under which the report was written.

8b, 8c, & 8d. PROJECT NUMBER: Enter the appropriate military department identification, such aa project number, subproject number, system numbers, task number, etc.

9a. ORIGINATOR'S REPORT NUMBER(S): Enter the official report number by which the document will be identified and controlled by the originating activity. This number must be unique to this report.

9b. OTHER REPORT NUMBER(S): If the report has been assigned any other report numbera *(either by the originator or by the sponsor)*, also enter thia number(s).

10. AVAILABILITY/LIMITATION NOTICES: Enter any limitations on further disaemination of the report, other than those imposed by security classification, using standard statements such as:

(1) "Qualified requesters may obtain copies of this report from DDC."

(2) "Foreign announcement and dissemination of this report by DDC is not authorized."

(3) "U. S. Government agencies may obtain copies of this report directly from DDC. Other qualified DDC users shall request through _____."

(4) "U. S. military agencies may obtain copies of this report directly from DDC. Other qualified users shall request through _____."

(5) "All distribution of this report is controlled. Qualified DDC users shall request through _____."

If the report has been furnished to the Office of Technical Services, Department of Commerce, for sale to the public, indicate thia fact and enter the price, if known.

11. SUPPLEMENTARY NOTES: Use for additional explanatory notes.

12. SPONSORING MILITARY ACTIVITY: Enter the name of the departmental project office or laboratory sponsoring *(paying for)* the research and development. Include address.

13. ABSTRACT: Enter an abstract giving a brief and factual summary of the document indicative of the report, even though it may also appear elsewhere in the body of the technical report. If additional apace is required, a continuation sheet shall be attached.

It is highly desirable that the abstract of classified reports be unclassified. Each paragraph of the abstract shall end with an indication of the military security classification of the information in the paragraph, represented as *(TS)*, *(S)*, *(C)*, or *(U)*.

There is no limitation on the length of the abstract. However, the suggested length is from 150 to 225 words.

14. KEY WORDS: Key words are technically meaningful terms or short phrases that characterize a report and may be used as index entries for cataloging the report. Key words must be selected so that no security classification is required. Identifiers, such as equipment model designation, trade name, military project code name, geographic location, may be used as key words but will be followed by an indication of technical context. The assignment of links, rules, and weights is optional.